Monthly Notices of the ROYAL ASTRONOMICAL SOCIETY
MNRAS **450,** 3514–3548 (2015) doi:10.1093/mnras/stv821

New binaries among UV-selected, hot subdwarf stars and population properties⋆

A. Kawka,[1]†‡ S. Vennes,[1]‡ S. O'Toole,[2] P. Németh,[3]‡ D. Burton,[4] E. Kotze[5,6] and D. A. H. Buckley[5,7]

[1]*Astronomický ústav AV ČR, Fričova 298,CZ-251 65 Ondřejov, Czech Republic*
[2]*Australian Astronomical Observatory, PO Box 915, 1670 North Ryde NSW, Australia*
[3]*Dr. Remeis–Sternwarte, Institute for Astronomy, University Erlangen-Nürnberg, Sternwartstr. 7, D-96049 Bamberg, Germany*
[4]*Faculty of Sciences, University of Southern Queensland, Toowoomba, QLD 4350, Australia*
[5]*South African Astronomical Observatory, Observatory Road, Observatory 7935, South Africa*
[6]*Department of Astronomy, University of Cape Town, Rondebosch 7770, Cape Town, South Africa*
[7]*South African Large Telescope, PO Box 9, Observatory 7935, South Africa*

Accepted 2015 April 10. Received 2015 April 10; in original form 2014 November 17

ABSTRACT

We have measured the orbital parameters of seven close binaries, including six new objects, in a radial velocity survey of 38 objects comprising a hot subdwarf star with orbital periods ranging from ∼0.17 to 3 d. One new system, GALEX J2205−3141, shows reflection on an M dwarf companion. Three other objects show significant short-period variations, but their orbital parameters could not be constrained. Two systems comprising a hot subdwarf paired with a bright main-sequence/giant companion display short-period photometric variations possibly due to irradiation or stellar activity and are also short-period candidates. All except two candidates were drawn from a selection of subluminous stars in the *Galaxy Evolution Explorer* ultraviolet sky survey. Our new identifications also include a low-mass subdwarf B star and likely progenitor of a low-mass white dwarf (GALEX J0805−1058) paired with an unseen, possibly substellar, companion. The mass functions of the newly identified binaries imply minimum secondary masses ranging from 0.03 to 0.39 $M_{\odot}$. Photometric time series suggest that, apart from GALEX J0805−1058 and J2205−3141, the companions are most likely white dwarfs. We update the binary population statistics: close to 40 per cent of hot subdwarfs have a companion. Also, we found that the secondary mass distribution shows a low-mass peak attributed to late-type dwarfs, and a higher mass peak and tail distribution attributed to white dwarfs and a few spectroscopic composites. Also, we found that the population kinematics imply an old age and include a few likely halo population members.

Key words: binaries: close – binaries: spectroscopic – subdwarfs – white dwarfs – ultraviolet: stars.

1 INTRODUCTION

Hot subdwarf stars (see a review by Heber 2009) are core helium burning stars with very thin hydrogen envelopes and belong to the extreme horizontal branch (EHB). The mass of most hot subdwarfs is about 0.5 $M_{\odot}$. The origin of EHB stars, i.e. the hot, hydrogen-rich (sdB) and helium-rich subdwarf (sdO) stars, is closely linked to binarity. Mengel, Norris & Gross (1976) first proposed that sdB stars are formed in close binary systems and Dorman, Rood & O'Connell (1993) inferred the presence of an extremely thin hydrogen envelope (<0.001 $M_{\odot}$). Han et al. (2002, 2003) proposed three formation channels for sdB stars through binary interaction, i.e. common envelope (CE), Roche lobe overflow (RLOF), and binary merger. Han et al. (2003) predict a binary fraction of 76–89 per cent with orbital periods ranging from 0.5 h to 500 d. However, they caution that the observed frequency could be much lower due to selection effects. The proposed formation channels also predict single sdB stars that form via the merger of two helium white dwarfs. Approximately 11–26 per cent

⋆Based on observations made with ESO telescopes at the La Silla Paranal Observatory under programmes 076.D-0355, 077.D-0515, 078.D-0098, 086.D-0714, 089.D-0864, 090.D-0012 and 093.D-0273.

†E-mail: kawka@sunstel.asu.cas.cz
‡Visiting Astronomer, KPNO, National Optical Astronomy Observatory, which is operated by the Association of Universities for Research in Astronomy (AURA) under cooperative agreement with the National Science Foundation.

of subdwarfs are expected to form via this merger channel (Han et al. 2003).

Formation channels of helium-rich (He-sdO) stars are not as well defined. Justham, Podsiadlowski & Han (2011) proposed that these objects may form in a close double degenerate binary with the massive component accreting from a helium white dwarf companion and initiating helium-shell burning. A small number of sdO stars are known to exist as companions to Be stars (Gies et al. 1998; Peters et al. 2008, 2013). These sdO stars are formed through close binary interaction where the more massive primary star begins mass transfer on to its less massive companion during its shell-hydrogen burning phase. The result of this mass transfer leaves a spun up Be star with an sdO companion (Pols et al. 1991).

Cool companions to hot subdwarf stars can be revealed as infrared excess in the spectral energy distribution (SED). Thejll, Ulla & MacDonald (1995) and Ulla & Thejll (1998) detected infrared excess in over 20 per cent of the hot subdwarf stars studied in their sample. Girven et al. (2012) explored photometric surveys that cover a wide wavelength range, from the *Galaxy Evolution Explorer* (*GALEX*) ultraviolet survey through to the infrared, the Two Micron All Sky Survey (2MASS) and the UKIRT Infrared Deep Sky Survey (UKIDSS), and searched for main-sequence companions to hot subdwarf stars. They found that the most common companions to hot subdwarfs have a spectral type between F0 and K0, while M-type companions were found to be much rarer.

Radial velocity surveys (e.g. Maxted et al. 2001; Morales-Rueda et al. 2003; Copperwheat et al. 2011; Geier et al. 2011c) of sdB stars have shown that approximately half of all sdB stars reside in close binary systems with either a cool main-sequence star or a white dwarf companion. These surveys target binary systems with periods of a few hours to ≈30 d. Napiwotzki et al. (2004) reported a binary fraction of 39 per cent of sdB stars from the ESO Supernovae type Ia Progenitor surveY (SPY). Copperwheat et al. (2011) estimated a higher binary fraction of 46–56 per cent from their survey of sdB stars selected from the Palomar–Green and Edinburgh–Cape surveys.

A few rare sdB stars are found in close orbit with a massive white dwarf ($M_{\rm WD} \gtrsim 0.9\,{\rm M}_{\odot}$), making them Type Ia supernova progenitors. These systems would first evolve to AM CVn systems before detonating either as a Type Ia or the less energetic Type.Ia (Iax) supernova (Bildsten et al. 2007; Fink et al. 2010; Solheim 2010). The first such candidate is KPD 1930+2752 (Maxted, Marsh & North 2000b; Geier et al. 2007), with a second candidate, GALEX J1411−3053 (CD−30 11223), discovered as part of our radial velocity survey of *GALEX* selected hot subdwarf stars (Vennes et al. 2012).

Some sdB stars in close binary systems have stellar parameters that fall below the zero-age horizontal branch and probably did not initiate helium burning. Such objects have very low masses ($\approx 0.2\,{\rm M}_{\odot}$) and are the progenitors of extremely low mass (ELM) white dwarfs, which will in time evolve into AM CVn systems. If the companion to these low-mass stars is a massive enough white dwarf, then the system may become a Type Ia supernova. The first-known low-mass sdB star, HD 188112, was discovered by Heber et al. (2003).

Ahmad, Jeffery & Fullerton (2004) discovered the first double subdwarf binary, PG 1544+488. This helium rich sdB (He-sdB) binary remains, at the present time, unique. The mass ratio determined from the velocity semi-amplitude of the components show that they have a similar mass which suggests that the system emerged from a CE comprised of two nearly identical red giant cores (Şener & Jeffery 2014). Alternatively, Lanz et al. (2004) interpreted the peculiar atmospheric composition of He-sdB stars, such as PG 1544+488, with evolutionary models involving a delayed helium-core flash and convective mixing while descending on the white dwarf cooling track. Similarly, HE 0301−3039 is a close binary consisting of two sdO stars (Lisker et al. 2004; Stroeer et al. 2007) that may be the outcome of double-core CE evolution (Justham et al. 2011).

Surveys of hot subdwarfs involving photometric time series have uncovered several more low-mass sdB stars. *Kepler* observations revealed that KIC 6614501 is another low-mass sdB plus white dwarf system (Silvotti et al. 2012). Also, Maxted et al. (2014) presented 17 eclipsing systems from Wide Angle Search for Planets (WASP) survey that are likely to contain a pre-helium white dwarf, similar to the system 1SWASP J024743.37−251549.2 (Maxted et al. 2011). Follow-up spectroscopy for six of these systems confirmed them to be main-sequence A stars with very low mass ($\approx 0.2\,{\rm M}_{\odot}$) pre-He white dwarfs currently experiencing hydrogen-shell burning.

Wider binaries (orbital periods ∼ years) containing an sdB star with a cool main-sequence companion were reported by Barlow et al. (2012, 2013b) and Vos et al. (2013). The predicted period distribution by Han et al. (2003) is bimodal with some B- to F-type companions in the longer period range. The relative frequency of short- to long-period binaries depends on the actual value of the critical mass ratio for stable mass transfer; this ratio may be set with a study of potential subdwarf plus A-star binaries. Chen et al. (2013) showed that these long-period binaries are the result of stable RLOF.

Vennes, Kawka & Németh (2011) and Németh, Kawka & Vennes (2012) presented a new sample of sdB stars selected from the *GALEX* all-sky survey and we conducted a radial velocity survey of a subsample of stars from this selection. The first two systems (GALEX J0321+4727 and GALEX J2349+3844) discovered as part of this survey were presented by Kawka et al. (2010), followed by the aforementioned short-period system GALEX J1411−3053 (Vennes et al. 2012; Geier et al. 2013a). Additional spectroscopic and photometric observations of the first two systems were presented in Kawka et al. (2012) along with a progress report on the other systems that were observed as part of this programme. The photometric observations confirmed the reflection effect in GALEX J0321+4727 originally reported by Kawka et al. (2010) and based on Northern Sky Variability Survey (NSVS) photometry. The observations also showed that both GALEX J0321+4727 and GALEX J2349+3844 are V2093 Her type pulsating subdwarfs (Green et al. 2003).

In this paper, we present spectroscopic and photometric observations of a sample of *GALEX*-selected hot subdwarf stars with the aim of determining their binary properties. Sections 2.1 and 2.2 present details of our spectroscopic observations, while Section 2.3 present archival photometric time series. In Section 3, we present an analysis of stellar properties (3.1), and of binary properties supplemented by our analysis of photometric time series (3.2). Finally, we present a review of the properties of known binaries comprising a hot subdwarf star, including the properties of the components (Section 4.1), the population kinematics (4.2), and the properties of some outstanding individual cases (4.3), followed by a summary of this work (4.4).

2 SAMPLE SELECTION AND OBSERVATIONS

Table 1 lists the stars originally included in our radial velocity survey with notable properties described in Section 3.1. The sample includes 38 spectroscopically confirmed hot subdwarf stars, and two

Table 1. Target summary.

GALEX J	Other names	$T_{\rm eff}$ (K)	log g c.g.s.	log (He/H)	Notes[a]
004759.6+033742	BPS BS 17579-0012, PB 6168	38620^{+2250}_{-970}	$6.14^{+0.22}_{-0.18}$	$-2.63^{+0.44}_{-1.17}$	sdB+F6V; IR; nearby star
004729.4+095855	HD 4539, HIP 3701	24650^{+590}_{-200}	$5.38^{+0.03}_{-0.05}$	$-2.42^{+0.20}_{-0.07}$	
004917.2+205640	PG 0046+207	27520^{+500}_{-450}	$5.55^{+0.07}_{-0.06}$	$-2.48^{+0.16}_{-0.23}$	
005956.7+154419	HIP 4666, PG 0057+155, PHL 932	33530^{+190}_{-310}	$5.83^{+0.04}_{-0.05}$	$-1.69^{+0.06}_{-0.04}$	
020656.1+143900	CHSS 3497	30310^{+660}_{-80}	$5.77^{+0.05}_{-0.06}$	$-2.61^{+0.15}_{-0.24}$	
023251.9+441126	FBS 0229+439	33260^{+420}_{-380}	$5.73^{+0.09}_{-0.10}$	$-1.70^{+0.08}_{-0.12}$	
040105.3−322348	CD-32 1567, EC 03591-3232	30490^{+250}_{-220}	$5.71^{+0.06}_{-0.04}$	$-1.92^{+0.06}_{-0.04}$	
050018.9+091203	HS 0457+0907	36270^{+490}_{-1130}	$5.75^{+0.15}_{-0.13}$	$-1.46^{+0.14}_{-0.15}$	
050735.7+034814		23990^{+630}_{-610}	$5.42^{+0.08}_{-0.11}$	$-3.05^{+0.48}_{-0.78}$	Ca H&K, RV
061325.3+342053		34250^{+330}_{-390}	$5.75^{+0.10}_{-0.06}$	$-1.28^{+0.04}_{-0.08}$	RV
065736.7−732447	CPD-73 420	29940^{+900}_{-160}	$5.45^{+0.07}_{-0.15}$	<-3.21	nearby star
070331.5+623626	FBS 0658+627	28750^{+370}_{-340}	$5.40^{+0.07}_{-0.04}$	$-2.76^{+0.22}_{-0.26}$	
071646.9+231930	TYC 1909-865-1	11140/9310	4.39/3.67	...	close B+A V binary, RV
075147.1+092526		30620^{+490}_{-460}	$5.74^{+0.11}_{-0.12}$	$-2.49^{+0.27}_{-0.30}$	nearby star (6 arcsec), RV
080510.9−105834	TYC 5417-2552-1	22320^{+330}_{-280}	$5.68^{+0.03}_{-0.06}$	<-3.44	ELM WD progenitor, RV
081233.6+160123		31580^{+440}_{-490}	$5.56^{+0.10}_{-0.13}$	<-2.90	RV
104148.6−073034	TYC 5492-642-1	27440^{+620}_{-450}	$5.63^{+0.09}_{-0.06}$	$-2.44^{+0.16}_{-0.23}$	
111422.0−242130	EC 11119-2405, TYC 6649-111-1	23430^{+480}_{-450}	$5.29^{+0.08}_{-0.07}$	$-2.46^{+0.19}_{-0.31}$	
135629.2−493403	CD-48 8608, TYC 8271-627-1	33070^{+230}_{-660}	$5.74^{+0.07}_{-0.16}$	$-2.75^{+0.25}_{-0.43}$	sdB+G8V; IR
140747.6+310318	BPS BS 16082-0122	24900^{+50}_{-3050}	$4.25^{+0.03}_{-0.09}$	$-1.18^{+0.08}_{-0.09}$	high-v early B
141133.3+703737	TYC 4406-666-1	21170^{+1500}_{-1110}	$5.55^{+0.31}_{-0.23}$	<-2.36	sdB+F; IR; ELM WD progenitor?
142126.5+712427	TYC 4406-285-1	25620^{+320}_{-220}	5.67 ± 0.04	<-3.7	
142747.2−270108	EC 14248-2647, TYC 6740-942-1	31880^{+360}_{-290}	$5.70^{+0.05}_{-0.08}$	$-1.71^{+0.05}_{-0.11}$	
143519.8+001352	TYC 325-452-1, PG 1432+004	23090^{+780}_{-250}	$5.28^{+0.08}_{-0.08}$	$-2.39^{+0.18}_{-0.20}$	
163201.4+075940	TYC 960-1373-1, PG 1629+081	38110^{+570}_{-680}	$5.38^{+0.06}_{-0.09}$	$-2.71^{+0.27}_{-0.29}$	nearby star, RV
173153.7+064706		27780^{+1030}_{-470}	$5.35^{+0.18}_{-0.07}$	<-2.53	RV
173651.2+280635	TYC 2084-448-1	36160^{+6500}_{-4200}	$5.24^{+0.84}_{-0.84}$	$-1.09^{+0.69}_{-1.34}$	sdB+F7V; IR; variable
175340.5−500741		32430^{+880}_{-570}	$5.95^{+0.18}_{-0.18}$	$-2.25^{+0.31}_{-1.04}$	sdB+F7V; IR
184559.8−413826		35930^{+840}_{-4770}	$5.23^{+0.27}_{-0.23}$	$+2.10^{+1.10}_{-0.38}$	sdO; He I spectrum
190211.7−513005	CD-51 11879, TYC 8386-1370-1, LSE 263	72300^{+5380}_{-3260}	$5.49^{+0.11}_{-0.11}$	$+0.02^{+2.10}_{-0.03}$	sdO; He II spectrum
190302.4−352828	BPS CS 22936-0293	32100^{+1760}_{-1260}	$5.26^{+0.31}_{-0.30}$	<-1.96	RV
191109.2−140651	TYC 5720-292-1	55970^{+4540}_{-1780}	$5.69^{+0.71}_{-0.09}$	$+0.25^{+0.70}_{-0.60}$	sdO; He II spectrum
203850.3−265750	TYC 6916-251-1	58450^{+4600}_{-7920}	$5.04^{+0.39}_{-0.17}$	$-1.13^{+0.27}_{-0.29}$	sdO+G3.5III; IR; variable
215340.4−700430	EC 21494-7018, TYC 9327-1311-1	23720^{+260}_{-230}	$5.65^{+0.03}_{-0.02}$	$-3.22^{+0.13}_{-1.15}$	ELM WD progenitor?
220551.8−314105	TYC 7489-686-1, BPS CS 30337-0074	28650^{+930}_{-80}	$5.68^{+0.01}_{-0.03}$	$-2.09^{+0.12}_{-0.03}$	reflection, RV
225444.1−551505		31070^{+150}_{-190}	$5.80^{+0.04}_{-0.06}$	$-2.47^{+0.15}_{-0.13}$	RV
233451.7+534701	TYC4000-216-1	35680^{+340}_{-250}	$5.91^{+0.07}_{-0.06}$	-1.43 ± 0.07	
234421.6−342655	CD-35 15910, HE 2341-3443	28390^{+410}_{-120}	$5.39^{+0.05}_{-0.03}$	$-3.07^{+0.21}_{-0.26}$	
J	Other names	$T_{\rm eff}$ (K)	log g c.g.s.	log (He/H)	Notes
123723.5+250400	Feige 66	34300^{+160}_{-180}	5.82 ± 0.04	$-1.51^{+0.05}_{-0.07}$	
160011.8−643330	TYC 9044-1653-1	34640^{+590}_{-580}	$6.02^{+0.08}_{-0.11}$	$-0.30^{+0.05}_{-0.04}$	

[a]RV: confirmed radial velocity variable star; IR: SED of the stars shows significant IR excess.

objects that were, respectively, identified as an early B star and a A V+B V binary. The early B star GALEX J1407+3103 is notable for its high radial velocity, while the close A V+B V pair GALEX J0716+2319 shows significant radial velocity variations on a short time-scale. All except two objects were randomly selected from our catalogue of *GALEX*/Guide Star Catalog ultraviolet-excess objects (Vennes et al. 2011; Németh et al. 2012). Briefly, the source catalogue includes bright objects ($N_{\rm UV} < 14$) with an ultraviolet excess ($N_{\rm UV} - V < 0.5$). The latter criterion still allows for the selection of hot subdwarf plus F/G dwarf pairs (see Vennes et al. 2011). Two additional stars that were not observed by *GALEX*, including a blue-excess object (Jiménez-Esteban, Caballero & Solano 2011), are listed at the bottom of Table 1 with J2000 coordinates.

The *GALEX* name corresponds to the coordinates of the ultraviolet source detected in the near ultraviolet (NUV) band (Section 2.3); for convenience, the names are abbreviated to four digits right ascension and declination. The ultraviolet coordinates are generally close to the Guide Star Catalog (GSC2.3.2) optical coordinates (<1 arcsec), but, in a few cases, offsets as large as 4–9 arcsec occurred (GALEX J1421+7124, J1427−2701, J1902−5130, J2344−3426). Despite the offsets, the ultraviolet and optical sources must be one and the same. These offsets cannot be attributed to a high proper motion and are most likely due to a distorted point spread function (PSF) in bright off-centred sources in the *GALEX* images (Section 2.3).

Throughout this paper, we will refer to the hot subdwarf as the primary and its companion as the secondary. Table 1 lists some notable particularities such as the presence of a nearby star, whether unrelated or physically associated with the hot subdwarf, a bright main-sequence companion, or photometric variability due to reflection on a late-type companion or stellar activity (see Section 3.1). Most stars display H I-dominated line spectra, but we also noted the presence of He-rich subdwarfs characterized by He I and He II-dominated line spectra. The stellar parameters of a handful of subdwarfs locate them below the zero-age EHB (ZAEHB) and these objects are likely progenitors of ELM white dwarfs (Sections 3.1 and 3.2).

2.1 Intermediate to high-dispersion spectroscopy for radial velocity measurements

Our first extensive set of observations was obtained with the Wide Field Spectrograph (WiFeS; Dopita et al. 2007) attached to the 2.3 m telescope at the Siding Spring Observatory (SSO). The observations were conducted on UT 2011 July 14–18, UT 2011 December 2–3 and UT 2012 April 27–30. We used the B3000 and R7000 gratings with a slit width of 1 arcsec that provided spectral ranges of 3200–5900 Å at a resolution of $R = \lambda/\Delta\lambda = 3000$ and 5300–7000 Å at $R = 7000$, respectively. The RT560 dichroic beam splitter separated the incoming light into its red and blue components. WiFeS is an image-slicing spectrograph with 25 slitlets (38 × 1 arcsec) and depending on the seeing, the target can cover a few slitlets. The signal-to-noise ratio (S/N) of each observation was maximized by extracting the spectrum from the most significant ($\lesssim$6) traces. Each trace was wavelength- and flux-calibrated prior to co-addition. The spectra were wavelength-calibrated using NeAr arc spectra that were obtained either prior to or following each observation.

Next, our second set of observations was obtained using the Ritchey–Chrétien Focus (R–C) spectrograph attached to the 4 m telescope at Kitt Peak National Observatory (KPNO) on UT 2012 January 4–6. We used the KPC24 grating in second order combined with the T2KA CCD to provide a spectral range of 6030–6720 Å and a dispersion of 0.52 Å pixel^{-1}. The slit width was set to 1.5 arcsec which provided a resolution of ∼0.9 Å or $R = 7000$. Contamination from third order was removed using the GG495 filter. The spectra were wavelength-calibrated using HeNeAr spectra which were obtained following each observation.

We obtained a third set of observations using the ESO Faint Object Spectrograph and Camera (EFOSC2) attached to the 3.6 m New Technology Telescope (NTT) at La Silla Observatory in 2012 September. We used grism number 20 centred on Hα providing a spectral range from 6040 to 7140 Å and a dispersion of 0.55 Å pixel^{-1}. We set the slit width to 0.7 arcsec resulting in a 2 Å resolution or $R = 3500$. Next, we obtained additional spectra with EFOSC2 on the NTT on UT 2014 July 31 and August 1. We used grism number 19 that provided a spectral range from 4435 to 5120 Å and, after binning 2 × 2, a dispersion of 0.67 Å per binned pixel. The slit width was set to 1 arcsec resulting in a resolution of ∼2 Å or $R \approx 2000$. Additional EFOSC2 spectra of GALEX J1731+0647 were extracted from the ESO archive (programme 090.D-0012, PI S. Geier). The data were also obtained with grism 19, but binned 2 × 1 resulting in a dispersion of 0.34 Å pixel^{-1}. The slit width was set to 1 arcsec resulting in a resolution of ∼2 Å. All spectra were wavelength-calibrated using HeAr arc spectra which were obtained following each observation.

Also, we obtained a fourth set of spectra using the grating spectrograph attached to the 1.9 m telescope at the South African Astronomical Observatory (SAAO) on UT 2014 February 11. We used the 1200 lines mm^{-1} grating with a blaze wavelength of 6800 Å. This arrangement provided a range of 6023–6782 Å with a dispersion of 0.439 Å pixel^{-1}. The slit width was set to 1.05 arcsec resulting in $R = 7000$, or a resolution of ≈1 Å at Hα. A CuNe comparison arc was obtained following each target observation.

We assembled a fifth data set with observations of the bright objects HD 4539 (GALEX J0047+0958), the spectrophotometric standard Feige 66, GALEX J1421+7124, GALEX J1736+2806, and GALEX J2334+5347 using the 2 m telescope at Ondřejov Observatory. The observing configuration and procedure are described in Kawka et al. (2010). Briefly, for each star we obtained a series of spectra centred on Hα. We used the 830.77 lines mm^{-1} grating with a SITe 2030 × 800 CCD, this resulted in a spectral resolution of $R = 13\,000$. Each target exposure was immediately followed by a ThAr comparison arc.

Finally, and introducing our sixth and most recent observation programme, we obtained three high-dispersion echelle spectra of the short-period binary GALEX J2254−5515. From UT 2014 November 24 to December 4, we used the Fibre-fed Extended Range Optical Spectrograph (FEROS) attached to the 2.2 m telescope at La Silla. The spectra range from ≈3600 to ≈9200 Å at a resolution of $R \approx 48\,000$.

We supplemented our data sets with archival spectra. We extracted processed FEROS data from the ESO archive. The spectra were obtained under the programmes 076.D-0355, 077.D-0515, 078.D-0098 (PI: L. Morales-Rueda) and 086.D-0714 (PI: S. Geier).

We also extracted spectra from the Isaac Newton Group (ING) Archive. The first set of data (GALEX J1632+0759 and GALEX J1731+0647) was obtained with the Intermediate Dispersion Spectrograph (IDS) attached to the Isaac Newton Telescope (INT) on UT 2013 May 17 (run numbers 984 456 and 984 458) and on UT 2013 May 19 (run numbers 984 760, 984 762 and 984 763). The spectra were obtained with the R1200B grating which resulted in a useful range of 3900–5200 Å and a dispersion of 0.48 Å and delivering a resolution of 1.5 Å assuming a 3-pixel full width at half-maximum (FWHM). The spectra were wavelength-calibrated using CuAr and CuNe arcs and adjacent exposures were co-added to obtain the final radial velocity. A second set of data (GALEX J1632+0759) was obtained with the William Herschel Telescope (WHT) and the Intermediate dispersion Spectrograph and Imaging System (ISIS) on UT 2010 August 26 (run numbers 1483 813 and 1483 814). The spectra were obtained with the R600B and R600R gratings and calibrated with CuAr and CuNe arcs resulting in useful ranges of 3500–5100 Å and 5500–7030 Å and dispersion of 0.88 Å per binned pixel in the blue (2 × 2) and 0.49 Å pixel^{-1} in the red (binned 2 × 1), corresponding to spectral resolutions of 1.7 Å in the blue and 1.5 Å in the red assuming a 3-pixel FWHM.

On average, a high S/N was achieved with EFOSC2 on the NTT ($\overline{S/N} \approx 100$), the R–C Spectrograph on the KPNO 4 m telescope

($\overline{S/N} \approx 60$), and WiFeS on the SSO 2.3 m telescope ($\overline{S/N} \approx 80$). A lower S/N was achieved with the coudé spectrograph on the Ondřejov 2 m telescope, FEROS on the MPG 2.2 m telescope (La Silla), and the grating spectrograph on the SAAO 1.9 m telescope ($\overline{S/N} \approx 30$). The lower S/N achieved at Ondřejov and La Silla is largely compensated by the higher dispersion resulting in comparable or superior velocity accuracy (see next section). More than 70 per cent of our spectra had an S/N $\gtrsim$ 40 and spectra with ill-defined hydrogen or helium lines (S/N $\lesssim$ 15) were rejected.

2.1.1 *Tests of the wavelength and velocity scales*

We performed a series of tests of the wavelength scale of relevant spectra using the O I sky emission lines and atmospheric molecular absorption bands.

Diffuse O Iλ6300.304 emission helps set the accuracy of the wavelength scale, particularly in low- to intermediate-dispersion spectra. A strong emission line is detected in 93 per cent of all usable EFOSC2 spectra, 95 per cent of all KPNO and SSO spectra, and nearly all SAAO spectra. A short exposure time as well as the appearance of scattered moonlight usually limit the usefulness of this template. The O I velocity averaged $v(\mathrm{O\,I}) = 0.0$ km s^{-1} at KPNO with a dispersion $\sigma_v(\mathrm{O\,I}) = 2.1$ km s^{-1}, $v(\mathrm{O\,I}) = 1.9$ km s^{-1} with EFOSC2 and a dispersion $\sigma_v(\mathrm{O\,I}) = 5.4$ km s^{-1}, $v(\mathrm{O\,I}) = 3.7$ km s^{-1} at SSO and a dispersion $\sigma_v(\mathrm{O\,I}) = 7.4$ km s^{-1}, and $v(\mathrm{O\,I}) = 4.6$ km s^{-1} at SAAO and a dispersion $\sigma_v(\mathrm{O\,I}) = 4.4$ km s^{-1}. The emission line appeared blended in most spectra obtained during bright time at SSO. Based on this analysis, the expected accuracy should be of the order of 2–7 km s^{-1}. The accuracy of the wavelength scale using coudé or echelle spectrographs is normally of the order of 1 km s^{-1} or better.

Systematic velocity shifts are expected following an improper placement of the star on the slit, particularly if the stellar image is much narrower than the slit width. Excellent seeing conditions are often encountered at La Silla and KPNO. We cross-correlated telluric absorption features in the KPNO and EFOSC2 spectra with a telluric template of identical spectral resolution. We measured an average velocity of -0.8 km s^{-1} with a dispersion of 13.4 km s^{-1} in the EFOSC2 spectra and an average velocity of 2.4 km s^{-1} with a dispersion of 10.0 km s^{-1} in the KPNO spectra. Velocity deviations of up to 50 km s^{-1} were found in a few well-exposed EFOSC2 spectra. We corrected the measured stellar velocities at La Silla using the telluric template velocities.

In summary, after applying telluric corrections, we estimate that errors in stellar velocity measurements due to various systematic effects are better than $\sim$10 km s^{-1} provided that the photospheric lines are well defined. Ultimately, the accuracy of the wavelength is verifiable using actual stellar data and by plotting the velocity dispersion distribution (Section 3.1.3).

2.2 Low-dispersion spectroscopy for stellar parameter determinations

For stars not listed in Németh et al. (2012), we obtained additional low-dispersion spectra with the R–C spectrograph attached to the 4 m telescope at KPNO on UT 2013 July 12 (GALEX J1421+7124) and 2014 May 24 (GALEX J2334+5347). We used the KPC-10A grating and T2KA CCD with a dispersion of 2.77 Å pixel^{-1} in first order and centred on 5875 Å. We used the order sorting filter *WG*360 and set the slit width at 1.5 arcsec resulting in a spectral resolution of $\approx$5.5 Å. The spectra were wavelength-calibrated using the HeNeAr arc.

We extracted a set of spectra of the spectrophotometric standard Feige 66 from the ING archive. These spectra were obtained with ISIS attached to the WHT (run numbers 133198, 133200, 133201, 133223, 133226, 133227). The spectra were obtained using the *R*300*B* grating in the blue arm providing a dispersion of 1.54 Å pixel^{-1} and a spectral range from 3620 to 5190 Å. The slit width was set to 2.4 arcsec for each observation which corresponds to a resolution of $\approx$7.5 Å. The spectra were wavelength-calibrated using a CuAr arc.

Details of the low-dispersion spectroscopy obtained of other objects in the present sample are given by Vennes et al. (2011) and Németh et al. (2012).

2.3 Photometry and imaging

We compiled available optical and infrared photometric measurements and combined them with the *GALEX* NUV and FUV photometry from the all-sky imaging survey (AIS) to build an SED for each object in the sample. The ultraviolet data were collected from the site galex.stsci.edu/GalexView/. Morrissey et al. (2007) present details of the instrument calibration. Table A1 in the appendix lists the *GALEX* magnitudes, along with the available *V* magnitudes as well as 2MASS (Skrutskie et al. 2006) and *Wide-field Infrared Survey Explorer* (*WISE*; Wright et al. 2010) infrared measurements.

The PSF of *WISE* images ranges from 6 to 12 arcsec in the 3–24 μm wavelength range, while the PSF in 2MASS images is close to 2.5 arcsec. Because of its relatively broad PSF, stars located within its range and identified in higher resolution imaging are certainly contaminating the SED in the mid-IR range.

Also, we extracted photometric time series from the SuperWASP (SWASP; Pollacco et al. 2006) public archive, NSVS (Woźniak et al. 2004), All Sky Automated Survey (ASAS; Pojmanski 1997) and Catalina surveys (Drake et al. 2009). The Catalina photometry is unfiltered. Bright targets (<12 mag) are often saturated, but the photometric measurements are more precise with faint targets (>14 mag) than those obtained in the other three surveys consulted. The SWASP images are filtered (4000–7000 Å). Light-curve analysis of SWASP data is valuable because of the large number of measurements obtained for individual targets. We obtained ASAS times series in the *V* band and the NSVS images are unfiltered.

The calibrated *GALEX* magnitudes are obtained from the count rates extracted using elliptical apertures (fuv_flux_auto, nuv_flux_auto) fitted to the actual stellar profiles and converted into the AB system. The average *GALEX* PSF is matched approximately by Gaussian functions with FWHM of 5.3 and 4.2 arcsec in NUV and FUV images, respectively, and a positional accuracy of $\approx$0.5 arcsec. However, several factors affect the reliability of the *GALEX* photometric magnitudes. The *GALEX* imaging quality varies with the detector position with a strong dependency on the radial distance from the image centre. We recorded the target distance to the centre of the field of view (fov_radius), as well as the actual FWHM values in the FUV and NUV images (fuv_fwhm_world, nuv_fwhm_world) for each target. Measurements with a radial distance outside of 0.°4 combined with a large PSF (>0.″01) or measurements with an exceedingly large PSF (>0.″04) are marked in Table A1 as possibly unreliable. Finally, bright objects with unreliable non-linearity corrections outside the range of validity are marked. Non-linearity effects dominate the photometric error. A 10 per cent loss is observed at $N_{\mathrm{UV}} = 13.9$ and $F_{\mathrm{UV}} = 13.7$ so that

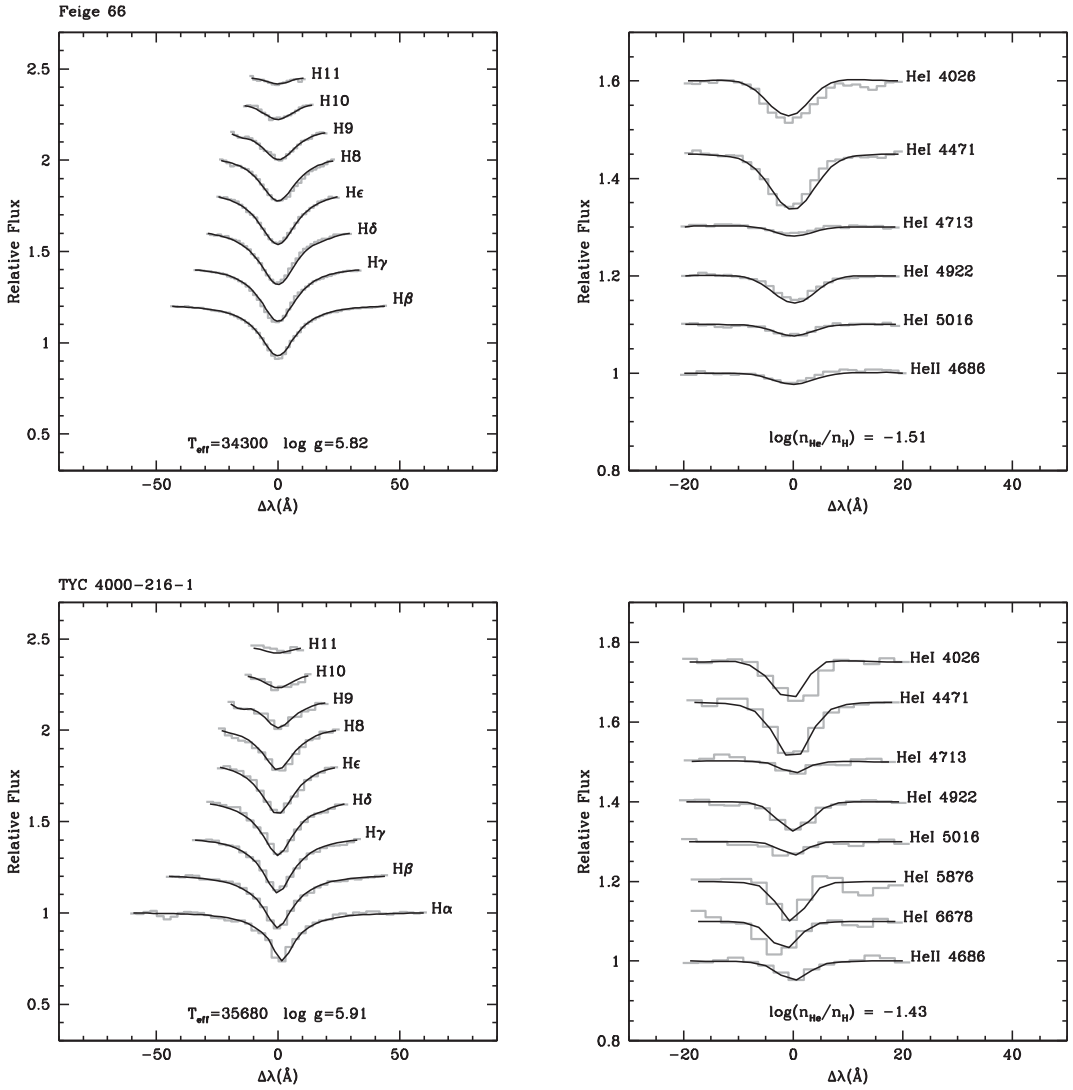

Figure 1. Line profile analysis of the WHT spectrum of Feige 66 (top) and KPNO spectrum of TYC4000-216-1 (bottom), labelled with best-fitting parameters.

most measurements in the present selection are affected. Morrissey et al. (2007) and Camarota & Holberg (2014) propose correction algorithms that are nearly identical. Camarota & Holberg (2014) presented a calibration sample sufficiently large to allow us to evaluate the scatter in the synthetic versus measured magnitude relations. For example, this scatter is of the order of 0.35 and 0.4 mag at $N_{\rm UV}$ and $F_{\rm UV} = 13$, respectively. We adopted *GALEX* magnitudes adjusted using the correction algorithm of Camarota & Holberg (2014) with errors estimated using the scatter in these corrections for a given magnitude.

The EFOSC2 acquisition images provide a deep, high-spatial resolution view of the fields surrounding target stars. These images were obtained with the Loral/Lesser 2048×2048 CCD. With a focal plane scale of 8.6 arcsec mm^{-1} and a pixel size of 15 μm, the sky images are sampled with a pixel size of 0.129 × 0.129 arcsec^2, or, after binning 2 × 2, a pixel size of 0.258 × 0.258 arcsec^2. The images allow for the identification of physical companions or unrelated, nearby stars.

Figs A1–A3 in the appendix compare all available photometry to synthetic spectra computed using stellar parameters listed in Table 1.

3 ANALYSIS

We present, in order, the properties of the sample including an overview of the stellar parameters ($T_{\rm eff}$, $\log g$, $\log$ He/H) and evolutionary history, the characteristics of the SEDs and photometric time series, and the radial velocity data set. We identify new binary candidates and present an analysis of individual binary properties from the combined data sets.

3.1 Sample properties

Table 1 lists the atmospheric parameters obtained from Németh et al. (2012). The Balmer line analysis for three additional objects (Feige 66, GALEX J1421+7124 and GALEX J2334+5347) is based on the model grids of Vennes et al. (2011). Best-fitting parameters ($T_{\rm eff}$, $\log g$, $\log$ He/H) are obtained using χ^2 minimization techniques with the observed line profiles (He I,II and H I) being simultaneously adjusted to interpolated spectra from the model grid. Examples of Balmer and helium line analyses are shown in Fig. 1.

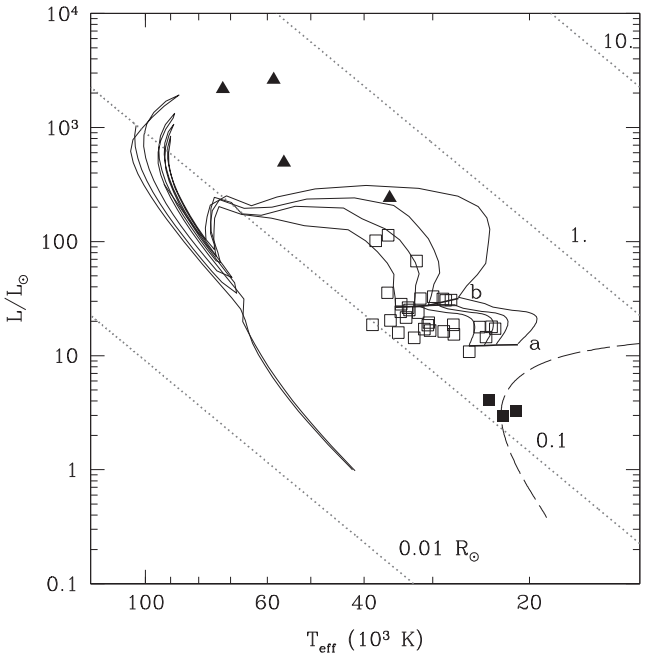

Figure 2. Physical properties, luminosity versus effective temperature, of the sample: sdO stars are shown with full triangles while sdB stars are shown with open squares (assuming 0.47 $M_\odot$) or full squares (assuming 0.234 $M_\odot$). The zero-age EHB is labelled 'a' while the terminal-age EHB is labelled 'b'. Evolutionary tracks computed by Dorman et al. (1993) with a helium core mass of 0.469 $M_\odot$ and hydrogen envelopes of, left to right, 0.002, 0.004, 0.006, and 0.01 $M_\odot$ are shown with full lines. The cooling track from Driebe et al. (1998) for progenitors of ELM white dwarfs of 0.234 $M_\odot$ is shown prior to hydrogen shell flashes with a dashed line. Lines of constant radii at 0.01, 0.1, 1, and 10 $R_\odot$ are labelled accordingly.

Fig. 2 shows properties of the sample presently investigated. Using the effective temperature ($T_{\rm eff}$) and surface gravity (g), we determined the total luminosity (in $L_\odot$) by adopting for most objects a sample-average mass of 0.47 $M_\odot$ (Fontaine et al. 2012),

$$L = 4\pi R^2 \sigma T_{\rm eff}^4,$$

where σ is the Stefan–Boltzmann constant and the radius (R) is calculated using

$$R = \sqrt{\frac{GM}{g}},$$

where M is the subdwarf mass and G is the gravitational constant.

The sdB stars form a sequence of approximately constant luminosity, $L = 10$–$30\ L_\odot$ or $M_V = 4.3$ ($\sigma = 0.9$) mag, and located between the ZAEHB and the TAEHB while a few ageing sdB stars and all He-rich sdO stars set out on a higher luminosity excursion beyond the stable He-burning stage. The objects lying below the ZAEHB ($L < 10\ L_\odot$) with a low temperature and a high gravity, GALEX J0805−1058 and, tentatively, J1411+7037 and J2153−7004, were singled-out and were attributed a mass of 0.23 $M_\odot$ based on their likely evolutionary status (Driebe et al. 1998). Most objects lie to the left of the EHB tracks suggesting that their hydrogen layer is thinner than 0.002 $M_\odot$, or, possibly, that their surface gravity is overestimated. To investigate the latter possibility, we compared the results of a model atmosphere analysis using the hydrogen Stark broadening tables of Lemke (1997), employed in this work, to those of Tremblay & Bergeron (2009), which include improved treatment of merging atomic energy levels. We found that improvements in Stark broadening theory may account for a shift of $\Delta\log g = +0.08$ dex near 30 000 K (see e.g. Østensen et al. 2014; Telting et al. 2014b) in agreement with a shift of $\Delta\log g = +0.06$ dex found at 40 000 K by Klepp & Rauch (2011). These systematic shifts are notable, but still cannot explain the model offsets apparent in Fig. 2. Metallicity has little effect on temperature and gravity below $T_{\rm eff}$=35 000 K as demonstrated by Latour et al. (2014). It is worth noting that, while an sdB mass of 0.47 $M_\odot$ may be typical, it does not necessarily apply to all objects (e.g. ELM progenitors).

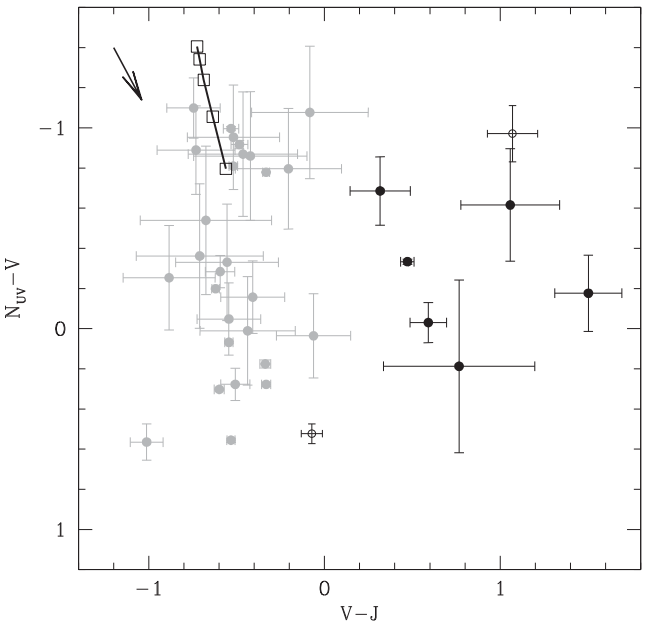

Figure 3. NUV − V versus $V - J$ colour–colour diagram. Stars with a composite IR excess are shown with full black circles and stars with an IR excess due to a nearby star are shown with open circles (see Section 3.1.1), while all others are shown in grey. Models at 24, 28, 32, 36, and 40 × 10^3 K ($\log g = 5.7$, $\log {\rm He/H} = -2.5$) are shown, from bottom to top, with open squares linked by a full line. The effect of interstellar extinction ($E_{B-V} = 0.05$) on the colours is shown with an arrow in the upper-left corner.

On the other hand, Schindler, Green & Arnett (2014) pointed out that current evolutionary models fail to reproduce some observed properties of EHB stars, such as the core mass derived from asteroseismology, and concluded that evolutionary models must be updated to match observed seismic and spectroscopic stellar parameters. Schindler et al. (2014) found that very high convective overshooting would be needed to reproduce the seismic core mass but that it would, quite improbably, double the EHB lifetime. Therefore, they conclude that the general treatment of convection in evolutionary models needs updating, and that new opacity tables and diffusion calculations are required.

3.1.1 Overview of the SEDs

Fig. 3 shows the NUV − V versus $V - J$ colour diagram for the sample of hot subdwarfs listed in Table A1. Figs 4 and 5 present the $V - J$ versus $J - H$ and $J - H$ versus $H - W1$ diagrams, respectively. The effect of interstellar extinction is evident in the NUV − V colour of some objects, but many are also affected by large systematic errors in the *GALEX* NUV photometry (non-linearity). For example, a larger extinction than observed in the interstellar line of sight is apparent towards GALEX J1632+0759. The

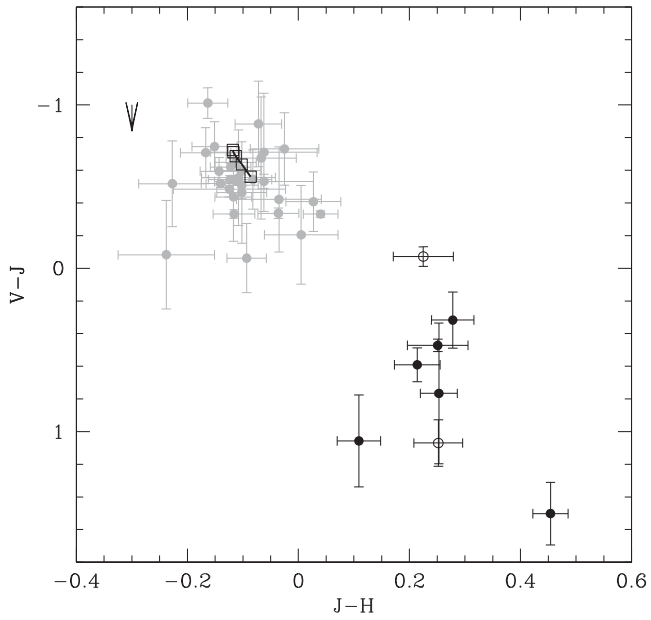

Figure 4. Same as Fig. 3 but showing $V - J$ versus $J - H$.

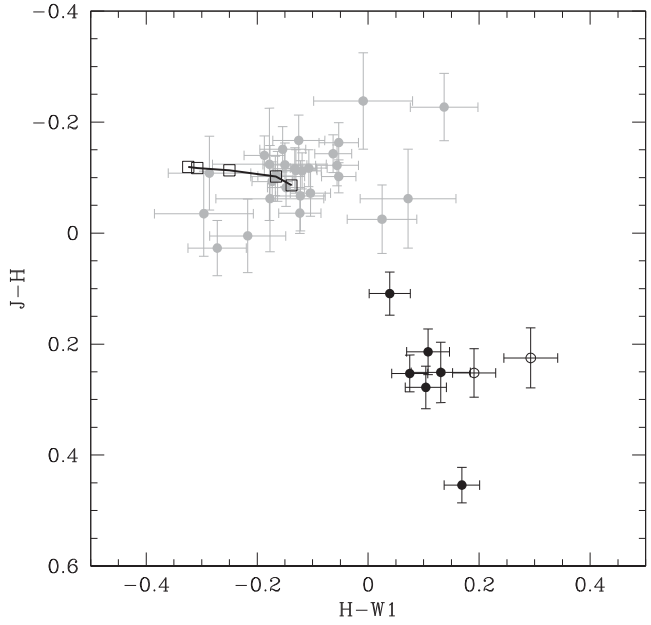

Figure 5. Same as Fig. 3 but showing $J - H$ versus $H - W1$.

International Ultraviolet Explorer (*IUE*) spectra that supplement uncertain *GALEX* photometric measurements indicate $E_{B-V} = 0.4$, largely in excess of that found in the extinction map of Schlegel, Finkbeiner & Davis (1998), $E_{B-V} = 0.08$. The effect on ultraviolet colours of an extinction coefficient $E_{B-V} = 0.05$ (see Fig. 3) is relatively modest, but coefficients in excess of 0.4 would displace colours from the upper left to the reddened, lower right corner in the vicinity of composite stars.

Individual SEDs may be contaminated by the presence of a nearby star, either physically associated or unrelated to the hot subdwarf. Inspection of the P82, P83, P85 and P89 EFOSC2 acquisition images obtained by Vennes et al. (2011) and Németh et al. (2012) revealed the presence of nearby companions (<3 arcsec) to J0047+0337, J0657−7324, and J1632+0759 (see below). Visual inspections of the guiding images displayed at KPNO did not reveal the presence of a nearby companion to any other objects. An inspection of photographic plate material (http://surveys.roe.ac.uk/ssa/index.html) helps locate other, more distant objects (>3 arcsec) that may contaminate photometric measurements with large PSF (e.g. *WISE*). For example, GALEX J0751+0925 is accompanied by a faint (Δm ∼5 mag), nearby star ∼6 arcsec away at a position angle of 200° (Epoch = 1993).

The composite nature of the spectra of GALEX J0047+0337, J1411+7037, J1736+2806, J1753−5007, J2038−2657 (Németh et al. 2012) are confirmed by their IR photometric colours. The flux contributions in the V band for these hot subdwarfs are offset by ∼0.7 (possibly contaminated), ∼0.0 (weak secondary detection in the optical), ∼1.2, ∼1.3, and ∼1.3 mag, respectively, relative to their observed composite V magnitudes. Although evident in the IR colours of GALEX J1356−4934 (Fig. A2), the presence of a companion was not detected by Németh et al. (2012). The flux contribution from the hot subdwarf in the V band is offset by ∼0.4 mag relative to the observed composite V magnitude. We re-examined the spectra of GALEX J1356−4934 and we found weak signatures of a cool main-sequence companion in the blue spectrum used by Németh et al. (2012), and stronger spectral lines representative of a cool main-sequence star in the red spectra used in this paper. We present our spectral decomposition of this system in Section 3.2.2. The IR colours for GALEX J0047+0337, J0657−7324, and J1632+0759 are almost certainly contaminated by their nearby, resolved companions.

3.1.2 Overview of the photometric time series

Table 2 summarizes the photometric time series analyses. We included objects showing significant radial velocity variations (e.g. GALEX J2205−3141), objects with composite optical spectra (e.g. GALEX J1736+2806), and, finally, three objects with previously published analyses from the present survey: GALEX J0321+4727 and GALEX J2349+3844 (Kawka et al. 2010), and GALEX J1411−3053 (Vennes et al. 2012). Photometric variations observed in the sdB plus white dwarf system GALEX J1411−3053 are an example of ellipsoidal variations in this class of objects. Fourier transform calculations of available light curves (Section 2.3) uncovered three objects with significant periodic variations. The light curves were analysed using fast Fourier transform analysis from Press et al. (1992). Both GALEX J1736+2806 and GALEX J2038−2657 are binaries comprising a hot subdwarf with a more luminous optical companion, while GALEX J2205−3141 is composed of a hot subdwarf and late-type companion. The photometric variations in the latter are clearly timed with the orbital period (see Section 3.2) and caused by reflection of the primary on the cool secondary. Variations in GALEX J1736+2806 and GALEX J2038−2657 may be caused by a spot on the surface of the secondary coupled to the rotation period. The variable, double-peaked Hα line profile of GALEX J2038−2657 also implies the presence of surface inhomogeneities (see Section 3.2.4).

An analysis of time series helps constrain the nature of the companion (Maxted et al. 2002). For example, a simple geometric model suggests that the presence of a late-type companion generally leads to detectable photometric variations phased on the orbital period. This reflection effect scales as R_2^2, where R_2 is the secondary radius, but only as $a^{-1/2}$, where a is the orbital separation

Table 2. Photometric time series.

Name	Survey	HJD range (2450000+)	Number	Period range (d)	Semi-amplitude (mmag)	Average magnitude (mag)	Standard deviation (mmag)
J0047+0337	ASAS	1868–5168	378	>0.02	4.4 ± 7.0	12.336	94.5
	NSVS	1382–1549	177	>0.01	17.8 ± 3.4	12.676	32.2
J0321+4727	NSVS	1373–1630	173	0.265 86[a]	61.3 ± 3.9	12.034	56.9
	SWASP	3196–4458	4575	0.265 86[a]	43.5 ± 1.0	11.490	49.4
J0401−3223	SWASP	3964–4485	14 208	>0.01	8.4 ± 0.1	11.268	12.4
				1.857 35[b]	0.8 ± 0.1		
J0507+0348	Catalina	3643–6592	347	>0.02	14.4 ± 1.8	14.172	23.8
				0.528 13[a]	2.1 ± 1.8		
J0613+3420	SWASP	3232–4573	4700	>0.03	12.7 ± 2.2	13.958	106.4
J0751+0925	ASAS	2623–5131	198	>0.1	80.3 ± 20.3	14.126	205.9
				0.178 32[a]	43.5 ± 20.8		
	Catalina	3466–6368	119	>0.1	12.0 ± 3.2	14.168	18.7
				0.178 32[a]	3.6 ± 3.0		
J0805−1058	ASAS	1868–5168	570	>0.1	19.9 ± 3.8	12.270	65.6
				0.173 70[a]	11.7 ± 4.8		
	NSVS	1488–1630	132	>0.01	33.0 ± 7.4	12.812	59.8
				0.173 70[a]	10.9 ± 7.2		
J1356−4934	ASAS	1900–5088	729	>0.04	3.3 ± 3.9	12.269	74.2
J1411−3053	ASAS	1902–5088	1060	0.024 49[c]	46.8 ± 3.8	12.342	88.2
	SWASP	3860–4614	13 079	0.024 49[c]	51.2 ± 2.0	12.723	165.6
J1632+0759	ASAS	2175–5106	399	>0.1	23.9 ± 5.1	12.763	74.5
				2.9515[a]	3.9 ± 5.2		
	Catalina	3466–6471	338	>0.02	49.8 ± 8.4	12.587	121.6
				2.9515[a]	7.5 ± 9.5		
	NSVS	1275–1417	115	>0.01	37.6 ± 8.6	13.248	69.3
				2.9515[a]	17.9 ± 8.9		
J1731+0647	ASAS	2727–5009	73	>0.1	98.7 ± 49.6	13.799	299.1
				1.173 34[a]	44.5 ± 51.5		
	Catalina	3466–6457	105	>0.1	74.9 ± 4.7	13.825	67.0
				1.173 34[a]	21.4 ± 9.2		
J1736+2806	SWASP	3128–4325	9140	1.333 20[d]	10.2 ± 0.2	11.639	17.0
J1753−5007	ASAS	1947–5137	544	>0.1	18.6 ± 5.7	12.955	94.2
J1903−3528	SWASP	3860–4551	7388	>0.01	3.6 ± 0.6	13.089	35.2
J2038−2657	NSVS	1348–1483	42	1.860[d]	56.4 ± 8.4	11.950	51.1
	SWASP	3958–4614	8332	1.870 22[d]	12.9 ± 0.4	11.856	28.2
J2205−3141	ASAS	1873–5166	521	0.341 56[d]	40.0 ± 5.0	12.381	81.4
	Catalina	3598–6217	252	0.341 56[d]	46.2 ± 6.2	12.07	64.4
	SWASP	3862–4614	22 731	0.341 56[d]	26.7 ± 1.0	12.409	110.1
J2254−5515	ASAS	1869–5168	672	>0.02	20.0 ± 3.8	12.113	70.9
				1.227 02[a]	4.7 ± 3.9		
	Catalina	3580–6076	78	>0.1	98.4 ± 16.8	12.442	103.1
				1.227 02[a]	28.1 ± 15.3		
J2349+3844	NSVS	1321–1579	261	>0.1	19.9 ± 3.9	12.287	44.7
				0.462 52[a]	5.0 ± 3.9		
	SWASP	3154–4669	12 175	>0.01	1.7 ± 0.2	11.640	15.6
				0.462 52[a]	1.1 ± 0.2		

[a]Spectroscopic period.
[b]Possible spectroscopic period.
[c]Ellipsoidal variations at half-spectroscopic period.
[d]Photometric period.

(Maxted et al. 2002). Interestingly, an application of these simple relations confirms the results of detailed light-curve modelling and most importantly that, for a given mass function, the effect of a lower binary inclination, which reduces the light contrast between inferior and superior conjunctions as well as its intensity through increased binary separation, is compensated by the increased mass and radius of the secondary calculated using the mass function, hence increasing the fraction of intercepted light. Following Maxted et al. (2002) and adding a slight modification to account for the effect of inclination on the visibility of the exposed hemisphere at inferior and superior conjunctions, the amplitude of the variations is given by

$$\delta m = 2.5 \log \left(\frac{f^+}{f^-} \right),$$

where

$$f^{\pm} = 1 + \left(\frac{R_2}{R_1} \right)^2 \left(\frac{R_1}{\sqrt{2}\, a} \right)^{1/2} \frac{1 \pm \sin i}{2},$$

where f^+ is the relative flux at superior conjunction, f^- is at inferior conjunction, i is the binary inclination and R_1 is the primary radius estimated from the measured surface gravity and assumed mass (0.23 or 0.47 $M_\odot$). The mass of the putative late-type secondary was estimated using the binary mass function, the assumed primary mass and by varying the inclination angle. The radius is then estimated following the mass-radius relation for late-type stars of Caillault & Patterson (1990). Applications of this approximate formula for δm lead to an overestimation of the amplitude of a factor of ≈3 when applied to the well-known case of GALEX J0321+4727 (Table 2). The semi-amplitude of the phased light curve of GALEX J0321+4727 reaches 44 and 61 mmag in the SWASP and NSVS data sets, respectively, and reveals the presence of an irradiated late-type companion. This simple model also shows that the amplitude of the variations is more or less constant (±30 per cent) when varying the inclination as shown in the detailed models of Maxted et al. (2002). Applying a factor of 0.3 to the amplitude calculated with the simple formula for δm presented above should allow us to confirm or rule out the presence of a late-type companion in the new binaries. For example, the companion to GALEX J2349+3844 (Kawka et al. 2010) is almost certainly a white dwarf. The predicted semi-amplitude of variations due to a late-type companion is ≈70 mmag, while the observed variations are less than 1 and 5 mmag in the SWASP and NSVS phased light curves, respectively (Table 2). Based on this insight, the photometric times series will help constrain in the following Sections the nature of the companion in the new binaries.

3.1.3 Overview of the radial velocity data set

We measured the radial velocities by fitting a Gaussian function to the deep and narrow Hα core for most red spectra, or He Iλ 6678.15 in a few instances described below. In the blue we used the Hβ core, He IIλ4685.698, or He Iλ4471.48 if necessary (see below). All measured velocities are heliocentric corrected and tabulated in Table B1 in Appendix B. For each target, Table B1 also includes the number of spectra, the average velocity ($\bar{v}$) and velocity dispersion (σ_v).

Fig. 6 shows the distribution of the measured velocity dispersion. The sample includes three objects published earlier (Kawka et al. 2010; Vennes et al. 2012) and seven new identifications described in the following section. Three additional objects show significant radial velocity variations ($\sigma_v > 10$ km s^{-1}), but with insufficient sampling to determine the orbital parameters. Adding two likely close binaries identified through photometric variations (GALEX J1736+2806 and J2038−2657, see Section 3.1.2) but for which we only dispose of radial velocity measurements of the secondary, we estimate that 15 out of 41 hot subdwarfs presently investigated are in close binaries, or a 37 per cent yield, lower than previously estimated (e.g. Copperwheat et al. 2011). Our survey strategy aimed at short-period binaries would be insensitive to long-period, low-amplitude variation (<10 km s^{-1}) systems. A detailed comparison with the sample of known hot subdwarf binaries should allow us to secure a global estimate of binarity in this population (Section 4.1).

3.2 Individual properties

Section 3.2.1 describes objects with variable radial velocities suggesting the presence of a close binary companion. Figs 7–13 show results of the period analysis ($1/\chi^2$ versus frequency) for this group of objects. The confidence level is set at 1σ (66 per cent) for a four-parameter ($p = 4$) analysis with the χ^2 normalized on the best-fitting solution and the radial velocity measurements phased on the best-fitting period. Sections 3.2.2, 3.2.3, and 3.2.4 review the properties of the remaining systems, i.e. those with composite spectra, unresolved radial velocity variations, or photometric

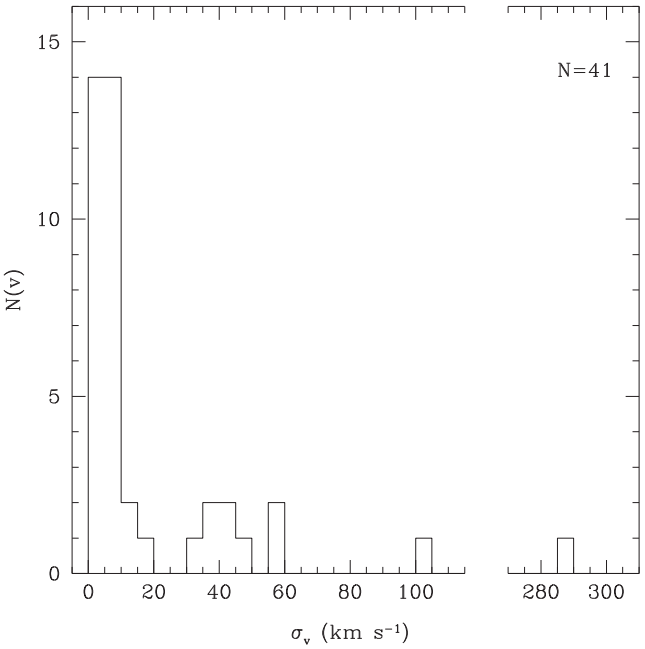

Figure 6. Number of objects per velocity dispersion bin (width = 5 km s^{-1}). The sample includes data from Table B1 in Appendix B and published results from the same survey (Kawka et al. 2010; Vennes et al. 2012).

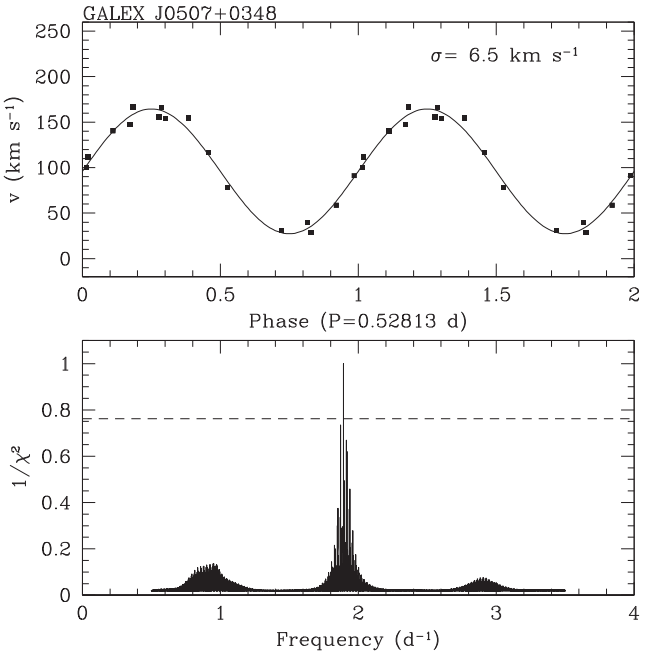

Figure 7. (Bottom) period analysis of radial velocity measurements of GALEX J0507+0348 (full line) and 66 per cent confidence level (dashed line). (Top) radial velocity measurements phased on the orbital period (0.52813 d) and best-fitting sine curve (full line) with the dispersion in velocity residuals shown in upper-right. The initial epoch T_0 corresponds to inferior conjunction of the sdB star. Details are presented in Section 3.2.1.

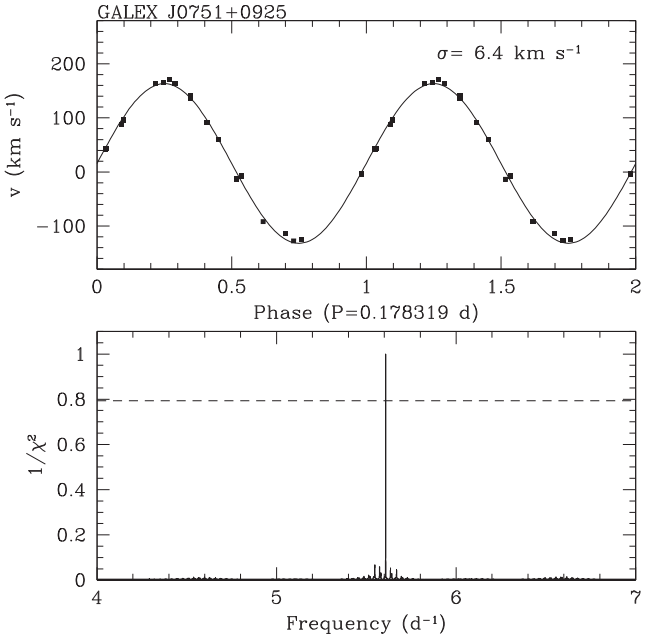

Figure 8. Same as Fig. 7 but for GALEX J0751+0925.

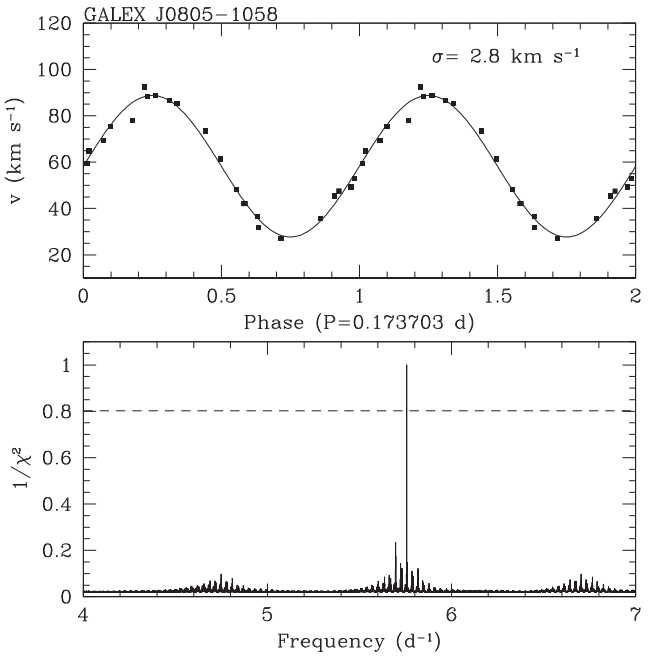

Figure 9. Same as Fig. 7 but for GALEX J0805−1058.

variability, respectively, and the likelihood that they might belong to the close binary population. Finally, Section 3.3 presents known facts concerning the remaining objects. In the following section, the subscript '1' refers to the hot subdwarf and the subscript '2' refers to its companion. Similarly, the suffix 'B' designates the companion. The binary parameters are listed in Table 3 including the number of spectra per object (N) and the dispersion in velocity residuals (σ_{vr}).

3.2.1 Close binaries

The sdB star GALEX J0507+0348 is part of a newly identified spectroscopic binary. The star is close to the ZAEHB and may

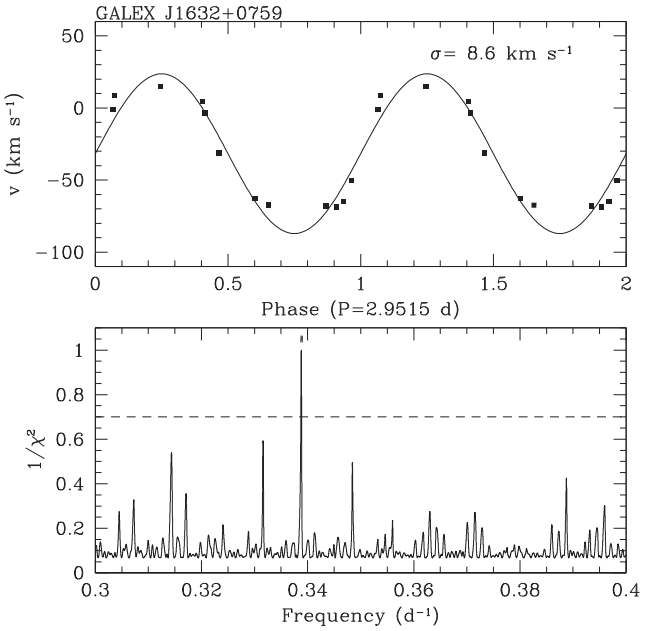

Figure 10. Same as Fig. 7 but for GALEX J1632+0759. The tick mark above the best-fitting period indicates the results of the period analysis of Barlow et al. (2014), $P = 2.951 \pm 0.001$ d.

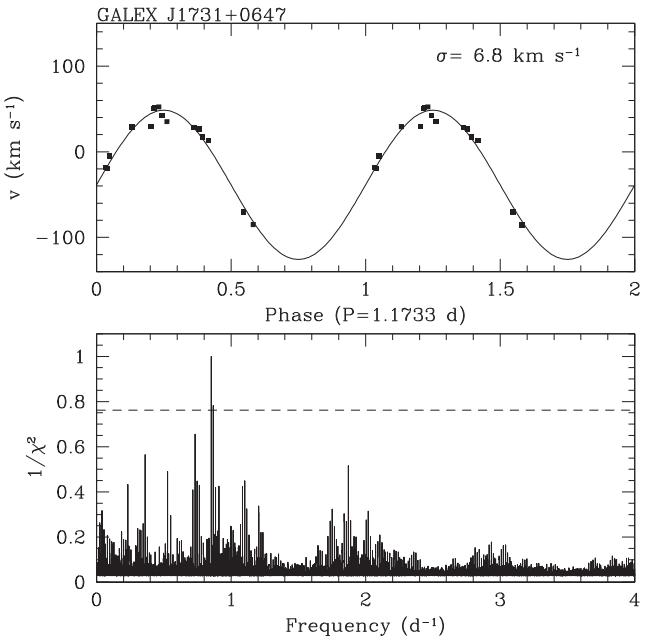

Figure 11. Same as Fig. 7 but for GALEX J1731+0647.

be a low-mass sdB star. The Hα radial velocity measurements are phased on a period of ∼0.528 d (Fig. 7). The SED of GALEX J0507+0348 shows an infrared excess but in the *WISE W3* band only. The nearby object (*sep.* = 17 arcsec) visible on photographic plates is not likely to affect the *WISE* measurements. Also, low-dispersion spectra show weak CaH&K lines with an equivalent width of EW(CaK) = 270 mÅ. The calcium doublet could indicate the presence of a late-type companion. However, no radial velocity measurements were obtained in that spectral region and we could not confirm variations in the line position. Moreover, we could not confirm the presence of other late-type spectral signatures such

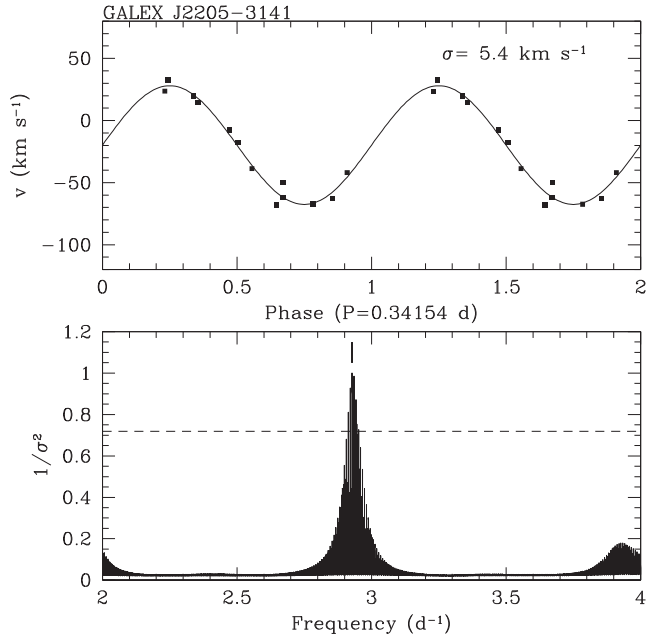

Figure 12. Same as Fig. 7 but for GALEX J2205−3141. The photometric period is marked close to the peak frequency of the velocity periodogram.

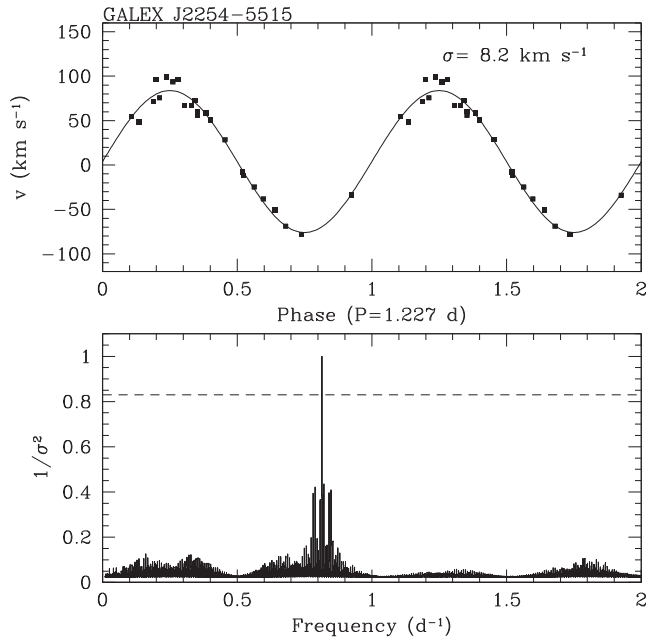

Figure 13. Same as Fig. 7 but for GALEX J2254−5515.

as Mg I lines, and our composite spectral analysis (Németh et al. 2012) rejects the presence of a companion with a flux contribution above 1 per cent in the optical range. A series of high-dispersion spectra is required to determine whether the CaH&K lines originate from the companion, the interstellar medium (ISM), or in the circumstellar environment. The mass function allows us to infer $M_2 > 0.20\,M_\odot$ assuming $M_1 = 0.47\,M_\odot$, or $M_2 > 0.15\,M_\odot$ assuming $M_1 = 0.30\,M_\odot$. A late-type (dM, dK) companion would satisfy these constraints. However, the Catalina time series folded on the orbital period constrains the photometric variations to a semi-amplitude lower than 2 mmag. Reflection effect on a late-type star with a mass exceeding $0.2\,M_\odot$ would result in variations of a semi-amplitude of ≈60 mmag as observed in the case of GALEX J0321+4727 (Kawka et al. 2010). We conclude that the companion is most likely a white dwarf. At a binary inclination $i < 30^\circ$, the mass function implies a minimum mass of $0.51\,M_\odot$ that would be consistent with a normal white dwarf star.

The sdB star GALEX J0751+0925 is part of a close binary with the largest velocity semi-amplitude measured in the present sample, $K \sim 148$ km s^{-1} (Fig. 8). The mass function implies the presence of a companion relatively more massive than in other similar systems with $M_2 > 0.34\,M_\odot$ assuming $M_1 = 0.47\,M_\odot$. The SED of this system also appears to show an infrared excess in the *W*1, *W*2, and *W*3 bands which may be caused, in part, by a nearby star only 6 arcsec away (particularly in the *W*3 band). The Catalina and ASAS light curves do not show significant variations at the orbital period. Again, a comparison with the photometrically variable system GALEX J0321+4727 indicates that the companion is probably a white dwarf. The semi-amplitude of the phased light curve of GALEX J0751+0925 is limited to 4 mmag in the Catalina observations although the minimum secondary mass in this shorter period system is larger than in GALEX J0321+4727, i.e. 0.34 versus $0.13\,M_\odot$, and the predicted semi-amplitude of variations due to a late-type companion would be ≈190 mmag. Therefore, the absence of a reflection effect in GALEX J0751+0925 rules out the presence of a late-type companion leaving only the possibility of a $>0.34\,M_\odot$ white dwarf companion, or $>0.50\,M_\odot$ if $i < 50^\circ$.

The sdB GALEX J0805−1058 clearly lies below the ZAEHB (Fig. 2); following the evolutionary tracks of Driebe et al. (1998) the mass of the subdwarf is estimated to be in the range 0.2–0.3 $M_\odot$. The low-velocity amplitude (Fig. 9) and small mass function imply a very low mass for the companion, $M_2 > 0.03\,M_\odot$, assuming $M_1 = 0.234\,M_\odot$. At inclinations higher than $i = 26^\circ$, the secondary mass remains lower than $0.08\,M_\odot$ and the object is substellar. Assuming a probability distribution for the inclination angle i of the form $P_i\,\mathrm{d}i = \sin i\,\mathrm{d}i$, inclinations higher than 26° have $P(>26) = 89.9$ per cent probability of occurring. At lower inclinations ($10^\circ < i < 26^\circ$, i.e. $P(10\text{–}26) = 8.6$ per cent), the secondary mass does not exceed $0.3\,M_\odot$ and the object would be a low-mass M dwarf. At very low inclinations ($i < 7^\circ$, i.e. $P(<7) = 0.7$ per cent), the secondary would be a normal white dwarf star ($M > 0.5\,M_\odot$). The SED shows a single, hot subdwarf star, i.e. as far as the *WISE* *W*2 band, and the faint ($\Delta m \sim 6$ mag), nearby (*sep.* ∼11 arcsec) object visible in photographic plates does not appear to contaminate the SED. The ASAS and NSVS light curves do not show significant variations when folded on the orbital period, i.e. $\lesssim$12 mmag, while the predicted semi-amplitude of variations due to a substellar object ($R_2 \approx 0.1\,R_\odot$, see a review by Chabrier et al. 2009) would be ≈20 mmag. Variations of the order of 10 mmag have been observed in brown dwarf plus hot subdwarf binaries (see e.g. Schaffenroth et al. 2014c) and such variations would be detectable in GALEX J0805−1058 in quality photometric time series. We conclude that the apparent lack of variations is a consequence of the small radius of a substellar secondary.

Barlow et al. (2012) recorded radial velocity variations in spectra of the sdB star GALEX J1632+0759. Their data suggested a period ranging from 2 to 11 d. Our measurements, based on Hα and He I 5875.621 in the red, and Hβ and He I 4685.698 in the blue, also revealed large velocity variations (Fig. 10). Recently, Barlow et al. (2014) obtained new radial velocity measurements and determined a period of 2.951 ± 0.001 d. We restricted our period analysis to frequencies between 0.3 and 0.4 d^{-1} and recovered an identical period. The mass function implies a secondary mass $M_2 > 0.31\,M_\odot$, assuming $M_1 = 0.47\,M_\odot$. The SED shows a large flux excess

Table 3. Spectroscopic binary parameters.

Parameter	J0507+0348	J0751+0925	J0805−1058	J1632+0759	J1731+0647	J2205−3141	J2254−5515
P (d)	0.528127	0.178319	0.173703	2.9515[a]	1.17334	0.341543	1.22702
σ_P (d)	0.000013	0.000005	0.000002	0.0006	0.00004	0.000008	0.00005
T_0 (HJD)	2456315.349	2455972.827	2456299.0335	2456150.701	2456313.119	2456313.3387	2456444.616
σ (T_0)	0.015	0.001	0.0026	0.016	0.004	0.0005	0.001
K (km s^{-1})	68.2 ± 2.5	147.7 ± 2.2	29.2 ± 1.3	54.9 ± 4.6	87.7 ± 4.1	47.8 ± 2.2	79.7 ± 2.6
γ (km s^{-1})	96.2 ± 1.8	15.5 ± 1.6	58.2 ± 0.9	-31.6 ± 2.7	-39.1 ± 3.0	-19.4 ± 1.7	4.2 ± 2.0
$f_{\rm sec}$ (M$_\odot$)	0.017 ± 0.002	0.059 ± 0.003	$(4.4 \pm 0.6) \times 10^{-4}$	0.048 ± 0.013	0.080 ± 0.012	0.0037 ± 0.0005	0.063 ± 0.006
M_1 (M$_\odot$)	(0.47)	(0.47)	(0.234)	(0.47)	(0.47)	(0.47)	(0.47)
M_2 (M$_\odot$)	>0.20	>0.34	>0.03	>0.31	>0.39	>0.11	>0.35
N	16	19	23	12	16	13	24
σ_v (km s^{-1})	6.5	6.4	2.8	8.6	6.8	5.4	8.2
Notes	probable WD secondary	probable WD secondary	low-mass sdB, possible BD secondary	probable WD secondary	probable WD secondary	reflection, dM secondary	probable WD secondary

[a]Based in part on the period obtained by Barlow et al. (2014): $P = 2.951 \pm 0.001$ d.

apparent in the 2MASS and *WISE* bands as well as heavy extinction in the ultraviolet range. The measured extinction coefficient ($E_{B-V} = 0.4$) largely exceeds the coefficient inferred from the maps of Schlegel et al. (1998), $E_{B-V} = 0.08$. The additional extinction probably originates in the immediate, possibly dusty, circumstellar environment of the system. An inspection of our acquisition images of GALEX J1632+0759 reveals the presence of a nearby star; we measured a separation of 2.3 arcsec at a position angle of 225°. The 2MASS and *WISE* photometric measurements are likely contaminated by this object. Østensen, Heber & Maxted (2005) also resolved GALEX J1632+0759 and the nearby star and measured a separation of 2.1 arcsec. In addition to GALEX J1632+0759, Barlow et al. (2014) obtained radial velocity measurements of the nearby star which they classified as a late G dwarf or early K dwarf that is itself in a close binary. The radial velocity varied with a period of 1.42 ± 0.01 d. Barlow et al. (2014) also found that the systems share the same systemic velocity suggesting that this is a quadruple system. The ASAS, Catalina, and NSVS time series constrain photometric variations to semi-amplitudes lower than 4, 8, and 18 mmag. The predicted semi-amplitude of photometric variations due to the presence of a late-type companion would be ≈60 mmag. We conclude that the secondary star is most probably a white dwarf with a mass ranging from 1.3 to 0.5 M$_\odot$ assuming a low inclination ($24 \lesssim i \lesssim 46°$), or with a peculiar low mass (0.3–0.5 M$_\odot$) assuming $i \gtrsim 46°$.

The new binary system GALEX J1731+0647 (Fig. 11) harbours the heaviest binary companion identified in our sample. The mass function implies a mass $M_2 > 0.39$ M$_\odot$, assuming $M_1 = 0.47$ M$_\odot$. The field surrounding this subdwarf is relatively crowded but only two objects are found between 13 and 15 arcsec away and with photographic magnitude differentials $\Delta m \sim 3$ and 5 mag. These objects would not affect the SED which shows a single hot subdwarf. The lack of photometric variations, <45 mmag in ASAS time series and <21 mmag in Catalina time series, compared to expected variations of ≈90 mmag due to a relatively large M or K dwarf suggests that the companion is most likely a white dwarf. We infer a mass between 1.3 and 0.5 M$_\odot$ assuming an inclination of $29 \lesssim i \lesssim 58°$, or a peculiar low mass (0.4–0.5 M$_\odot$) assuming $i \gtrsim 58°$.

GALEX J2205−3141 is a close binary with $P \approx 0.34$ d (Fig. 12) showing a reflection effect in the SWASP time series (semi-amplitude $\Delta m \approx 27$ mmag). Similar variations were also observed in the ASAS and Catalina time series. The mass function is consistent with the presence of a late-type companion ($M_2 > 0.11$ M$_\odot$). Photometric time series from the Catalina survey, SWASP (1SWASP J220551.98−314103.9), and ASAS show variability with mutually consistent periods of 0.341 559 ± 0.000 003, 0.341 563 ± 0.000 002, and 0.341 561 ± 0.000 002 d, respectively. The photometric periods are somewhat longer than the spectroscopic orbital period $P = 0.341\,543 \pm 0.000\,008$ d. The radial velocity measurements are based on the He I 4471.48 and 6678.15 lines. We noted that the Balmer Hα and Hβ lines cores are asymmetric and are possibly contaminated by emission from the companion as noted in the case of AA Dor (Vučković et al. 2008). Fig. 14 shows the SWASP measurements phased on the photometric period. We identify the initial epoch with the passage of the secondary star at superior conjunction corresponding to maximum reflected light. Although the photometric variations are clearly caused by the reflection of the primary light on a late-type dwarf companion, the phasing error between photometric and spectroscopic ephemeris is $\Delta\Phi \approx 0.1$. We attribute this error to a large gap between the epoch of the spectroscopic observations and that of the photometric observations. The SED shows a mild flux excess in the IR to mid-IR range possibly due to the late-type companion. A star found 9 arcsec away and 4 mag fainter does not affect the SED. However, renormalizing on the *J* band rather than the *V* band nearly eradicates this excess. Assuming a possible *K*-band contribution from the companion of 15–40 per cent, we estimated for the M dwarf companion $M_{K,2} \approx 7.5$–6.5 if $M_{K,1} \approx 5.5$. Bearing in mind that reprocessing of ultraviolet radiation from the hot primary into the cool secondary atmosphere should contribute to this IR excess, the absolute *K* magnitude of the secondary star corresponds to a spectral type later than M3–4, or a mass $M_2 \lesssim 0.24$–0.4 M$_\odot$ which requires an orbital inclination $i \gtrsim 20$–30°. We find possible evidence of extinction in the ultraviolet range in excess of the extinction expected from the Schlegel et al. (1998) map, although the *GALEX* NUV dip may be the result of larger uncertainties than estimated. This system is the only confirmed binary in our sample comprised of a hot subdwarf and late-type companion.

The sdB GALEX J2254−5515 shows large radial velocity variations (Fig. 13) although the Catalina and ASAS time series indicate that the star is not photometrically variable with semi-amplitudes lower than 28 and 5 mmag, respectively. The minimum mass of

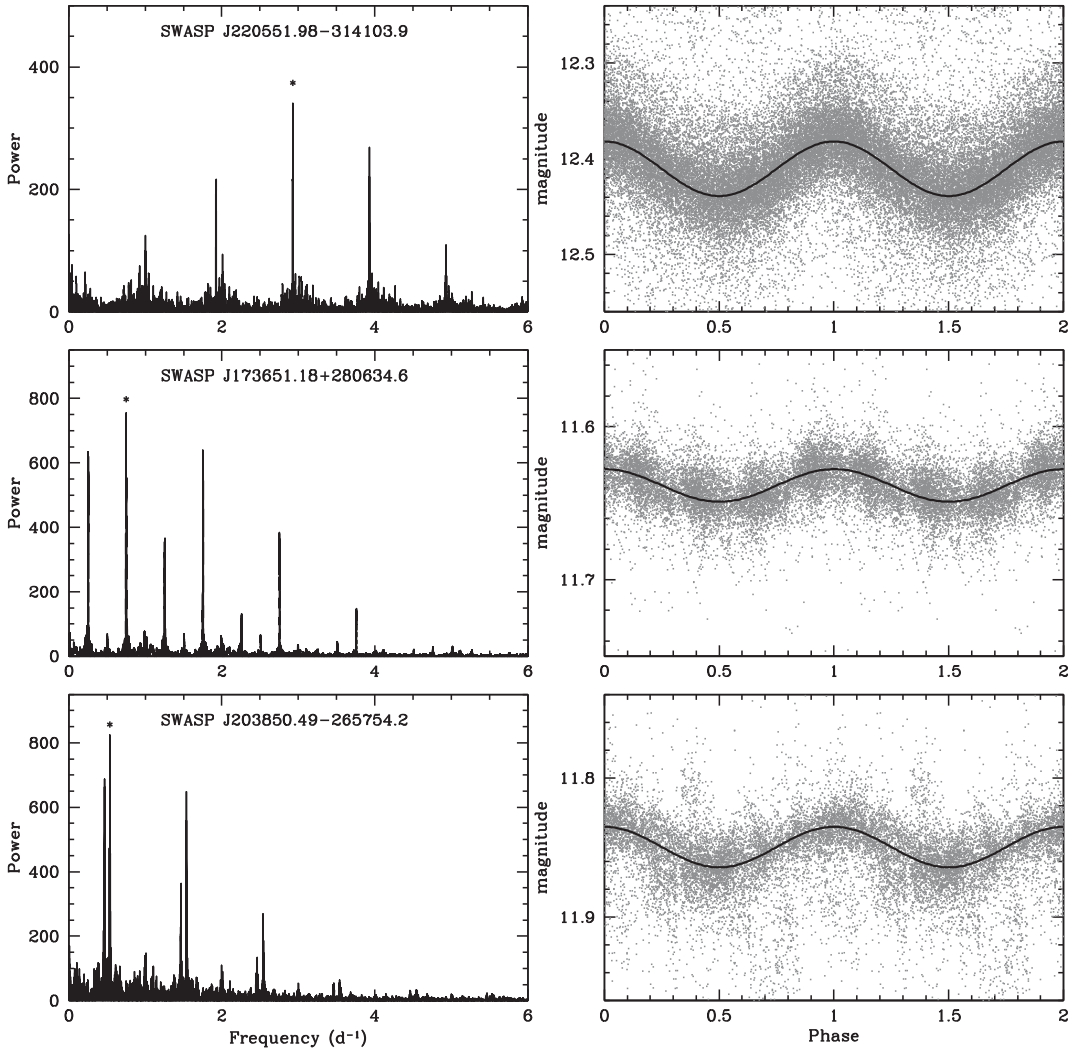

Figure 14. (Left-hand panels) Fourier transform analysis of the variable stars GALEX J2205−3141 (top), J1736+2806 (middle) and J2038−2657 (bottom), and phased light curves (right-hand panels). The identification of the photometric period with the spectroscopic period clearly indicates that the light curve of GALEX J2205−3141 shows the effect of reflection of the bright primary on the secondary star. The initial epoch T_0 in GALEX J2205−3141 corresponds to the passage of the secondary star at superior conjunction. Without knowing their orbital periods, we can only state that the cool, secondary stars in both GALEX J1736+2806 and J2038−2657 are variable. The photometric periods are marked with star symbols: $P = 0.341\,563$ d (J2205−3141), 1.333 204 d (J1736+2806), and 1.870 221 d (J2038−2657).

the secondary, $M_2 > 0.35\,M_\odot$ assuming $M_1 = 0.47\,M_\odot$, combined with the lack of photometric variability when compared to expected variations of 150 mmag caused by a reflection effect on a putative late-type companion imply that the companion is a white dwarf.

We neglected the possible effect of orbital eccentricity in the period analysis. The orbits of post-CE binaries is expected to be circular due to the synchronization during the post-CE phase. However, eccentric orbits in close binaries containing a subdwarf were reported by Edelmann et al. (2005) and Kawka et al. (2012). In these cases, the eccentricity was small ($e < 0.1$). Larger eccentricities were reported for long-period binaries, such as BD+20°3070, BD+34°1543, Feige 87 (Vos et al. 2013) and PG 1449+653 (Barlow et al. 2013b). Eccentric orbits may indicate the presence of a circumbinary disc (Artymowicz et al. 1991).

Now, we summarize additional constraints on the properties of spectroscopic composites, other likely systems showing radial velocity variations, and systems displaying photometric variability.

3.2.2 *Composite spectra*

Using spectral decomposition, Németh et al. (2012) classified GALEX J0047+0337 as a binary consisting of a hot sdB and a main-sequence F star. The radial velocity measurements obtained for GALEX J0047+0337B imply a constant velocity with standard deviation of only 6.3 km s^{-1} and include a single measurement deviating from the average velocity by more than 10 km s^{-1}. The ASAS and NSVS photometry do not show evidence of significant variations. The ASAS data constrain potential variations to a semi-amplitude lower than 4.4 mmag for all periods larger than 0.5 h. The EFOSC acquisition images revealed a nearby star approximately ∼3 arcsec away at a position angle of 344°. The object is about 1.2 mag fainter in *R* and the quoted *WISE* and 2MASS magnitudes include both stars since they would not be resolved in either surveys. Fortunately, our optical spectra were not contaminated by the nearby star and the composite nature of the object is not affected.

GALEX J1411+7037 and J1753−5007 are sdB stars with F-type companions. Their SEDs are consistent with the presence

of a luminous companion derived from the spectral decomposition of Németh et al. (2012). The Hα line profile in each star is dominated by the main-sequence star and no significant radial velocity variations have been found for these objects. The ASAS times series of GALEX J1753−5007 constrain photometric variations to a semi-amplitude lower than 19 mmag.

The SED of GALEX J1356−4934 shows significant infrared excess. An inspection of the acquisition images did not reveal a resolvable, nearby companion and radial velocity measurements show only marginal variability with radial velocity maxima reaching a span of 20 km s^{-1}. First, we performed an SED decomposition to estimate the spectral type of the companion. We adopted the sdB parameters determined by Németh et al. (2012) and calculated sdB absolute magnitudes of $M_K = 5.47$ and $M_V = 4.46$. Adopting the apparent visual magnitude $V = 12.3$ and 2MASS magnitude $K = 11.633$ and using the main-sequence colour and absolute magnitude relations from Pecaut & Mamajek (2013), we determined the absolute visual and infrared magnitudes of the late-type companion, $M_{K,2} = 3.57$ and $M_{V,2} = 5.36$, and a distance of 444 pc. Consequently, the companion mass is 0.94 $M_\odot$ corresponding to a G8V star. Next, we performed a spectral decomposition with XTGRID (Németh et al. 2012) making use of both the blue and red spectra of GALEX J1356−4934. The spectral decomposition showed that the companion contributes 27 per cent of the flux at 7000 Å. The new parameters of the sdB star are $T_{\rm eff} = 32370^{+230}_{-660}$ K, $\log g = 5.72^{+0.07}_{-0.16}$, $\log {\rm He/H} = -2.75^{+0.25}_{-0.43}$ and do not differ significantly from our earlier measurements. The parameters of the companion are $T_{\rm eff} = 5470$, $\log g = 4.47$, [Fe/H] = 0.003, also corresponding to a G8 main-sequence star. These values supersede those of Németh et al. (2012) for GALEX J1356−4934. The ASAS time series limits the photometric variations to a semi-amplitude of 3 mmag.

Optical spectra of subdwarf plus early-type F-stars are dominated in the red by the companion. Because the mass ratio is $\gtrsim$3, high-dispersion spectroscopy is required to detect the secondary star motion.

3.2.3 *Radial velocity variable*

Other objects, in addition to the confirmed binaries listed in Table 3, are likely close systems. The measured radial velocity extrema suggest that these subdwarfs are in close orbit with a companion, but the small number of spectra did not allow us to perform a period analysis.

We measured velocity extrema $\Delta v \approx 80$ km s^{-1} for GALEX J0613+3420, $\Delta v \approx 28$ km s^{-1} for GALEX J0812+1601, and $\Delta v \approx 35$ km s^{-1} for GALEX J1903−3528. The SWASP time series for GALEX J0613+3420 and GALEX J1903−3528 constrain photometric variations to maximum semi-amplitudes of 13 and 4 mmag, respectively, which exclude the presence of close late-type companions. Further investigations are required to clarify their binary status.

The SED of each object does not reveal the presence of a companion, however the SED of GALEX J0613+3420 shows evidence of a large interstellar extinction (Schlegel et al. 1998), and a possible excess ($E_{B-V} = 0.64$) above the interstellar value ($E_{B-V} = 0.36$).

3.2.4 *Photometrically variable*

The SWASP light curve of the sdB plus F7V pair GALEX J1736+2806 (1SWASP J173651.18+280634.6) varies with a period $P = 1.33$ d and a semi-amplitude of 11 mmag (Fig. 14). No significant variations were observed in a nearby comparison object (1SWASP J173635.80+280902.2). The grouping of data points observed in the light curve are also observed in the light curve of the nearby object and, therefore, it must be an artefact of data sampling. Using the SED, we found that the absolute V magnitude of the companion is ∼0.72 mag brighter than the sdB star consistent with a value of ∼0.81 mag obtained by Németh et al. (2012). The absolute magnitude of a late F7 star, M_V ∼4, would imply for the hot subdwarf M_V ∼4.7. The atmospheric parameters of the hot subdwarf are very uncertain (Németh et al. 2012) but would be reconciled with the companion spectral type at the lowest acceptable temperature (30 000K at $\log g = 5.7$). The photometric variability may be caused by irradiation of the exposed hemisphere of the F star although we failed to detect radial velocity variations at the same period.

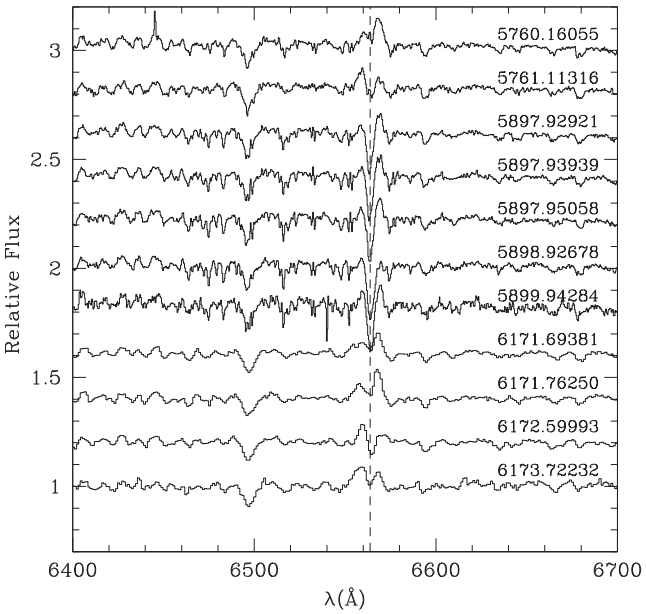

Figure 15. Spectra of the photometrically variable sdO+G8III star GALEX J2038−2657 obtained at SSO and La Silla and showing short-term variable Hα emission.

GALEX J2038−2657 is a relatively luminous hot sdO star with a G-type companion (Németh et al. 2012). Our spectroscopic observations revealed variability in the Hα profile (Fig. 15) on a timescale of a day or less. However, cross-correlation measurements in the spectral series dominated by the G companion show little variations with a dispersion $\sigma_v = 7.8$ km s^{-1} comparable to the expected accuracy of the wavelength scale. The measurements imply that the velocity semi-amplitude of the G8III star does not exceed ≈16 km s^{-1}. Fig. 16 shows the SED of GALEX J2038−2657 where the ultraviolet range is dominated by the hot subdwarf and the optical range by the red giant. The SWASP time series (1SWASP J203850.49−265754.2) reveals variations of 12 mmag semi-amplitude over a period of 1.87022 d (Fig. 14) that are confirmed by similar variations in a short NSVS time series. Again, no significant variations were observed in a nearby comparison object (1SWASP J203851.22−265943.1). These variations are most likely linked to the observed spectroscopic variability, but they cannot yet be clearly associated with a possible orbital period.

The system shares some properties with the sdB plus K III–IV system HD 185510 (Jeffery, Simon & Lloyd Evans 1992; Fekel et al. 1993) and the sdO plus K0 III system FF Aqr (Vaccaro & Wilson 2003). All three systems have an evolved secondary star, from subgiant to giant, and all three are photometrically variable. However, the hot subdwarf in HD 185510 is possibly

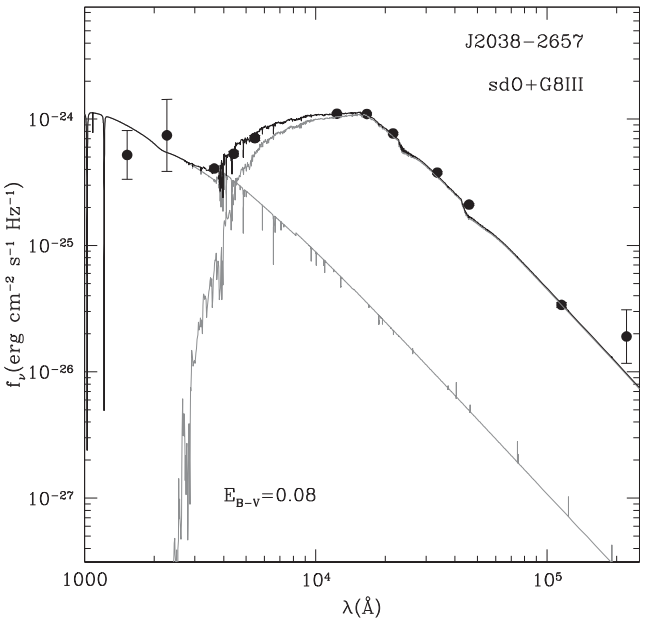

Figure 16. SED of GALEX J2038−2657 combining a cool G8III secondary and an sdO primary star (full line). Individual contributions are shown with grey lines. The effect of interstellar extinction ($E_{B-V} = 0.08$) is included.

the progenitor of a low-mass, helium white dwarf (0.3 $M_\odot$; Jeffery & Simon 1997). Photometric variations in HD 185510 and FF Aqr coincide with the orbital period and are caused by irradiation of the exposed hemisphere of the secondary stars. Moreover, the orbital periods HD 185510 and FF Aqr are 20.7 and 9.2 d, respectively, with orbital separations of ∼43 and ∼25 $R_\odot$, respectively, and well outside the radius of a subgiant or giant star (R(K0 III) ≈ 16 $R_\odot$).

Without an estimate of the orbital period, we can only set limits to the orbital parameters, such as the binary separation. The identification of the late-type giant secondary is based on spectral decomposition (Németh et al. 2012). The absolute V magnitude of the hot sdO star is only about ∼1.0 mag fainter than its companion. Adopting a G8 III type from the spectral decomposition shown in Fig. 16, the absolute magnitude of the companion is M_V(G8 III) = 0.9, implying an absolute magnitude M_V(sdO) = 1.9 for the primary in agreement with the estimate of Németh et al. (2012), M_V(sdO) = 2.0. The minimum orbital period for a systemic mass of 2–3 $M_\odot$ and an orbit outside the G8 III radius (15 $R_\odot$) is $P \gtrsim 3.1$ d. Adopting a radius of 15 $R_\odot$ for the G8 III star, the photometric period of 1.87 d implies a rotation velocity $v_{\rm rot} \approx 350$ km s^{-1}. The narrowest features in the SSO spectra have a width of $v_{\rm rot} \sin i = 130$ km s^{-1}, that would enforce a low inclination $i \lesssim 22^\circ$. High-dispersion spectroscopy is necessary to help determine the orbital parameters and help clarify the origin of the photometric variations. The most likely scenario is that the photometric variations are caused by a surface spot coupled to the rotation of the star, and that the orbital period probably exceeds several days with a low-velocity amplitude ($K \lesssim 20$ km s^{-1}).

3.3 Notes on other objects from this survey

GALEX J0047+0958 (HD 4539) is a well-known hot sdB star (see e.g. Kilkenny 1984). Spectropolarimetric measurements hint at the presence of a weak magnetic field (∼0.5 kG; Landstreet et al. 2012). Schoenaers & Lynas-Gray (2007) reported line profile variations and radial velocity variations of a few km s^{-1} that may be due to g-mode pulsations. Lynas-Gray (2012) obtained photometric series and measured variations with a frequency of 9.285 ± 0.003 d^{-1} and an amplitude of 0.0023 ± 0.0003 mag. This photometric frequency is consistent with one of the frequencies (9.2875 ± 0.0003 d^{-1}) determined from low-amplitude radial velocity variations, and both are possibly associated with stellar pulsation.

The SED of GALEX J0049+2056 (Fig. A1) shows an IR excess that could be attributed to a yet unidentified companion or nearby object, or to a dusty environment.

The sdB GALEX J0059+1544 (PHL 932) is embedded in an emission nebula. However, Frew et al. (2010) have shown that the association is only coincidental, but that PHL 932 does contribute and ionize a dense region of the ISM surrounding it. The SED of this object shows, as in the case of GALEX J0049+2056, a considerable IR excess (Fig. A1). Several radial velocity measurements of PHL 932 were reported in literature. Arp & Scargle (1967) measured 15 ± 20 km s^{-1} using two low-dispersion spectra. Edelmann (2003) measured 18 ± 2 km s^{-1} using echelle spectra. These velocities are in agreement with our measurements ($\bar{v} = 16.7$, $\sigma = 3.1$ km s^{-1}) and, therefore, it does not appear that PHL 932 is in a close binary. Geier & Heber (2012) report a rotational velocity of $v_{\rm rot} = 9.0 \pm 1.3$ km s^{-1}. Landstreet et al. (2012) obtained spectropolarimetric measurements of PHL 932 but did not detect a magnetic field with an upper limit of ∼300 G.

Brown et al. (2008) classified GALEX J0206+1438 (CHSS 3497) as a hot subdwarf. Our radial velocity measurements vary only marginally ($\sigma_v < 10$ km s^{-1}), and we do not dispose of sufficient data to determine a period. A radial velocity measurement of $V_{\rm r} = 7 \pm 16$ km s^{-1} was obtained by Brown et al. (2008) and is consistent with our measurements ($\bar{v} = 13.8$, $\sigma_v = 7.5$ km s^{-1}).

GALEX J0232+4411 (FBS 0229+439) was classified as an sdB star in the First Byurakan Survey of blue stellar objects (Mickaelian 2008).

Copperwheat et al. (2011) presented a set of radial velocity measurements for GALEX J0401−3223 which suggest that the sdB star is in a close binary system, but were unable to determine the orbital period with limited data. Copperwheat et al. (2011) measured an average velocity and dispersion of $v \pm \sigma_v = 55.2 \pm 4.4$ km s^{-1}, consistent with our own measurements. We have combined the Copperwheat et al. (2011) data with ours and conducted a period search. We found a best period of 1.8574 d, however two significant aliases at $P = 0.64$ and 0.066 d cannot be ruled out. The velocity semi-amplitude at all three periods does not exceed 10 km s^{-1} and excludes a white dwarf or late-type companion. The relatively short-period and low-velocity amplitude imply a minimum mass in the substellar range, 0.01–0.04 $M_\odot$. The SWASP data folded on the best period (1.8574 d) constrain photometric variations to a semi-amplitude of only 1 mmag, or 8 mmag when folded on any periods larger than 0.01 d. The expected variations due to a substellar companion would be as low as 6 mmag at the two longest periods or 20 mmag at the shortest, but are all significantly larger than the SWASP limit. It is not possible to describe the companion with present data, although a substellar companion is a distinct possibility.

Østensen et al. (2010c) obtained series of photometric observations of GALEX J0500+0912 in order to search for pulsations and concluded that it is not photometrically variable. Our limited radial velocity data set does not indicate variability.

An inspection of the acquisition images of GALEX J0657−7324 shows a nearby companion and, therefore, the 2MASS and *WISE* colours of the hot subdwarf are certainly contaminated. Heintz (1992) reported that GALEX J0657−7324 (HEI 714) is a visual

double star with a separation of 1.9 arcsec, and our own acquisition image locates the companion 1.8 arcsec away at a position angle of 270°. Also, our optical spectra do not appear to be contaminated by this object and do not indicate variability.

GALEX J1845−4138 is a relatively cool He-rich subdwarf displaying a strong He I line series and weaker Balmer lines. The velocity measurements based on He I 6678.154 ($v = -59.7 \pm 3.3$ km s^{-1}) are consistent with the measurements based on Hα and do not suggest any variability.

GALEX J1902−5130 is a helium sdO star. Landstreet et al. (2012) obtained spectropolarimetry of GALEX J1902−5130 with a measurement that shows that this star does not have a magnetic field down to a few hundred gauss. Our radial velocity measurements suggest there may be long-period, low-amplitude variations. The measurements are based on He II 6560.088 Å. The object is very hot and our spectra display He I emission.

GALEX J1911−1406 is also a very hot He-rich subdwarf. The velocity measurements are based on He II 6560.088 Å.

Geier & Heber (2012) report a rotational velocity of $v_{\rm rot} = 8.6 \pm 1.8$ km s^{-1} for GALEX J2153−7003. Copperwheat et al. (2011) obtained several radial velocity measurements of this star and found that it is not variable. Their average velocity and dispersion, 39.4 ± 7.5 km s^{-1}, are in a close agreement with our own measurements (43.4 ± 4.2 km s^{-1}).

GALEX J2344−3426 is a well-known sdB star. Østensen et al. (2010c) obtained photometric series of the star and found it to be non-variable. Geier & Heber (2012) measured a rotational velocity of $v_{\rm rot} = 7.3 \pm 1.0$ km s^{-1}. Mathys et al. (2012) and Landstreet et al. (2012) obtained spectropolarimetry of the star and constrained the longitudinal field to 261 G and 246 ± 232 G, respectively.

4 DISCUSSION

The new binary identifications are placed into context with a compilation of all known spectroscopically identified binaries (Appendix C). Table C1 lists the orbital parameters of these systems. The compilation includes hot subdwarfs with an unseen companion and spectroscopically identified late- to early-type companions in a range of periods from 0.05 to 1363 d. Table C2 lists the properties of the primary as well as kinematical properties of the systems.

Throughout this discussion, we assume for most subdwarfs a mass of 0.47 M$_\odot$ with a few exceptions such as the ELM progenitors (0.23 M$_\odot$) and hot sdO companions to early-type stars (1 M$_\odot$). Using pulsating properties of sdB stars and binary systems for which the sdB mass was measured, Fontaine et al. (2012) found that the average mass of an sdB star is 0.47 M$_\odot$ with a standard deviation of 0.031 M$_\odot$. Zhang, Chen & Han (2009) found that most sdB stars have a mass between 0.42 and 0.54 M$_\odot$ and an average mass of about 0.50 M$_\odot$. Zhang et al. (2009) used evolutionary models and the parameters of a sample of 164 sdB stars.

4.1 Properties of known binaries: period and mass function

Fig. 17 (top) shows the cumulative distribution of orbital periods in the population of binaries with a hot subdwarf primary. The derivative of the function with respect to the logarithm of the period provides an estimate of the period distribution (Fig. 17, bottom). Several peaks stand-out, particularly at 0.1, 0.5–2.0, 10, and 1000 d. The last two peaks are clearly separated by a gap within which few binaries are known. A few Be stars with a hot subdwarf companion populate the gap and the distribution includes spectroscopically (UV) confirmed Be+sdO (Peters et al. 2008, 2013). We noticed a

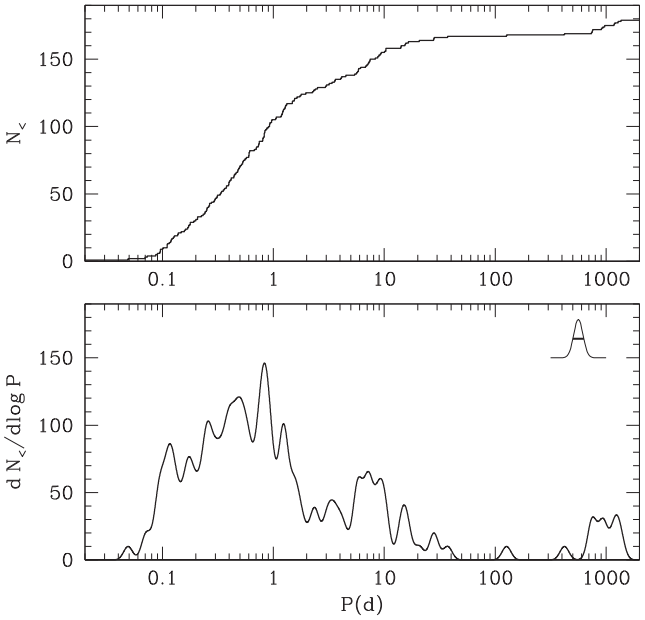

Figure 17. Cumulative function of period (top), $N_<$ versus log P, and its first derivative (bottom). The derivative was smoothed with a Gaussian function (FWHM = 0.1 dex), and shown in the upper-right corner.

hint of a hierarchy in the period distribution. The shortest periods coincide with dM companions emerging from a CE phase (low-mass ratio $M_2/M_1 < 1/2$), white dwarfs ($M_2/M_1 \approx 1$), and, at high-mass ratio ($M_2/M_1 > 2$), subdwarfs with a subgiant/giant or Be companion, and, finally, subdwarfs with an FGK companion at the longest periods and emerging from a RLOF. Following a RLOF, the orbital separation increases the least for more massive companions. It is remarkable that main-sequence A-type star companions are still missing although they are predicted in population syntheses (Han et al. 2003). Subdwarfs with A-type main-sequence companions should be detectable as UV excess objects or as low-amplitude radial velocity variations similar to Be+subdwarf binaries. In summary, binaries near the main peak are mostly white dwarfs plus subdwarfs after possibly two episodes of mass-transfer. Note that the orbital parameters of many systems with large velocity amplitudes remain unresolved (see e.g. Copperwheat et al. 2011; Geier et al. 2011c) and are not included in this analysis.

Fig. 18 shows the sample of known binaries in the velocity amplitude versus period plane. Most eclipsing systems have secondary masses between 0.08 and 0.15 M$_\odot$. Systems with known white dwarf secondaries have secondary masses close to or above 0.60 M$_\odot$.

Fig. 19 also shows the sample of known binaries in the velocity amplitude versus period plane but with the velocity scale corrected for an average inclination of 57°. The correction allows us to draw class properties but should not be applied to individual objects. Secondary masses for systems showing a reflection effect range, with the exception of FF Aqr and HD 185510, from 0.08 to 0.30 M$_\odot$. Remarkably, secondary masses for most non-reflecting systems cluster near 0.60 M$_\odot$ and the unseen objects are probably white dwarfs. Secondary stars in the long-period range and with masses in excess of 0.60 M$_\odot$ are identifiable as G and K stars. All eclipsing systems with $K < 100$ km s^{-1}, i.e. with an estimated $M_2 < 0.3$ M$_\odot$, also show a reflection effect indicative of a late-type secondary, while the remaining systems cluster at a higher secondary mass $M_2 \approx 0.6$ M$_\odot$ and almost certainly harbour a white dwarf secondary. Fig. 20 shows

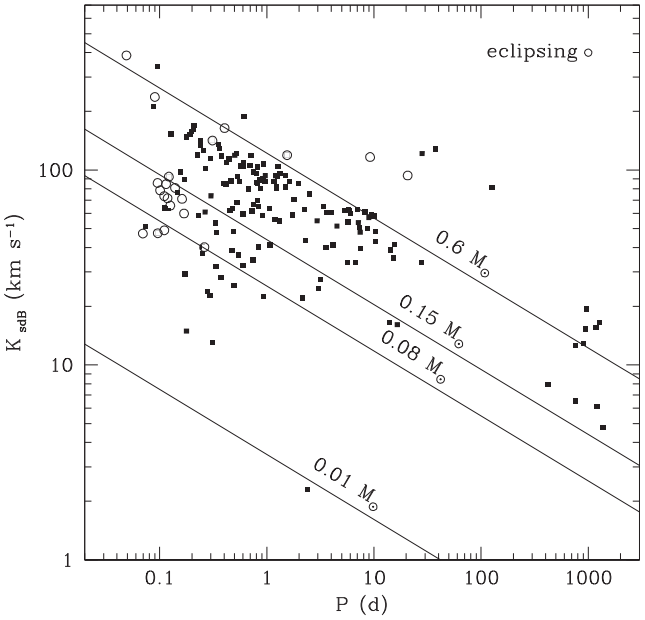

Figure 18. Measured velocity amplitude versus period with a subsample of eclipsing binaries shown with open circles. Full lines are labelled with the mass of secondary stars which were computed for $i = 90°$.

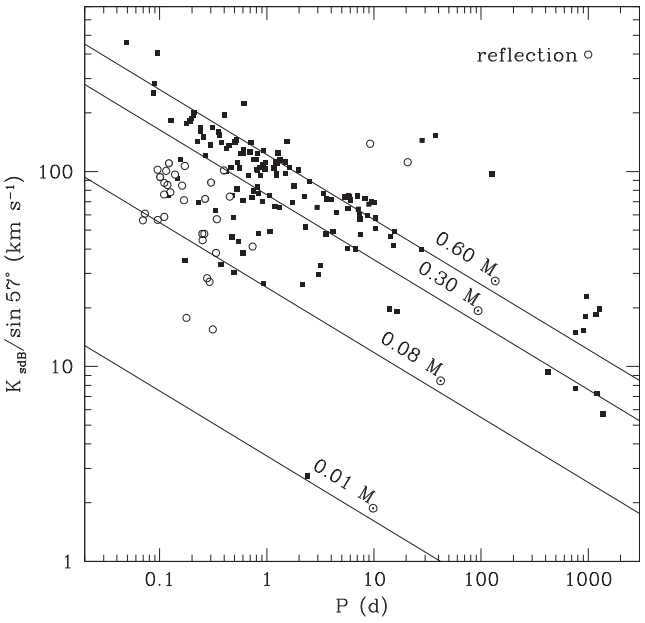

Figure 19. Same as Fig. 18 but with reflection binaries shown with open circles. The velocity scale is corrected for the effect of an average inclination of 57°. Secondary masses cluster between 0.08 and 0.30 $M_\odot$.

secondary mass distribution assuming average system inclination of 57°. This distribution may be described by a superposition of two power laws. A shallow distribution with $M_2 > 0.08\,M_\odot$, i.e. $\alpha = 1.3$ between 0.08 and 0.5 $M_\odot$ and $\alpha = 2.3$ above 0.5 $M_\odot$ following the initial mass function $\xi(m) \propto m^{-\alpha}$ of Kroupa (2001), and a steeper distribution ($\alpha \approx 6$) with $M_2 > 0.48\,M_\odot$. The former power law encompasses mostly M-type dwarfs, many of them showing a reflection effect, while the latter encompasses white dwarfs in the 0.5–1.0 $M_\odot$ mass range. This simplified white dwarf distribution represents well the peak and high-mass tail of the white dwarf mass

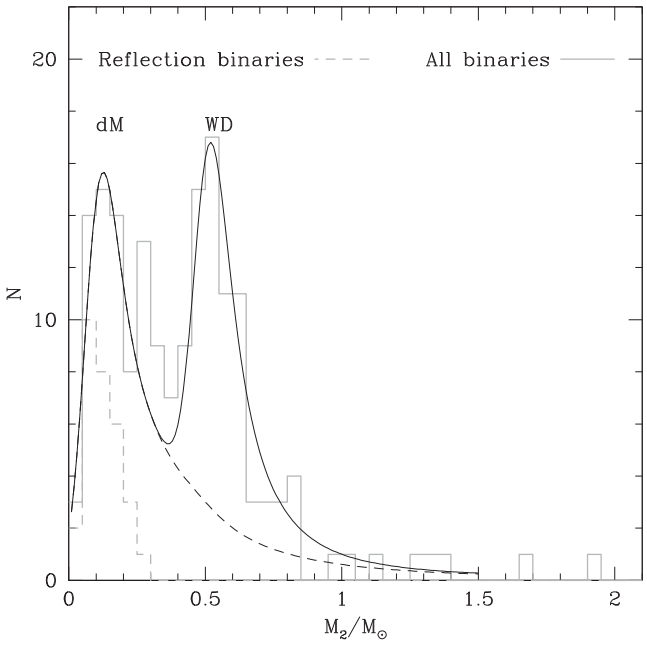

Figure 20. Mass distribution of all known binaries with a hot subdwarf primary star as a function of the secondary mass, assuming an average inclination of 57° (full histogram). The peak distribution of low-mass stars is marked 'dM' and that of white dwarfs, 'WD'. Binaries showing reflection effect in their light curves are shown with a dashed histogram. The full lines show synthetic distributions smoothed to two-bins width for a combination of late-type stars and white dwarfs (double-peaked full line), and that excluding white dwarfs (dashed line).

distribution (see e.g. Kepler et al. 2007) but excludes possible low-mass white dwarfs (<0.48 $M_\odot$). On the other hand, the late-type stellar mass distribution follows the initial mass function and the expectation of a randomly drawn set of late-type stars. The reflection effect is common in short-period binaries ($P < 0.5$ d) but is relatively rare at longer periods (see Fig. 19) due to increased binary separations and weaker photometric variations. The actual late-type mass distribution appears as a scaled-up version of the secondary mass distribution in the subsample of reflection binaries, but it also includes longer period binaries with an indiscernible reflection effect. Note that a third narrow peak is possibly present at ≈0.3 $M_\odot$. Since this peak is mostly made up of companions that do not show the reflection effect, the origin of this peak maybe be low-mass white dwarfs. It may also be due to an incorrect mass estimate of the subdwarf, for example an ELM progenitor is assumed rather than a normal subdwarf. Most objects (60–70 per cent) are low-mass main-sequence stars, while 30–40 per cent are white dwarfs.

Our own survey delivered a 37 per cent fraction of hot subdwarfs in close binaries (Section 3.1.3). Our survey strategy was aimed at and successfully uncovered short-period binaries. Fig. 19 shows that setting our detection threshold at 10 km s^{-1} would have allowed for the detection of any stellar companion with an orbital period $\lesssim$20 d, any late-type companion with a mass of 0.3 $M_\odot$ and $P \lesssim 600$ d, or just about any white dwarf companion. However, a close examination of data sampling shows that 60 per cent were obtained with a span of 2 d or less with another 30 per cent with a span of 100–400 d, i.e. during a subsequent observing run or season. Systems with periods of 10–20 d or longer would have only been partially covered and most likely avoided detection. Note that the longest period detected in our survey is only 3 d long. Setting our detection threshold at 10 d, i.e. some 155 objects out of 179 known

binaries, the total yield including longer period binaries could be ≈15 per cent larger for a total binary fraction of 43 per cent. The four additional hot subdwarfs with composite spectra (see Table 1) which are likely to have longer orbital periods ($\gtrsim$10 d) are such objects.

4.2 Properties of known binaries: kinematics

We calculated the Galactic velocity components (U, V, W), which are relative to the local standard of rest (LSR), of all known hot subdwarf binary systems (listed in Appendix C) using their positions, systemic (γ) velocities, proper motions and apparent magnitudes. We adopted the right-handed system for the velocity components, where U is positive in the direction of the Galactic Centre, V is positive in the direction of Galactic rotation and W is positive towards the North Galactic Pole. We assumed that the solar motion relative to the LSR is (U, V, W) = (10.1, 4.0, 6.7) km s^{-1} as determined by Hogg et al. (2005). The distribution of systemic velocities, i.e. radial velocities, follows $N \approx e^{-|\gamma|/\sigma}$, where $\sigma_r = 41$ km s^{-1}. The σ_r value is the one-dimension equivalent of the two-dimension transversal velocity dispersion $\sigma_T = 59$ km s^{-1} measured by Vennes et al. (2011), where $\sigma_T = \sqrt{2}\,\sigma_r$. In their study of the kinematics of EHB stars, Altmann, Edelmann & de Boer (2004) measured significantly larger radial velocities with a distribution following $\sigma_r = 65$ km s^{-1} compared to our sample, but they measured a transversal velocity distribution consistent with the present one.

To calculate the Galactic velocity vectors, we employed the method outlined in Johnson & Soderblom (1987) using as an input the radial velocity, proper motion (Zacharias et al. 2013) and distance measurements. We determined the distance towards each subdwarf using the distance modulus $V - M_V = 5 \log d - 5$, where the magnitude V is listed in Table C1. We estimated the absolute magnitude M_V from the measured stellar parameters, i.e.

$$M_V = -2.5 \log (4\pi\Omega\, \bar{H}_V),$$

where $\Omega = r^2/d^2$, with $d = 10$ pc and $r^2 = GM/g$. The Eddington flux is averaged ($\bar{H}_V$) over the Johnson V transmission curve. We assumed $M = 0.23\,M_\odot$ for low-mass objects, $0.47\,M_\odot$ for normal objects and $1.0\,M_\odot$ for subdwarfs in massive binaries, and the published surface gravity measurements were usually obtained using a spectroscopic method similar to that described in Section 3.1.

Fig. 21 shows the U and V velocity components for all hot subdwarf binary systems. Table 4 lists the (U, V, W) velocity components and dispersions for the sample of known binaries. The distribution appears asymmetric with several objects trailing at large negative Galactic V velocity. We computed the straight average and dispersion ('All') but excluding the extreme case of OGLE BUL-SC16335. We also fitted the distributions with Gaussian functions excluding outliers, i.e. all bins with less than three members ('$N > 3$'). The sample velocity dispersion is significantly smaller than that calculated by Altmann et al. (2004) for single hot subdwarf stars ($\sigma_U = 74$ km s^{-1}, $\sigma_V = 79$ km s^{-1}, $\sigma_W = 64$ km s^{-1}). However, our velocity dispersion is in better agreement with the dispersion ($\sigma_U = 62 \pm 8$ km s^{-1}, $\sigma_V = 52 \pm 7$ km s^{-1}, $\sigma_W = 59 \pm 8$ km s^{-1}) calculated by de Boer et al. (1997) based on a sample of 41 hot subdwarf stars. Possible explanations for the inflated Galactic velocities of Altmann et al. (2004) are that their sample included yet unidentified binaries or that lower dispersion spectroscopy resulted in larger measurement errors. In summary, the hot subdwarf population and the confirmed binaries among them are kinematically indistinguishable and drawn from the same, general population of EHB stars.

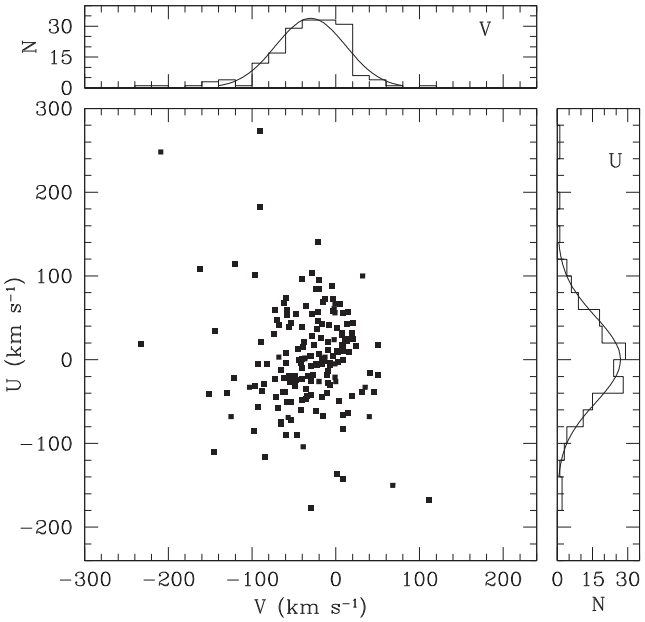

Figure 21. Galactic velocity vectors U and V of all known binaries containing a hot subdwarf. The individual distributions are shown in the upper panel (V) and right-hand panel (U). Details of the measurements are shown in Table 4 and discussed in Section 4.2.

Table 4. Kinematical properties of the hot subdwarf binary population.

Vel.[a]	$N > 3$[b]	All[c]	sdB[d]	WD[e]	WD_{thin}[f]	WD_{thick}[f]
$\bar{U}$	0 ± 5	2	−8	−7.8	–	–
σ_U	52 ± 3	62	74	42.8	34	79
$\bar{V}$	−30 ± 2	−32	−37	−40.1	–	−52
σ_V	42 ± 2	47	79	31.9	24	36
$\bar{W}$	−5 ± 3	−6	12	−5.9	–	–
σ_W	34 ± 2	41	64	27.4	18	46

[a] All velocities expressed in km s^{-1}.
[b] This work, but excluding outliers.
[c] This work.
[d] Altmann et al. (2004).
[e] Kawka et al. (2012).
[f] Pauli et al. (2006).

Also, Table 4 compares results for the hot subdwarf population with that of field white dwarf stars. Pauli et al. (2006) list 361 thin disc members and 27 thick disc members, while Kawka et al. (2012) list 57 old disc white dwarfs, which is a mix of old thin-disc and thick-disc populations, and at least one halo white dwarf. A comparison of the velocity dispersions shows that the binary population may be an even older population than field white dwarf stars with some population members belonging to the old disc or even the halo.

Four systems display peculiar kinematics. Three of these, SDSS J1622+4730, PHL 861 and SDSS J1505+1108, have Galactic velocities that make them halo candidates with a few additional objects lagging in the V component making them thick-disc candidates. The fourth object, OGLE BUL-SC16335, is in a crowded field and there is a possibility that the proper motion measurements are incorrect.

Barlow et al. (2013b) calculated kinematics for five long-period systems and found that two of these (PG 1449+653 and PG 1701+359) have kinematics suggesting that they belong either to the thick disc or halo. They also report that there is a high probability

that PG 1104+243 belongs to the thick disc. Our calculated Galactic velocities are similar to those of Barlow et al. (2013b). Note that Barlow et al. (2013b) includes the disc rotation (220 km s^{-1}) in their *V* velocity.

A comparison of the velocity components of the hot subdwarf binary population to that of Kawka et al. (2012) shows that the dispersion is larger for all velocity components than that of the white dwarf population, suggesting that the subdwarf population appears to be older than the white dwarf population. Finally, a comparison with the work of Pauli et al. (2006) shows that the hot subdwarf binary population has a velocity dispersion between the thin and thick disc dispersions for white dwarfs.

4.3 Low-mass subdwarfs as progenitors of ELM white dwarfs

The first-known ELM white dwarf progenitor, HD 188112, was discovered by Heber et al. (2003). As part of their survey of ELM white dwarfs, Kilic et al. (2011) found that SDSS J1625+3632 is similar to HD 188112. Other recently discovered systems are KIC 6614501 (Silvotti et al. 2012) and NGC 6121-V46 (O'Toole et al. 2006). Our radial velocity survey adds one more object to the small sample of ELM white dwarf progenitors. Vennes et al. (2011) showed that GALEX J0805−1058 has atmospheric properties representative of ELM white dwarf progenitors ($M \lesssim 0.3\,M_{\odot}$) and, therefore, it was selected for radial velocity follow-up measurements. New radial velocity measurements proved that GALEX J0805−1058 is in a close binary, and, because it also lies below the ZAEHB (see Section 3.1), we conclude that it is a genuine ELM white dwarf progenitor. It is also the first ELM white dwarf progenitor without a more massive white dwarf companion, and this is likely to have significant implications for the origin and evolution of ELM white dwarfs. Two other objects from our sample lie below the ZAEHB, J1411+7037, which is paired with an F star, and J2153−7004, although we did not detect significant radial velocity variations.

4.4 Summary

We presented an analysis of the orbital properties of seven new systems comprising a hot subdwarf primary. The secondary in one system is a late-type star showing a reflection effect (GALEX J2205−3141), while we found evidence that the secondary star in GALEX J0805−1058 is a very low mass M dwarf or possibly a substellar object. The mass function of the other objects implies the likely presence of a white dwarf companion. The period of photometric variability of two additional systems is, in the case of GALEX J1736+2806 probably coincident with the orbital period, and, in the case of J2038−2657, probably coincident with the rotation period of the giant companion. Our survey results, taking into account the survey strategy, imply an incidence of binarity of ∼43 per cent in the hot subdwarf population.

We have compiled a list of all known hot subdwarfs in binary systems and performed a binary population analysis. We found that systems showing the reflection effect have components that are of a lower mass (0.08 to 0.30 $M_{\odot}$) than those that do not show the reflection (∼0.6 $M_{\odot}$). It is very likely that the companion to the hot subdwarf in most of the systems not showing the reflection effect in the short-period binaries ($P \lesssim 1$ d) are white dwarfs. The inferred secondary mass distribution is a superposition of two approximate power laws, one low-mass power law ($\gtrsim 0.1\,M_{\odot}$) and composed of low-mass main-sequence stars, and another, high-mass power law ($\gtrsim 0.5\,M_{\odot}$) and primarily composed of white dwarfs with a few early-type main-sequence stars. White dwarfs constitute ≈30–40 per cent of all binary companions.

We have calculated the Galactic velocity components for all known hot subdwarfs in a binary system and showed that this population may be older than the field white dwarf population. In this sample, we found three systems that possibly belong to the halo.

Future work will involve high-dispersion spectroscopic follow-up of low-velocity amplitude binary candidates, and of binaries comprising a hot subdwarf and an early-type main-sequence, or giant companion.

ACKNOWLEDGEMENTS

AK and SV acknowledge support from the Grant Agency of the Czech Republic (P209/12/0217 and 13-14581S) and Ministry of Education, Youth and Sports (LG14013). We wish to thank S. Ehlerová and team members for their assistance with observations obtained with the MPG 2.2-m telescope at La Silla. We thank the referee for a thorough report and for stimulating further work on the paper. This work was also supported by the project RVO:67985815 in the Czech Republic. This paper uses observations made at the SAAO. This paper makes use of data obtained from the ING Archive which is maintained as part of the CASU Astronomical Data Centre at the Institute of Astronomy, Cambridge. This publication makes use of data products from the *WISE*, which is a joint project of the University of California, Los Angeles, and the Jet Propulsion Laboratory/California Institute of Technology, funded by the National Aeronautics and Space Administration. This publication makes use of data products from the 2MASS, which is a joint project of the University of Massachusetts and the Infrared Processing and Analysis Center/California Institute of Technology, funded by the National Aeronautics and Space Administration and the National Science Foundation.

NOTE ADDED IN PRESS

A close examination of the *WISE* images reveals the presence of a nearby object in all four *WISE* bands (separation ∼6 arcsec, PA ∼270°). The nearby object dominates in the *W*3 and *W*4 bands.

REFERENCES

Ahmad A., Jeffery C. S., Fullerton A. W., 2004, A&A, 418, 275
Almeida L. A., Jablonski F., Tello J., Rodrigues C. V., 2012, MNRAS, 423, 478
Altmann M., Edelmann H., de Boer K. S., 2004, A&A, 414, 181
Arp H., Scargle J. D., 1967, ApJ, 150, 707
Artymowicz P., Clarke C. J., Lubow S. H., Pringle J. E., 1991, ApJ, 370, L35
Aznar Cuadrado R., Jeffery C. S., 2001, A&A, 368, 994
Barlow B. N. et al., 2010, MNRAS, 403, 324
Barlow B. N., Dunlap B. H., Clemens J. C., 2011, ApJ, 737, L2
Barlow B. N., Wade R. A., Liss S. E., Østensen R. H., Van Winckel H., 2012, ApJ, 758, 58
Barlow B. N. et al., 2013a, MNRAS, 430, 22
Barlow B. N., Liss S. E., Wade R. A., Green E. M., 2013b, ApJ, 771, 23
Barlow B. N., Wade R. A., Liss S. E., Stark M. A., 2014, ASP Conf. Ser. Vol. 481, Hot Subdwarf Stars and Related Objects. Astron. Soc. Pac., San Francisco, p. 301
Bildsten L., Shen K. J., Weinberg N. N., Nelemans G., 2007, ApJ, 662, L95
Billéres M., Fontaine G., Brassard P., Charpinet S., Liebert J., Saffer R. A., 2000, ApJ, 530, 441
Billéres M., Fontaine G., Brassard P., Liebert J., 2002, ApJ, 578, 515
Bloemen S. et al., 2011, MNRAS, 410, 1787

Božić H., Harmanec P., Horn J., Koubsky P., Scholz G., McDavid D., Hubert A.-M., Hubert H., 1995, A&A, 304, 235
Brown W. R., Beers T. C., Wilhelm R., Allende Prieto C., Geller M. J., Kenyon S. J., Kurtz M. J., 2008, AJ, 135, 564
Caillault J.-P., Patterson J., 1990, AJ, 100, 825
Camarota L., Holberg J. B., 2014, MNRAS, 438, 3111
Cardelli J. A., Clayton G. C., Mathis J. S., 1989, ApJ, 345, 245
Chabrier G., Baraffe I., Leconte J., Gallardo J., Barman T., 2009, in Stempels E., ed., AIP Conf. Proc. Vol. 1094, Cool Stars, Stellar Systems and the Sun. Am. Inst. Phys., New York, p. 102
Chen X., Han Z., Deca J., Podsiadlowski P., 2013, MNRAS, 434, 186
Copperwheat C. M., Morales-Rueda L., Marsh T. R. Maxted P. F. L., Huber U., 2011, MNRAS, 415, 1381
de Boer K. S., Aguilar Sánchez Y., Altmann M., Geffert M., Odenkirchen M., Schmidt J. H. K., Colin J., 1997, A&A, 327, 577
Deca J. et al., 2012, MNRAS, 421, 2798
Dopita M., Hart J., McGregor P., Oates P., Blozham G., Jones D., 2007, Ap&SS, 310, 255
Dorman B., Rood R. T., O'Connell R. W., 1993, ApJ, 419, 596
Drake A. J. et al., 2009, ApJ, 696, 870
Drechsel H. et al., 2001, A&A, 379, 893
Driebe T., Schoenberner D., Bloecker T., Herwig F., 1998, A&A, 339, 123
Edelmann H., 2003, PhD thesis, Friedrich-Alexander-Univ. Erlangen-Nuremberg
Edelmann H., 2008 in Heber U., Jeffery C. S., Napiwotzki R., eds, ASP Conf. Ser. Vol. 392, Hot Subdwarf Stars and Related Objects. Astron. Soc. Pac., San Francisco, p. 187
Edelmann H., Heber U., Napiwotzki R., Reid I. N., Saffer R. A., 1999, in Solheim S.-E., Meistas E. G., eds, ASP Conf. Ser. Vol. 169, White Dwarfs. Astron. Soc. Pac., San Francisco, p. 546
Edelmann H., Heber U., Hagen H.-J., Lemke M., Dreizler S., Napiwotzki R., Engels D., 2003, A&A, 400, 939
Edelmann H., Heber U., Lisker T., Green E. M., 2004, Ap&SS, 291, 315
Edelmann H., Heber U., Altmann M., Karl C., Lisker T., 2005, A&A, 442, 1023
Fekel F., Henry G. W., Busby M. R., Eitter J. J., 1993, AJ, 106, 2370
Fink M., Röpke F. K., Hillebrandt W., Seitenzahl I. R., Sim S. A., Kromer M., 2010, A&A, 514, A53
Fontaine G., Brassard P., Charpinet S., Green E. M., Randall S. K., Van Grootel V., 2012, A&A, 539, A12
For B.-Q. et al., 2006, ApJ, 642, 1117
For B.-Q., Edelmann H., Green E. M., Drechsel H., Nesslinger S., Fontaine G., 2008, in Heber U., Jeffery C. S., Napiwotzki R., eds, ASP Conf. Ser. Vol. 392, Hot Subdwarf Stars and Related Objects. Astron. Soc. Pac., San Francisco, p. 203
For B.-Q. et al., 2010, ApJ, 708, 253
Foss D., Wade R. A., Green R. F., 1991, ApJ, 374, 281
Frew D. J., Madsen G. J., O'Toole S. J., Parker Q. A., 2010, Publ. Astron. Soc. Aust., 27, 203
Geier S., Heber U., 2012, A&A, 543, A149
Geier S., Nesslinger S., Heber U., Przybilla N., Napiwotzki R., Kudritzki R.-P., 2007, A&A, 464, 299
Geier S., Nesslinger S., Heber U., Randall S. K., Edelmann H., Green E. M., 2008, A&A, 477, L13
Geier S., Edelmann H., Heber U., Morales-Rueda L., 2009, ApJ, 702, L96
Geier S., Heber U., Kupfer T., Napiwotzki R., 2010a, A&A, 515, A37
Geier S., Heber U., Podsiadlowski Ph., Edelmann H., Napiwotzki R., Kupfer T., Müller S., 2010b, A&A, 519, A25
Geier S. et al., 2011a, A&A, 526, A39
Geier S., Napiwotzki R., Heber U., Nelemans G., 2011b, A&A, 528, L16
Geier S. et al., 2011c, A&A, 530, A28
Geier S. et al., 2011d, ApJ, 731, L22
Geier S. et al., 2013a, A&A, 554, A54
Geier S., Heber U., Edelmann H., Morales-Rueda L., Kilkenny D., O'Donoghue D., Marsh T. R., Copperwheat C., 2013b, A&A, 557, A122
Geier S. et al., 2014, A&A, 562, A95
Gies D. R., Bagnuolo W. G., Ferrara E. C., Kaye A. B., Thaller M. L., 1998, ApJ, 493, 440
Girven J. et al., 2012, MNRAS, 425, 1013
Green E. M. et al., 2003, ApJ, 583, L31
Green E. M. et al., 2004, Ap&SS, 291, 267
Green E. M., For B.-Q., Hyde E. A., 2005, in Koester D., Moehler S., eds, ASP Conf. Ser. Vol. 334, 14th European Workshop on White Dwarfs. Astron. Soc. Pac., San Francisco, p. 363
Han Z., Podsiadlowski Ph., Maxted P. F. L., Marsh T. R., Ivanova N., 2002, MNRAS, 336, 449
Han Z., Podsiadlowski Ph., Maxted P. F. L., Marsh T. R., 2003, MNRAS, 341, 669
Heber U., 1986, A&A, 155, 33
Heber U., 2009, ARA&A, 47, 211
Heber U., Reid I. N., Werner K., 2000, A&A, 363, 198
Heber U., Moehler S., Napiwotzki R., Thejll P., Green E. M., 2002, A&A, 383, 938
Heber U., Edelmann H., Lisker T., Napiwotzki R., 2003, A&A, 411, L477
Heber U. et al., 2004, A&A, 420, 251
Heintz W. D., 1992, ApJS, 83, 351
Hogg D. W., Blanton M. R., Roweis S. T., Johnston K. V., 2005, ApJ, 629, 268
Jeffery C. S., Ramsay G., 2014, MNRAS, 442, L61
Jeffery C. S., Simon T., 1997, MNRAS, 286, 487
Jeffery C. S., Simon T., Lloyd Evans T., 1992, MNRAS, 258, 64
Jester S. et al., 2005, AJ, 130, 873
Jiménez-Esteban F. M., Caballero J. A., Solano E., 2011, A&A, 525, A29
Johnson D. R. H., Soderblom D. R., 1987, AJ, 93, 864
Justham S., Podsiadlowski P., Han Z., 2011, MNRAS, 410, 984
Karl C., Heber U., Napiwotzki R., Geier S., 2006, Balt. Astron., 15, 151
Kawaler S. D. et al., 2010, MNRAS, 409, 1509
Kawka A., Vennes S., 2012, MNRAS, 425, 1394
Kawka A., Vennes S., Németh P., Kraus M., Kubát J., 2010, MNRAS, 408, 992
Kawka A. et al., 2012, in Kilkenny D., Jeffery C. S., Koen C., eds, ASP Conf. Ser. Vol. 452, Fifth Meeting on Hot Subdwarf Stars and Related Objects. Astron. Soc. Pac., San Francisco, p. 121
Kepler S. O., Giovannini O., Kanaan A., Wood M. A., Claver C. F., 1995, Balt. Astron., 4, 157
Kepler S. O., Kleinman S. J., Nitta A., Koester D., Castanheira B. G., Giovannini O., Costa A. F. M., Althaus L., 2007, MNRAS, 375, 1315
Kilic M., Brown W. R., Allende Prieto C., Agüeros M. A., Heinke C., Kenyon S. J., 2011, ApJ, 727, 3
Kilkenny D., 1984, MNRAS, 211, 969
Kilkenny D., Keuris S., Marang F., Roberts G., van Wyk F., Ogloza W., 2000, The Observatory, 120, 48
Kilkenny D., Koen C., Worters H., 2010, MNRAS, 404, 376
Klepp S., Rauch T., 2011, A&A, 531, L7
Koen C., 2009, MNRAS, 395, 979
Koen C., Green E. M., 2010, MNRAS, 406, 2701
Koen C., Orosz J. A., Wade R. A., 1998, MNRAS, 300, 695
Koen C., Kilkenny D., Pretorius M. L., Frew D. J., 2010, MNRAS, 401, 1850
Kroupa P., 2001, MNRAS, 322, 231
Kupfer T. et al., 2014, in van Grootel V., Green E., Fontaine G., Charpinet S., eds, ASP Conf. Ser. Vol. 481, Sixth Meeting on Hot Subdwarf Stars and Related Objects. Astron. Soc. Pac., San Francisco, p. 293
Kupfer T. et al., 2015, A&A, 576, A44
Landstreet J. D., Bagnulo S., Fossati L., Jordan S., O'Toole S. J., 2012, A&A, 541, A100
Lanz T., Brown T. M., Sweigart A. V., Hubeny I., Landsman W. B., 2004, ApJ, 602, 342
Latour M., Fontaine G., Green E. M., Brassard P., Chayer P., 2014, ApJ, 788, 65
Lemke M., 1997, A&AS, 122, 285
Liebert J., Saffer R. A., Green E. M., 1994, AJ, 107, 1408
Lisker T., Heber U., Napiwotzki R., Christlieb N., Reimers D., Homeier D., 2004, Ap&SS, 291, 351

Lisker T., Heber U., Napiwotzki R., Christlieb N., Han Z., Homeier D., Reimers D., 2005, A&A, 430, 223
Lynas-Gray A. E., 2012, in Kilkenny D., Jeffery C. S., Koen C., eds, ASP Conf. Ser. Vol. 452, Fifth Meeting on Hot Subdwarf Stars and Related Objects. Astron. Soc. Pac., San Francisco, p. 213
Mathys G., Hubrig S., Mason E., Michaud G., Schöller M., Wesemael F., 2012, Astron. Nachr., 333, 30
Maxted P. F. L., Moran C. K. J., Marsh T. R., Gatti A. A., 2000a, MNRAS, 311, 877
Maxted P. F. L., Marsh T. R., North R. C., 2000b, MNRAS, 317, L41
Maxted P. F. L., Heber U., Marsh T. R., North R. C., 2001, MNRAS, 326, 1391
Maxted P. F. L., Marsh T. R., Heber U., Morales-Rueda L., North R. C., Lawson W. A., 2002, MNRAS, 333, 231
Maxted P. F. L. et al., 2011, MNRAS, 418, 1156
Maxted P. F. L. et al., 2014, MNRAS, 437, 1681
Mengel J. G., Norris J., Gross P. G., 1976, ApJ, 204, 488
Mereghetti S., La Palombara N., Tiengo A., Sartore N., Esposito P., Israel G. L., Stella L., 2013, A&A, 553, A46
Mickaelian A. M., 2008, AJ, 136, 946
Moehler S., Heber U., de Boer K. S., 1990, A&A, 239, 265
Morales-Rueda L., Maxted P. F. L., Marsh T. R., North R. C., Heber U., 2003, MNRAS, 338, 752
Moran C., Maxted P., Marsh T. R., Saffer R. A., Livio M., 1999, MNRAS, 304, 535
Morrissey P. et al., 2007, ApJS, 173, 682
Müller S., Geier S., Heber U., 2010, Ap&SS, 329, 101
Napiwotzki R., Edelmann H., Heber U., Karl C., Drechsel H., Pauli E.-M., Christlieb N., 2001, A&A, 378, L17
Napiwotzki R., Karl C. A., Lisker T., Heber U., Christlieb N., Reimers D., Nelemans G., Homeier D., 2004, Ap&SS, 291, 321
Naslim N., Geier S., Jeffery C. S., Behara N. T., Woolf V. M., Classen L., 2012, MNRAS, 423, 3031
Németh P., Kawka A., Vennes S., 2012, MNRAS, 427, 2180
O'Toole S. J., Heber U., 2006, A&A, 452, 579
O'Toole S. J., Heber U., Benjamin R. A., 2004, A&A, 422, 1053
O'Toole S. J., Jordan S., Friedrich S., Heber U., 2005, A&A, 437, 227
O'Toole S. J., Napiwotzki R., Heber U., Drechsel H., Frandsen S., Grundahl F., Bruntt H., 2006, Balt. Astron., 15, 61
Orosz J. A., Wade R. A., 1999, MNRAS, 310, 773
Østensen R. H., Van Winckel H., 2012, in Kilkenny D., Jeffery C. S., Koen C., eds, ASP Conf. Ser. Vol. 452, Fifth Meeting on Hot Subdwarf Stars and Related Objects. Astron. Soc. Pac., San Francisco, p. 163
Østensen R., Heber U., Maxted P., 2005, in Koester D., Moehler S., eds, ASP Conf. Ser. Vol. 334, 14th European Workshop on White Dwarfs. Astron. Soc. Pac., San Francisco, p. 435
Østensen R., Oreiro R., Drechsel H., Heber U., Baran A., Pigulski A., 2007, in Napiwotzki R., Burleigh M. R., eds, ASP Conf. Ser. Vol. 372, 15th European Workshop on White Dwarfs. Astron. Soc. Pac., San Francisco, p. 483
Østensen R. et al., 2010a, MNRAS, 408, L51
Østensen R. et al., 2010b, MNRAS, 409, 1470
Østensen R. H. et al., 2010c, A&A, 513, A6
Østensen R. et al., 2011, MNRAS, 414, 2860
Østensen R. et al., 2013, A&A, 559, A35
Østensen R., Telting J. H., Reed M. D., Baran A. S., Németh P., Kiaeerad F., 2014, A&A, 569, A15
Pablo H., Kawaler S. D., Green E. M., 2011, ApJ, 740, L47
Pauli E.-M., Napiwotzki R., Heber U., Altmann M., Odenkirchen M., 2006, A&A, 447, 173
Pecaut M. J., Mamajek E. E., 2013, ApJS, 208, 9
Peters G. J., Gies D. R., Grundstrom E. D., McSwain M. V., 2008, ApJ, 686, 1280
Peters G. J., Pewett T. D., Gies D. R., Touhami Y. N., Grundstrom E. D., 2013, ApJ, 765, 2
Pojmanski G., 1997, Acta Astron., 47, 467
Pollacco D. L. et al., 2006, PASP, 118, 1407
Pols O. R., Coté J., Waters L. B. F. M., Heise J., 1991, A&A, 241, 419
Polubek G., Pigulski A., Baran A., Udalski A., 2007, in Napiwotzki R., Burleigh M. R., eds, ASP Conf. Ser. Vol. 372, 15th European Workshop on White Dwarfs. Astron. Soc. Pac., San Francisco, p. 487
Press W. H., Teukolsky S. A., Vetterling W. T., Flannery B. P., 1992, Numerical Recipes in FORTRAN. The Art of Scientific Computing, 2nd edn. Cambridge Univ. Press, Cambridge
Reed M. D. et al., 2004, ApJ, 607, 445
Reed M. D. et al., 2010, Ap&SS, 329, 83
Saffer R. A., Bergeron P., Koester D., Liebert J., 1994, ApJ, 432, 351
Saffer R. A., Livio M., Yungelson L. R., 1998, ApJ, 502, 394
Schaffenroth V., Geier S., Drechsel H., Heber U., Wils P., Østensen R., Maxted P. F. L., di Scala G., 2013, A&A, 553, A18
Schaffenroth V., Geier S., Barbu-Barna I., Heber U., Kupfer T., Cordes O., 2014a, in van Grootel V., Green E., Fontaine G., Charpinet S., eds, ASP Conf. Ser. Vol. 481, 6th Meeting on Hot Subdwarf Stars and Related Objects. Astron. Soc. Pac., San Francisco, p. 253
Schaffenroth V., Geier S., Heber U., Kupfer T., Ziegerer E., Heuser C., Classen L., Cordes O., 2014b, A&A, 564, A98
Schaffenroth V., Classen L., Nagel K., Geier S., Koen C., Heber U., Edelmann H., 2014c, A&A, 570, A70
Schindler J.-T., Green E. M., Arnett W. D., 2014, preprint (arXiv:1410.8204)
Schlegel D. J., Finkbeiner D. P., Davis M., 1998, ApJ, 500, 525
Schoenaers C., Lynas-Gray A. E., 2007, Commun. Asteroseismol., 151, 67
Şener H. T., Jeffery C. S., 2014, MNRAS, 440, 2676
Silvotti R. et al., 2012, MNRAS, 424, 1752
Skrutskie M. F. et al., 2006, AJ, 131, 1163
Solheim J.-E., 2010, PASP, 122, 1133
Stroeer A., Heber U., Lisker T., Napiwotzki R., Dreizler S., Christlieb N., Reimers D., 2007, A&A, 462, 269
Telting J. H., Østensen R., Oreiro R., Reed M., Farris L., O'Toole S., Aerts C., 2012a, in Kilkenny D., Jeffery C. S., Koen C., eds, ASP Conf. Ser. Vol. 452, Fifth Meeting on Hot Subdwarf Stars and Related Objects. Astron. Soc. Pac., San Francisco, p. 147
Telting J. H. et al., 2012b, A&A, 544, A1
Telting J. H., Østensen R., Reed M., Kiaeerad F., Farris L., Baran A., Oreiro R., O'Toole S., 2014a, in van Grootel V., Green E., Fontaine G., Charpinet S., eds, ASP Conf. Ser. Vol. 481, 6th Meeting on Hot Subdwarf Stars and Related Objects. Astron. Soc. Pac., San Francisco, p. 287
Telting J. H. et al., 2014b, A&A, 570, A129
Thackeray A. D., 1970, MNRAS, 150, 215
Thejll P., Ulla A., MacDonald J., 1995, A&A, 303, 773
Tremblay P.-E., Bergeron P., 2009, ApJ, 696, 1755
Ulla A., Thejll P., 1998, A&AS, 132, 1
Vaccaro T. R., Wilson R. E., 2003, MNRAS, 342, 564
Vaccaro T. R., Silver I., Kawka A., Vennes S., Németh P., Wilson R. E., 2007, BAAS, 39, 728
Vennes S., Kawka A., Németh P., 2011, MNRAS, 410, 2095
Vennes S., Kawka A., O'Toole S. J., Németh P., Burton D., 2012, ApJ, 759, L25
Verbeek K. et al., 2012, MNRAS, 426, 1235
Vos J., Østensen R., Németh P., Green E. M., Heber U., Van Winckel H., 2013, A&A, 559, A54
Vos J., Østensen R., Van Winckel H., 2014, in van Grootel V., Green E., Fontaine G., Charpinet S., eds, ASP Conf. Ser. Vol. 481, 6th Meeting on Hot Subdwarf Stars and Related Objects. Astron. Soc. Pac., San Francisco, p. 265
Vučković M., Aerts C., Östensen R., Nelemans G., Hu H., Jeffery C. S., Dhillon V. S., Marsh T. R., 2007, A&A, 471, 605
Vučković M., Østensen R., Bloemen S., Decoster I., Aerts C., 2008, in Heber U., Jeffery C. S., Napiwotzki R., eds, ASP Conf. Ser. Vol. 392, Hot Subdwarf Stars and Related Objects. Astron. Soc. Pac., San Francisco, p. 199
Woźniak P. R. et al., 2004, AJ, 127, 2436
Wright E. L. et al., 2010, AJ, 140, 1868
Zacharias N., Finch C. T., Girard T. M., Henden A., Bartlett J. L., Monet D. G., Zacharias M. I., 2013, AJ, 145, 44
Zhang X., Chen X., Han Z., 2009, A&A, 504, L13

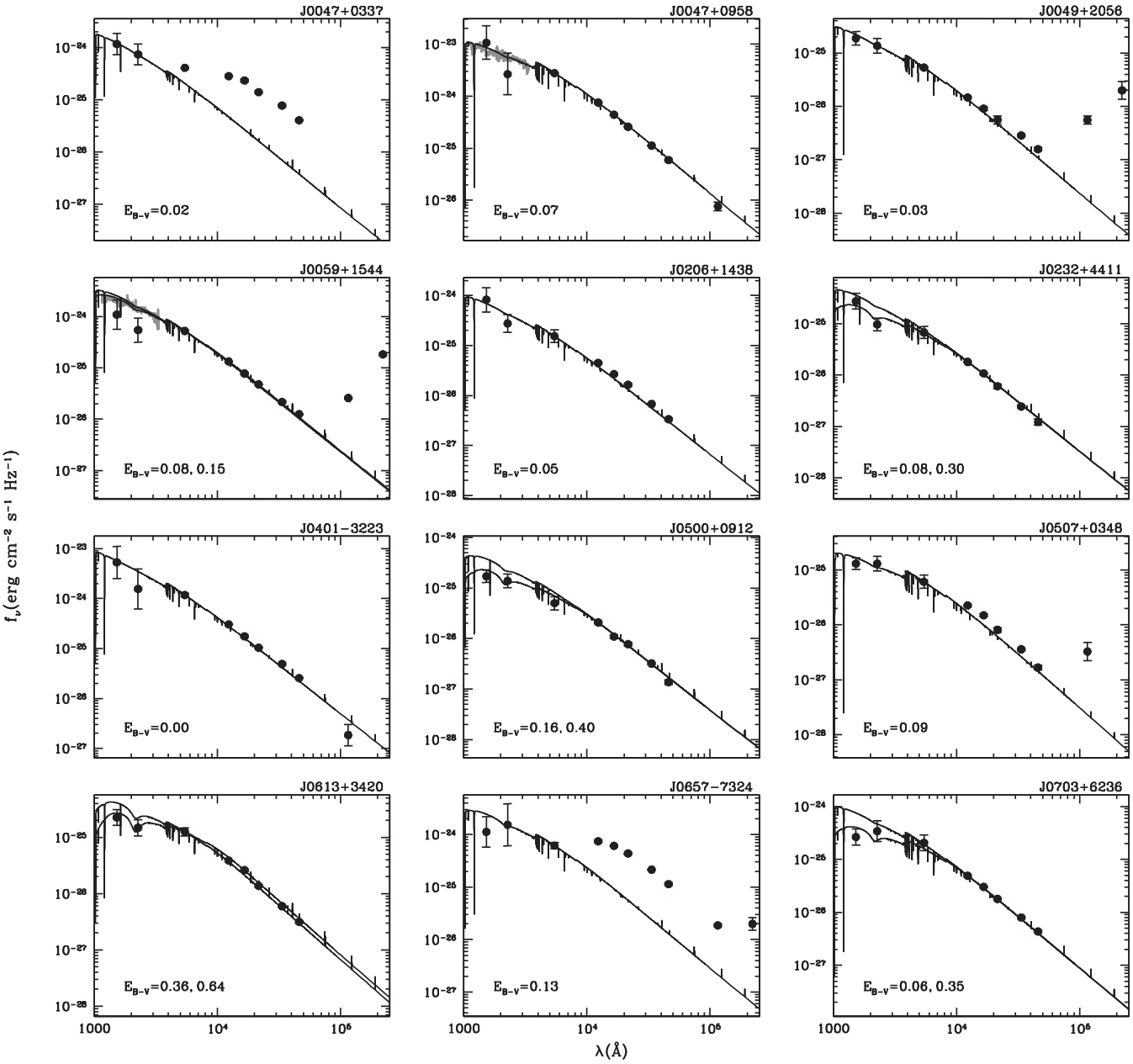

Figure A1. SED of the observed *GALEX* sample.

APPENDIX A: PHOTOMETRY AND SEDS

Figs A1–A3 show available photometry from Table A1 compared to model spectra. The extinction was determined by comparing the observed photometry with the model spectrum. Extinction was measured towards several sdB stars (e.g. Moehler, Heber & de Boer 1990; Aznar Cuadrado & Jeffery 2001) and given that these stars are spread throughout the Galaxy, i.e. at high latitudes and in the Galactic plane, the extinction coefficients $E(B-V)$ can vary from 0 to as much as 0.4. In these cases, the extinction was measured using *IUE* spectra combined with optical and infrared photometry. We used the parametrized extinction law as defined by Cardelli, Clayton & Mathis (1989) with $R = 3.2$.

We acquired from the Mikulski Archive for Space Telescopes (MAST) the following set of *IUE* spectra:

J0047+0958: swp26276mxlo and lwp07169mxlo,
J0059+1544: swp27142mxlo and lwp07144mxlo,
J1435+0013: swp23176mxlo and lwp03501mxlo,
J1632+0759: swp33790mxlo and lwp13481mxlo,
J1902−5130: swp17051mxlo and lwr13321mxlo,
J2344−3426: swp17981mxlo.

The model distributions include the effect of interstellar extinction with the line-of-sight extinction coefficient obtained from Schlegel et al. (1998). Also, we experimented with larger coefficients in an attempt to match SEDs showing possible intrinsic absorption. For example, the SED of J1632+0759 reveals the presence of an infrared flux excess as well as a larger extinction that revealed in Schlegel et al. (1998)'s maps.

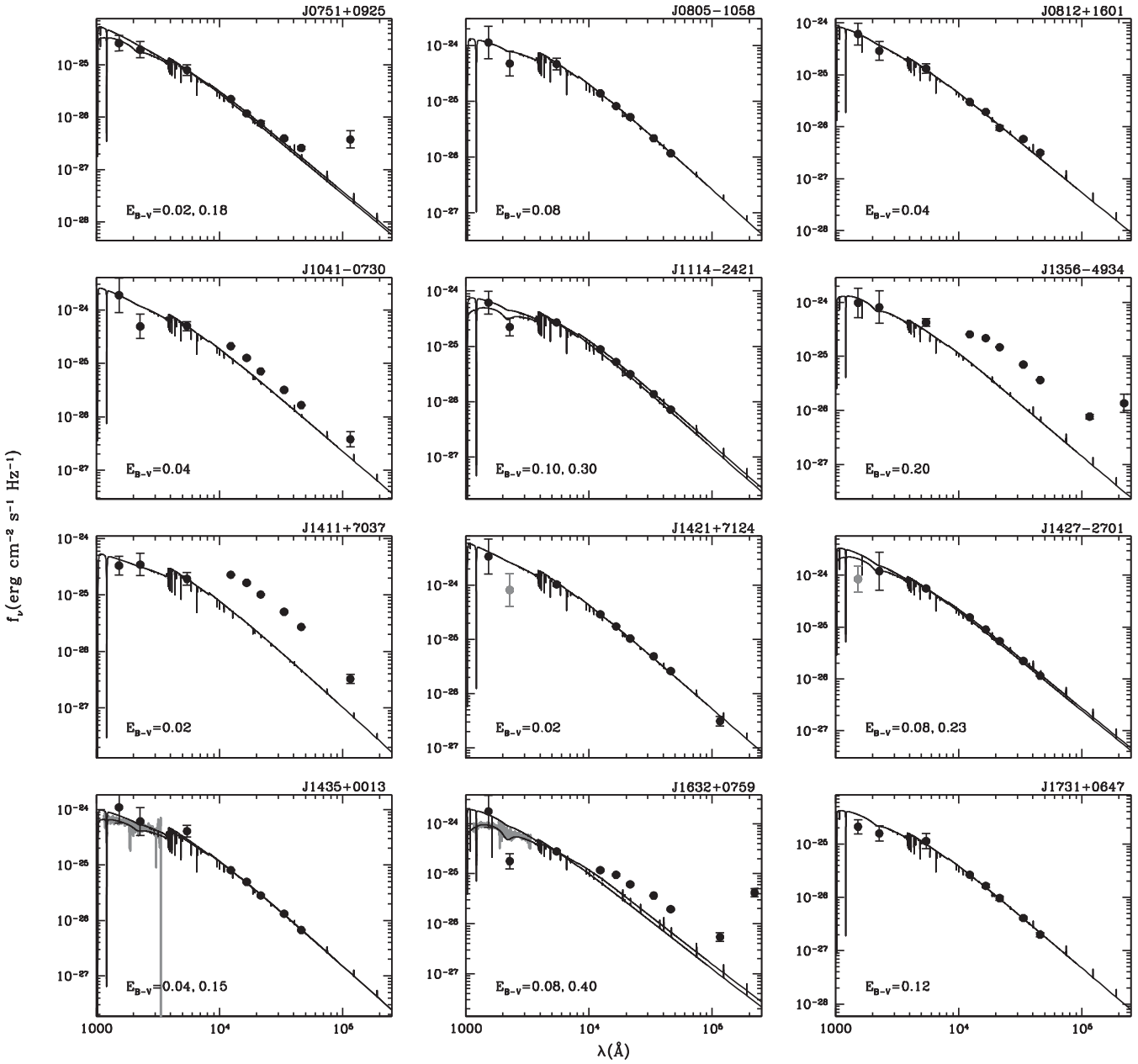

Figure A2. SED of the observed *GALEX* sample.

APPENDIX B: RADIAL VELOCITY MEASUREMENTS

Table B1 lists the heliocentric-corrected velocity measurements (v), the mid-exposure heliocentric julian dates (HJD) and data sources. The instrument configurations and error estimates are described in Sections 2.1 and 2.2, respectively, and the measurement procedures are described in Section 3.1.3.

Stars labelled with the suffix 'B' are the 'secondary' components of each system. The radial velocities are those of that secondary component.

The label 'SSO' refers to spectra obtained with the WiFeS attached to the 2.3 m telescope at Siding Spring Observatory; the label 'KPNO' refers to spectra obtained with the 4-m telescope and R.-C. Spectrograph at Kitt Peak National Observatory; the label 'NTT' refers to spectra obtained using EFOSC2 attached to the New Technology Telescope at La Silla; the label 'OND' refers to spectra obtained using the coudé spectrograph and the 2-m telescope at Ondřejov Observatory; the label 'SAAO' refers to spectra obtained at the South African Astronomical Observatory using the 74-inch telescope and the Cassegrain spectrograph; and new and archival spectra are labelled 'FEROS' for the Fiber-fed Extended Range Optical Spectrograph on the MPG 2.2-m telescope at La Silla, and 'INT' and 'WHT' for spectrographs attached to the Isaac Newton Telescope and William Herschel Telescope at La Palma.

APPENDIX C: HOT SUBDWARF BINARY SYSTEMS

We have compiled a list of all known hot subdwarf binary systems. Table C1 lists the name of the system, its coordinates, proper motion, V magnitudes, orbital period in days, the systemic velocity (γ) and

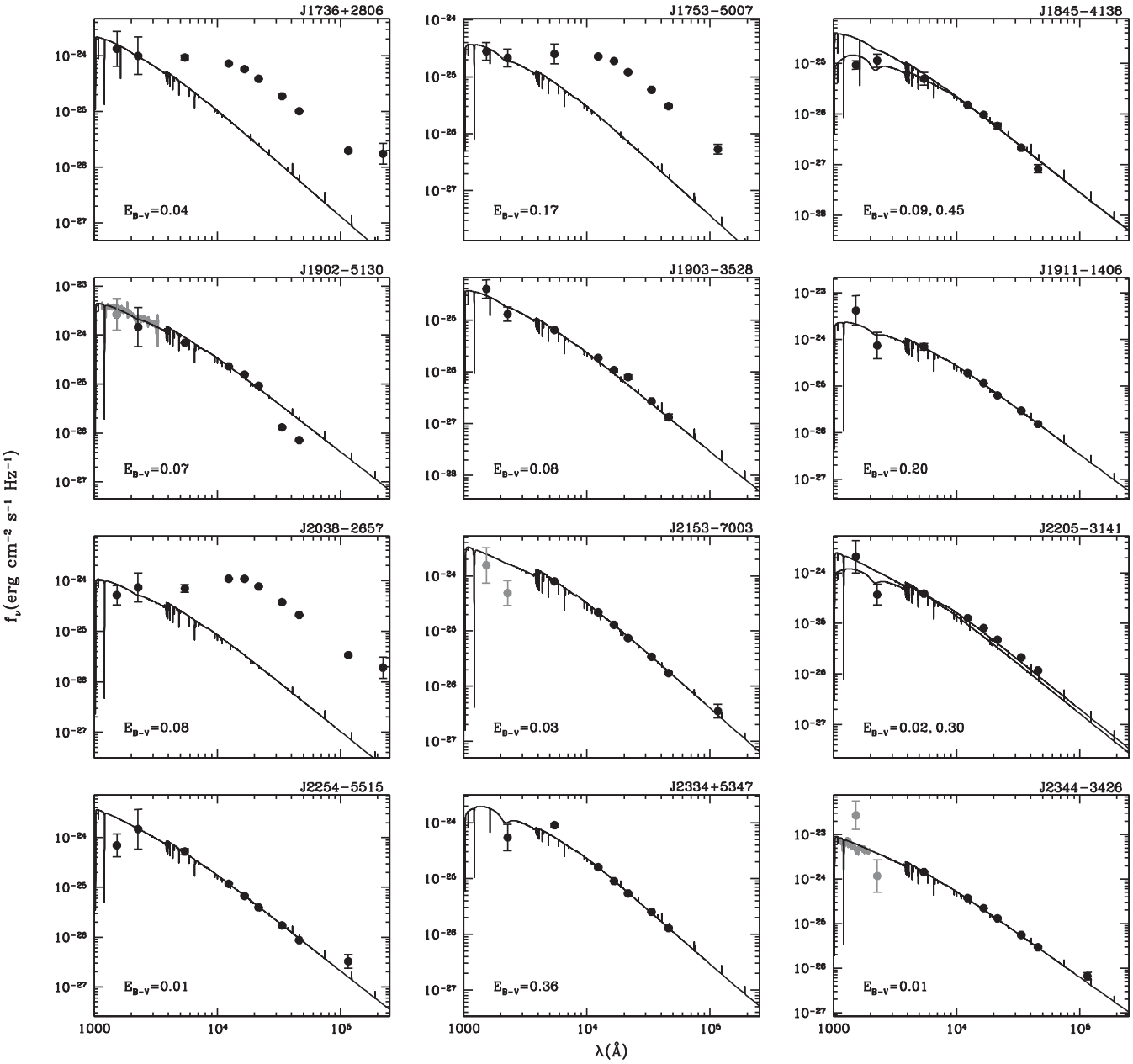

Figure A3. SED of the observed *GALEX* sample.

the velocity semi-amplitude of the hot subdwarf (K). The table also lists the eccentricity (e) of the system if the orbit of the binary was found to be eccentric. If the companion to the hot subdwarf is known, it is listed and also if the system is photometrically variable, this is also noted in the table. The proper motions and V magnitudes for the objects are from The fourth US Naval Observatory CCD Astrograph Catalog (UCAC4; Zacharias et al. 2013). For those objects that are not in the UCAC4 and has Sloan Digital Sky Survey (SDSS) photometry, we calculated V magnitudes using the transformation equation of Jester et al. (2005),

$$V = g - 0.58(g - r) - 0.01.$$

The references for the binary system properties are provided in the final column. GALEX J1736+2806 and J2038−2657 are not included in Table C1 because the photometric variations are not clearly associated with orbital periodicities. New Kepler identifications (KIC) are added to the list despite current lack of radial velocity data because of the higher quality of light-curve analysis and the timeliness of the results. Table C2 lists published stellar parameters (with relevant references) and calculated absolute V magnitude and Galactic velocity vectors (U, V, W). The mass of sdO companions to Be stars is assumed to be $1\,M_{\odot}$ and that of low-mass sdB stars is assumed to be $0.23\,M_{\odot}$.

Table A1. Photometric measurements.

GALEX J	F_{UV} 1528 Å (mag)	N_{UV} 2271 Å (mag)	V 5455 Å (mag)	J 1.235 μm (mag)	H 1.662 μm (mag)	K 2.159 μm (mag)	$W1$ 3.353 μm (mag)	$W2$ 4.603 μm (mag)	$W3$ 11.561 μm (mag)	$W4$ 22.088 μm (mag)
004759.6+033742	11.24 ± 0.52	11.74 ± 0.40	12.352 ± 0.013	*11.880 ± 0.036*[a]	*11.629 ± 0.041*[a]	*11.697 ± 0.038*[a]	11.498 ± 0.034	11.569 ± 0.039	–	–
004729.4+095855	8.84 ± 0.80	10.34 ± 1.00	10.272 ± 0.004	10.816 ± 0.023	10.939 ± 0.032	11.027 ± 0.020	11.089 ± 0.023	11.148 ± 0.021	11.449 ± 0.209	–
004917.2+205640	13.22 ± 0.32	13.56 ± 0.34	14.559 ± 0.009	15.091 ± 0.043	15.153 ± 0.078	15.189 ± 0.190	15.081 ± 0.037	15.077 ± 0.086	11.796 ± 0.194	9.047 ± 0.413
005956.7+154419	11.30 ± 0.71	12.06 ± 0.59	12.076 ± 0.004	12.696 ± 0.021	12.818 ± 0.030	12.865 ± 0.028	12.874 ± 0.024	12.838 ± 0.027	–	–
020656.1+143900	11.62 ± 0.62	12.80 ± 0.44	13.41 ± 0.31	13.874 ± 0.024	13.976 ± 0.038	14.017 ± 0.058	14.139 ± 0.030	14.266 ± 0.047	–	–
023251.9+441126	12.80 ± 0.38	13.93 ± 0.31	14.30 ± 0.29	14.855 ± 0.036	14.963 ± 0.056	15.096 ± 0.106	15.249 ± 0.049	15.360 ± 0.145	–	–
040105.3−322348	9.59 ± 0.80	10.92 ± 1.00	11.20 ± 0.08	11.794 ± 0.024	11.937 ± 0.024	12.017 ± 0.025	12.000 ± 0.023	12.062 ± 0.023	12.992 ± 0.525	–
050018.9+091203	13.32 ± 0.30	13.55 ± 0.35	14.63 ± 0.33	14.713 ± 0.036	14.951 ± 0.079	14.840 ± 0.099	14.960 ± 0.041	15.236 ± 0.118	–	–
050735.7+034814	13.62 ± 0.26	13.62 ± 0.34	14.42 ± 0.30	14.625 ± 0.037	14.620 ± 0.055	14.786 ± 0.105	14.837 ± 0.041	15.029 ± 0.105	12.374 ± 0.407	–
061325.3+342053	13.01 ± 0.35	13.48 ± 0.35	13.63 ± 0.18	14.038 ± 0.028	14.011 ± 0.041	14.212 ± 0.063	14.283 ± 0.033	14.335 ± 0.062	–	–
065736.7−732447	11.27 ± 0.72	10.93 ± 1.00	11.90 ± 0.14	10.830 ± 0.030	10.578 ± 0.032	10.462 ± 0.023	10.387 ± 0.022	10.438 ± 0.020	10.477 ± 0.052	9.042 ± 0.303
070331.5+623626	12.84 ± 0.37	12.56 ± 0.49	13.10 ± 0.37	13.775 ± 0.054	13.842 ± 0.033	13.925 ± 0.054	13.964 ± 0.030	13.991 ± 0.052	–	–
075147.1+092526	12.85 ± 0.37	13.17 ± 0.38	14.12 ± 0.26	14.638 ± 0.036	14.865 ± 0.049	14.850 ± 0.116	14.728 ± 0.036	14.549 ± 0.076	12.221 ± 0.414	–
080510.9−105834	11.27 ± 0.72	12.21 ± 0.56	12.21 ± 0.27	12.647 ± 0.024	12.764 ± 0.023	12.762 ± 0.030	12.871 ± 0.024	12.912 ± 0.027	–	–
081233.6+160123	11.93 ± 0.52	12.74 ± 0.45	13.57 ± 0.22	14.301 ± 0.030	14.326 ± 0.054	14.605 ± 0.099	14.301 ± 0.032	14.322 ± 0.064	–	–
104148.6−073034	10.72 ± 0.80	12.17 ± 0.57	12.14 ± 0.21	12.202 ± 0.023	12.295 ± 0.027	12.437 ± 0.027	12.468 ± 0.024	12.541 ± 0.026	12.211 ± 0.363	–
111422.0−242130	11.93 ± 0.52	13.03 ± 0.40	12.80 ± 0.01	13.132 ± 0.024	13.248 ± 0.029	13.322 ± 0.043	13.380 ± 0.026	13.447 ± 0.036	–	–
123723.5+250400[b]	–	–	10.509 ± 0.002	11.157 ± 0.022	11.270 ± 0.030	11.367 ± 0.022	11.400 ± 0.023	11.477 ± 0.021	11.591 ± 0.184	–
135629.2−493403	11.42 ± 0.67	11.62 ± 0.75	12.30 ± 0.17	11.983 ± 0.025	11.705 ± 0.029	11.633 ± 0.023	11.601 ± 0.023	11.677 ± 0.022	11.443 ± 0.105	9.468 ± 0.430
141133.3+703737	12.60 ± 0.41	12.55 ± 0.49	13.17 ± 0.28	12.113 ± 0.026	12.004 ± 0.029	12.036 ± 0.027	11.965 ± 0.023	12.000 ± 0.022	12.369 ± 0.203	–
142126.5+712427	10.08 ± 0.80	*11.62 ± 0.75*[a]	11.34 ± 0.08	11.848 ± 0.021	11.950 ± 0.021	12.017 ± 0.028	12.003 ± 0.023	12.047 ± 0.022	12.432 ± 0.219	–
142747.2−270108	*11.58 ± 0.62*[a]	11.20 ± 0.92	12.01 ± 0.01	12.529 ± 0.022	12.669 ± 0.027	12.732 ± 0.029	12.856 ± 0.025	12.926 ± 0.027	–	–
143519.8+001352	11.30 ± 0.71	11.94 ± 0.63	12.36 ± 0.26	13.244 ± 0.032	13.316 ± 0.027	13.436 ± 0.044	13.420 ± 0.024	13.521 ± 0.032	–	–
160011.8−643330[b]	–	–	11.86 ± 0.15	12.568 ± 0.028	12.735 ± 0.036	12.786 ± 0.036	12.860 ± 0.030	12.951 ± 0.037	–	–
163201.4+075940	10.79 ± 0.80	13.28 ± 0.37	12.764 ± 0.049	*12.836 ± 0.034*[a]	12.611 ± 0.042	12.597 ± 0.033	12.318 ± 0.024	12.362 ± 0.028	11.823 ± 0.220	8.248 ± 0.215
173153.7+064706	13.09 ± 0.34	13.40 ± 0.36	13.74 ± 0.36	14.450 ± 0.033	14.512 ± 0.090	14.599 ± 0.090	14.689 ± 0.037	14.832 ± 0.088	–	–
173651.2+280635	11.08 ± 0.78	11.40 ± 0.84	11.44 ± 0.10	10.849 ± 0.027	10.635 ± 0.031	10.592 ± 0.022	10.527 ± 0.023	10.563 ± 0.021	10.410 ± 0.057	9.187 ± 0.462
175340.5−500741	12.79 ± 0.38	13.07 ± 0.39	12.88 ± 0.43	12.114 ± 0.024	11.861 ± 0.023	11.853 ± 0.024	11.786 ± 0.023	11.862 ± 0.024	11.839 ± 0.206	–
184559.8−413826	13.97 ± 0.20	13.76 ± 0.32	14.63 ± 0.32	15.052 ± 0.037	15.087 ± 0.067	15.148 ± 0.137	15.383 ± 0.059	15.785 ± 0.198	–	–
190211.7−513005	*10.35 ± 0.80*[a]	11.00 ± 1.00	11.771 ± 0.001	12.103 ± 0.020	12.063 ± 0.024	12.158 ± 0.023	13.437 ± 0.026	13.451 ± 0.034	–	–
190302.4−352828	12.40 ± 0.44	13.61 ± 0.34	14.35 ± 0.02	14.834 ± 0.044	14.958 ± 0.091	14.813 ± 0.109	15.136 ± 0.047	15.274 ± 0.150	–	–
191109.2−140651	9.84 ± 0.80	11.72 ± 0.71	11.77 ± 0.18	12.314 ± 0.024	12.396 ± 0.024	12.561 ± 0.031	12.544 ± 0.023	12.616 ± 0.031	–	–
203850.3−265750	12.11 ± 0.48	11.72 ± 0.71	11.90 ± 0.19	10.398 ± 0.024	9.944 ± 0.021	9.843 ± 0.022	9.775 ± 0.024	9.772 ± 0.020	–	–
215340.4−700430	*10.92 ± 0.80*[a]	*12.17 ± 0.57*[a]	11.62 ± 0.01	12.152 ± 0.021	12.264 ± 0.025	12.375 ± 0.027	12.383 ± 0.024	12.486 ± 0.027	12.287 ± 0.303	–
220551.8−314105	10.61 ± 0.80	12.47 ± 0.51	12.41 ± 0.02	12.747 ± 0.024	12.783 ± 0.028	12.863 ± 0.034	12.906 ± 0.026	12.903 ± 0.030	–	–
225444.1−551505	11.79 ± 0.56	10.98 ± 1.00	12.08 ± 0.15	12.825 ± 0.024	12.976 ± 0.033	13.068 ± 0.031	13.130 ± 0.025	13.238 ± 0.031	12.373 ± 0.352	–
233451.7+534701	–	12.06 ± 0.59	11.49 ± 0.09	12.502 ± 0.025	12.665 ± 0.026	12.726 ± 0.021	12.718 ± 0.024	12.812 ± 0.027	–	–
234421.6−342655	*7.82 ± 0.80*[a]	*11.23 ± 0.91*[a]	10.982 ± 0.006	11.581 ± 0.028	11.684 ± 0.022	11.771 ± 0.023	11.851 ± 0.023	11.915 ± 0.024	11.604 ± 0.201	–

[a]Possibly unreliable.
[b]Not a *GALEX* source.

Table B1. Radial velocities.

HJD (2450000+)	v (km s^{-1})	Source	HJD (2450000+)	v (km s^{-1})	Source	HJD (2450000+)	v (km s^{-1})	Source	HJD (2450000+)	v (km s^{-1})	Source
GALEX J0047+0337B			$N = 4,\ \bar{v} = 45.3,\ \sigma_v = 4.4$			5930.74878	31.3	KPNO	6047.05680	29.3	SSO
5898.04458	−19.9	SSO	GALEX J0401−3223			5930.80712	18.8	KPNO	6047.08829	31.4	SSO
5899.04507	−23.4	SSO	3953.91980	53.0	FEROS	5930.86267	13.6	KPNO	6700.41812	22.9	SAAO
5930.57007	−22.1	KPNO	4014.75477	52.1	FEROS	5930.91715	5.7	KPNO	6700.47565	34.4	SAAO
5930.57406	−23.5	KPNO	5500.79501	49.3	FEROS	5931.00340	0.5	KPNO	6700.52813	30.5	SAAO
5930.66341	−23.2	KPNO	5900.02546	45.2	SSO	5932.71032	50.9	KPNO	$N = 6,\ \bar{v} = 29.8,\ \sigma_v = 3.5$		
5931.56622	−26.2	KPNO	6171.78071	55.8	NTT	5932.86851	42.3	KPNO	GALEX J1114−2421		
5932.55868	−27.1	KPNO	6171.83654	66.3	NTT	5932.95043	36.1	KPNO	6046.17066	20.2	SSO
6172.84455	−5.7	NTT	6172.75132	56.8	NTT	5933.00770	30.1	KPNO	6047.00935	19.7	SSO
$N = 8,\ \bar{v} = -21.4,\ \sigma_v = 6.3$			6172.78790	52.3	NTT	$N = 9,\ \bar{v} = 25.5,\ \sigma_v = 16.0$			6047.04136	15.7	SSO
GALEX J0047+0958 (HD 4539)			6173.74065	72.0	NTT	GALEX J0751+0925			6047.10305	15.9	SSO
3227.46321	3.7	OND	6173.80204	63.0	NTT	5898.15513	164.5	SSO	6047.99465	16.9	SSO
3227.48556	−0.4	OND	6173.88283	64.4	NTT	5898.20329	−13.8	SSO	6700.43054	7.6	SAAO
3227.50802	−1.4	OND	6700.28962	54.0	SAAO	5899.12739	−113.9	SSO	6700.48786	4.8	SAAO
3229.51947	−2.4	OND	6700.34266	49.4	SAAO	5899.22915	170.8	SSO	6700.53977	16.3	SAAO
3229.54285	−0.2	OND	6700.40330	46.9	SAAO	5930.75957	87.8	KPNO	$N = 8,\ \bar{v} = 14.6,\ \sigma_v = 5.2$		
3255.46637	−0.5	OND	$N = 14,\ \bar{v} = 55.8,\ \sigma_v = 7.6$			5930.81729	92.2	KPNO	Feige 66		
3255.49221	−2.4	OND	GALEX J0500+0912			5930.87413	−127.6	KPNO	5311.46603	−5.5	OND
3255.54837	−3.0	OND	5930.62297	48.5	KPNO	5930.92836	42.6	KPNO	5311.48899	−7.9	OND
3255.57093	−2.1	OND	5930.73469	47.7	KPNO	5930.93931	96.5	KPNO	5311.51191	−4.2	OND
5499.73722	−3.2	FEROS	5931.65783	50.2	KPNO	5930.98374	135.2	KPNO	5311.53487	5.8	OND
5500.56785	−3.7	FEROS	5932.74346	45.0	KPNO	5931.03215	−91.9	KPNO	5311.55792	−7.1	OND
5500.70433	−2.7	FEROS	$N = 4,\ \bar{v} = 47.8,\ \sigma_v = 1.9$			5931.73038	−8.1	KPNO	5312.46039	−3.2	OND
5500.78859	−3.2	FEROS	GALEX J0507+0348			5931.87541	141.4	KPNO	5312.48335	−5.0	OND
5930.55564	−5.0	KPNO	5931.67914	77.7	KPNO	5931.99730	41.9	KPNO	5312.50638	0.0	OND
5930.55774	0.0	KPNO	5931.83227	39.7	KPNO	5932.75723	163.1	KPNO	5312.52952	−4.2	OND
5930.65685	−3.4	KPNO	5931.92094	91.2	KPNO	5932.88029	−4.4	KPNO	5312.55266	−4.7	OND
5931.57524	−3.7	KPNO	5932.69831	116.5	KPNO	5933.01902	−125.4	KPNO	$N = 10,\ \bar{v} = -3.6,\ \sigma_v = 3.7$		
5932.55265	−6.4	KPNO	5932.83768	30.7	KPNO	6046.91015	60.7	SSO	GALEX J1356−4934		
6172.83793	0.1	NTT	5932.89420	28.6	KPNO	6047.93820	163.7	SSO	6046.15529	0.2	SSO
6173.77623	−1.4	NTT	6171.78863	147.5	NTT	$N = 19,\ \bar{v} = 46.1,\ \sigma_v = 101.1$			6046.27506	17.2	SSO
$N = 20,\ \bar{v} = -2.1,\ \sigma_v = 2.1$			6171.84440	155.4	NTT	GALEX J0805−1058			6047.13503	4.8	SSO
GALEX J0049+2056			6171.85811	153.7	NTT	5898.12316	52.8	SSO	6172.47898	12.8	NTT
5930.59893	15.1	KPNO	6171.90134	154.1	NTT	5898.12983	64.7	SSO	6172.49297	7.1	NTT
5930.68516	17.7	KPNO	6172.81341	140.7	NTT	5898.13875	69.2	SSO	6172.51996	15.8	NTT
5931.58588	14.6	KPNO	6172.90675	166.4	NTT	5898.25067	26.9	SSO	6172.54716	8.9	NTT
5932.57896	18.2	KPNO	6173.81997	99.9	NTT	5899.08066	61.3	SSO	6700.49865	20.6	SAAO
$N = 4,\ \bar{v} = 16.4,\ \sigma_v = 1.6$			6173.90692	166.6	NTT	5899.20870	88.4	SSO	6700.56149	8.7	SAAO
GALEX J0059+1544			6700.31140	58.5	SAAO	5900.24103	78.0	SSO	$N = 9,\ \bar{v} = 10.7,\ \sigma_v = 6.1$		
3955.82658	20.6	FEROS	6700.36337	111.9	SAAO	5930.76915	47.5	KPNO	GALEX J1407+3103		
3986.81551	9.6	FEROS	$N = 16,\ \bar{v} = 108.7,\ \sigma_v = 47.9$			5930.82802	88.9	KPNO	5932.03194	−160.6	KPNO
5930.58194	15.5	KPNO	GALEX J0613+3420			5930.88403	42.1	KPNO	5932.97687	−157.3	KPNO
5930.58594	17.3	KPNO	5931.74486	−135.5	KPNO	5930.97349	75.2	KPNO	5933.05659	−164.7	KPNO
5930.67212	20.7	KPNO	5931.84915	−139.9	KPNO	5930.99445	92.6	KPNO	$N = 3,\ \bar{v} = -160.9,\ \sigma_v = 3.0$		
5931.60011	13.1	KPNO	5931.93741	−138.7	KPNO	5931.75141	42.1	KPNO	GALEX J1411+7037B		
5932.56969	14.9	KPNO	5932.72107	−40.9	KPNO	5931.88363	85.1	KPNO	5932.00693	−18.0	KPNO
5932.72419	18.3	KPNO	$N = 4,\ \bar{v} = -113.7,\ \sigma_v = 42.1$			5931.98199	45.6	KPNO	5932.04748	−17.6	KPNO
6172.83077	12.4	NTT	GALEX J0657−7324			5932.86147	49.1	KPNO	5932.99447	−14.9	KPNO
6173.78258	21.6	NTT	6047.87067	−7.0	SSO	5932.94370	73.5	KPNO	5933.06557	−20.9	KPNO
$N = 10,\ \bar{v} = 16.4,\ \sigma_v = 3.8$			6171.82808	−11.3	NTT	6046.92589	31.8	SSO	$N = 4,\ \bar{v} = -17.9,\ \sigma_v = 2.1$		
GALEX J0206+1438			6171.92035	−17.6	NTT	6046.96533	36.0	SSO	GALEX J1421+7124		
5932.64012	19.8	KPNO	6172.80377	−11.7	NTT	6047.95401	48.4	SSO	5461.35716	−24.2	OND
5932.76929	23.2	KPNO	6172.91817	1.1	NTT	6700.39670	36.6	SAAO	5461.38072	−22.3	OND
6172.76462	19.9	NTT	6172.92477	−12.6	NTT	6700.46184	59.2	SAAO	5461.40360	−25.5	OND
6172.79845	4.1	NTT	6700.33004	−16.0	SAAO	6700.51455	86.2	SAAO	5462.34435	−29.5	OND
6172.89971	9.8	NTT	6700.37998	−13.9	SAAO	$N = 23,\ \bar{v} = 60.1,\ \sigma_v = 20.0$			5462.36727	−19.9	OND
6173.75136	1.6	NTT	6700.44564	−19.7	SAAO	GALEX J0812+1601			5462.64138	−17.4	OND
6173.81315	12.5	NTT	$N = 9,\ \bar{v} = -12.1,\ \sigma_v = 5.8$			5898.18568	−26.7	SSO	5463.32822	−21.2	OND
6173.92187	19.6	NTT	GALEX J0703+6236			5898.23480	−20.9	SSO	5463.35791	−25.7	OND
$N = 8,\ \bar{v} = 13.8,\ \sigma_v = 7.5$			5931.04474	24.2	KPNO	5932.85141	1.3	KPNO	5464.32919	−23.3	OND
GALEX J0232+4411			5931.71772	18.3	KPNO	5932.93361	−1.6	KPNO	5464.35893	−24.2	OND
5931.61405	41.1	KPNO	5931.85802	17.6	KPNO	5933.02934	−4.1	KPNO	5470.25157	−24.4	OND
5931.81305	52.1	KPNO	5931.94502	19.8	KPNO	$N = 5,\ \bar{v} = -10.4,\ \sigma_v = 11.2$			5483.25104	−35.4	OND
5932.65498	46.2	KPNO	$N = 4,\ \bar{v} = 20.0,\ \sigma_v = 2.6$			GALEX J1041−0730			5794.51260	−28.6	OND
5932.81723	41.8	KPNO	GALEX J0716+2319			6046.11527	30.0	SSO	$N = 13,\ \bar{v} = -24.7,\ \sigma_v = 4.4$		

Table B1 – *continued*

HJD (2450000+)	v (km s^{-1})	Source	HJD (2450000+)	v (km s^{-1})	Source	HJD (2450000+)	v (km s^{-1})	Source	HJD (2450000+)	v (km s^{-1})	Source
GALEX J1427−2701			5757.01406	−4.4	SSO	5757.09665	7.1	SSO	5898.96627	66.8	SSO
6048.11285	−6.6	SSO	6048.21613	52.3	SSO	5757.10547	14.4	SSO	5898.99478	67.3	SSO
6171.47061	10.9	NTT	6171.57012	28.2	NTT	5760.12396	14.0	SSO	5899.02602	60.4	SSO
6171.48306	6.8	NTT	6171.59018	27.1	NTT	5761.03781	20.1	SSO	5899.98304	48.7	SSO
6171.49578	1.1	NTT	6171.60924	17.8	NTT	5761.09468	8.6	SSO	6171.72238	−38.2	NTT
6171.50953	3.5	NTT	6171.63315	13.7	NTT	6171.68438	10.4	NTT	6171.77618	−50.8	NTT
6171.52366	5.2	NTT	6172.56912	51.2	NTT	6171.74097	10.7	NTT	6171.82488	−69.0	NTT
6171.53666	−0.5	NTT	6172.60585	42.9	NTT	6172.65633	18.1	NTT	6171.89529	−78.4	NTT
6172.50574	0.6	NTT	6172.62568	35.3	NTT	6172.72634	4.9	NTT	6172.63823	72.5	NTT
6172.53333	−7.6	NTT	6361.86864	−70.0	NTT	$N = 9,\ \bar{v} = 12.0,\ \sigma_v = 4.7$			6172.70799	50.3	NTT
6700.57282	−12.0	SAAO	6361.90960	−84.9	NTT	GALEX J1903−3528			6172.77525	28.4	NTT
6700.60630	−5.0	SAAO	6429.53360	51.7	INT	6171.70234	−29.7	NTT	6172.85901	−11.3	NTT
$N = 11,\ \bar{v} = -0.3,\ \sigma_v = 6.6$			6870.49571	−17.8	NTT	6171.75097	−37.6	NTT	6173.67386	71.5	NTT
GALEX J1435+0013			6870.61105	29.4	NTT	6172.67409	−17.3	NTT	6173.73606	98.9	NTT
3829.84393	−5.5	FEROS	6870.69156	29.8	NTT	6172.73670	−25.6	NTT	6173.79014	96.8	NTT
4137.79323	−3.2	FEROS	$N = 16,\ \bar{v} = 11.4,\ \sigma_v = 40.0$			6173.70238	−2.9	NTT	6173.87812	55.8	NTT
5756.90232	−16.0	SSO	GALEX J1736+2806B			$N = 5,\ \bar{v} = -22.6,\ \sigma_v = 11.8$			6870.63480	96.2	NTT
6046.18707	−3.7	SSO	5045.37797	−14.2	OND	GALEX J1911−1406			6870.71233	93.8	NTT
6047.22908	−6.5	SSO	5045.39926	−16.5	OND	5760.14357	−156.8	SSO	6870.86537	58.6	NTT
6047.26718	2.2	SSO	5310.44503	−19.6	OND	5761.05696	−147.0	SSO	6989.54548	54.3	FEROS
6048.04105	3.6	SSO	5310.46808	−8.2	OND	5761.12734	−151.3	SSO	6990.55028	−34.2	FEROS
6048.07142	−5.9	SSO	5310.49159	−16.9	OND	$N = 3,\ \bar{v} = -151.7,\ \sigma_v = 4.0$			6994.58156	75.6	FEROS
6048.09997	−4.6	SSO	5310.51449	−7.4	OND	GALEX J2153−7003			$N = 24,\ \bar{v} = 32.6,\ \sigma_v = 55.0$		
6700.58473	−12.6	SAAO	5310.53754	−14.7	OND	3918.75562	43.4	FEROS	GALEX J2334+5347		
6700.62607	−6.0	SAAO	5310.56068	−9.3	OND	3956.76278	42.5	FEROS	5461.43461	40.3	OND
$N = 11,\ \bar{v} = -5.3,\ \sigma_v = 5.3$			5310.58391	−13.9	OND	5757.17717	41.8	SSO	5461.48740	36.1	OND
J1600−6433			5311.58102	−13.2	OND	5757.18600	43.1	SSO	5461.55799	31.5	OND
5756.93811	55.6	SSO	5311.60395	−18.7	OND	5761.21680	44.2	SSO	5461.58084	44.7	OND
5756.94716	55.1	SSO	5312.57540	−11.5	OND	5897.97485	41.4	SSO	5462.39976	46.5	OND
5757.03853	48.6	SSO	5312.59830	−7.9	OND	5897.98518	36.9	SSO	5462.42295	41.0	OND
5757.04736	53.6	SSO	5377.40465	−11.8	OND	5898.94745	39.8	SSO	5462.59518	31.6	OND
5757.96919	65.3	SSO	5377.42598	−6.9	OND	5898.95287	42.1	SSO	5462.61797	42.5	OND
5757.97801	56.6	SSO	5430.35500	−9.3	OND	5898.97969	40.3	SSO	5463.41196	37.9	OND
5760.98197	41.6	SSO	5430.37835	−10.7	OND	5899.96199	41.4	SSO	5463.44187	29.6	OND
6171.62174	37.8	NTT	5483.27549	−7.8	OND	6171.80243	50.5	NTT	5463.47292	26.0	OND
6171.66370	45.9	NTT	5675.52280	−16.0	OND	6171.87909	47.0	NTT	5464.41610	37.2	OND
6172.58713	56.0	NTT	5766.38926	−7.9	OND	6172.68364	42.9	NTT	5464.44582	50.4	OND
6172.66055	40.6	NTT	5794.39180	−6.5	OND	6173.79603	54.2	NTT	5483.37624	28.3	OND
6700.59333	43.1	SAAO	$N = 21,\ \bar{v} = -11.9,\ \sigma_v = 4.0$			$N = 15,\ \bar{v} = 43.4,\ \sigma_v = 4.2$			5483.56518	29.9	OND
6700.63352	37.7	SAAO	GALEX J1753−5007B			GALEX J2205−3141			5794.58849	34.8	OND
$N = 13,\ \bar{v} = 49.0,\ \sigma_v = 8.3$			5757.06955	−56.9	SSO	5757.23298	−67.4	SSO	5834.29578	29.0	OND
GALEX J1632+0759			5757.07837	−56.4	SSO	6171.77057	−17.9	NTT	$N = 17,\ \bar{v} = 36.3,\ \sigma_v = 6.9$		
5435.41483	−67.4	WHT	5761.02112	−65.7	SSO	6171.81889	−68.1	NTT	GALEX J2344−3426		
5756.97348	−62.5	SSO	5761.07352	−60.3	SSO	6171.88946	−62.9	NTT	3679.56424	21.5	FEROS
5761.00101	−50.0	SSO	6171.64403	−56.2	NTT	6172.70173	23.7	NTT	3957.88130	21.5	FEROS
6048.12788	15.2	SSO	6171.71118	−73.0	NTT	6172.78429	−8.0	NTT	5757.29066	12.9	SSO
6171.55953	−0.7	NTT	6172.61645	−75.6	NTT	6172.85277	−62.3	NTT	5898.02545	21.5	SSO
6171.57889	8.6	NTT	6173.71129	−74.9	NTT	6173.73046	32.9	NTT	5899.01277	19.2	SSO
6172.55735	4.8	NTT	$N = 8,\ \bar{v} = -64.9,\ \sigma_v = 8.0$			6173.76269	19.9	NTT	5899.06162	21.0	SSO
6172.57774	−3.1	NTT	GALEX J1845−4138			6173.83761	−38.8	NTT	6171.81182	29.0	NTT
6432.47442	−31.5	INT	6171.65588	−52.3	NTT	6870.62358	−49.9	NTT	6171.91775	26.4	NTT
6870.48215	−68.0	NTT	6171.73152	−52.3	NTT	6870.70432	−42.0	NTT	6172.69358	31.2	NTT
6870.59970	−69.0	NTT	6172.64693	−57.2	NTT	6870.85814	14.7	NTT	6173.76988	34.9	NTT
6870.68037	−65.0	NTT	6172.71683	−69.1	NTT	$N = 13,\ \bar{v} = -25.1,\ \sigma_v = 36.4$			$N = 10,\ \bar{v} = 23.9,\ \sigma_v = 6.1$		
$N = 12,\ \bar{v} = -32.4,\ \sigma_v = 33.3$			6173.68314	−56.9	NTT	GALEX J2254−5515					
GALEX J1731+0647			$N = 5,\ \bar{v} = -57.6,\ \sigma_v = 6.1$			5898.00341	−7.3	SSO			
5757.00524	−19.9	SSO	GALEX J1902−5130			5898.05579	−24.7	SSO			

Table C1. Properties of hot subdwarf binary systems.

Object	RA (J2000)	Dec. (J2000)	$\mu_\alpha \cos\delta$, μ_δ (mas yr^{-1})	V (mag)	Period (d)	γ (km s^{-1})	K (km s^{-1})	e	Sec. type	Variable	Ref.
CD-30 11223	14 11 16.0	−30 53 07	7.4 ± 1.0, −6.4 ± 1.8	12.34	0.048 979 06 ± 0.000 000 04	31.5 ± 1.3	386.9 ± 1.9		WD	ell,ecl	1,2
SDSSJ1622+4730	16 22 56.7	+47 30 51	−10.7 ± 7.4,−29.6 ± 8.0	16.19	0.069 69 ± 0.000 03	−54.7 ± 1.5	47.2 ± 2.0		bd	refl,ecl	3
PG1017−086	10 20 14.5	−08 53 46	−5.0 ± 2.5, 11.7 ± 4.0	14.42	0.072 9938 ± 0.000 0003	−9.1 ± 1.3	51.0 ± 1.7		dM	refl	4
NGC 6121−V46	16 23 47.1	−26 31 56	–	18.51	0.087 159	31.3 ± 1.6	211.6 ± 2.3		WD	ell	5
KPD0422+5421	04 26 06.9	+54 28 17	3.5 ± 3.7, −5.0 ± 4.3	14.66	0.090 179 45 ± 0.000 000 12	−57 ± 12	237 ± 18		WD	ecl,ell	6,7
KPD1930+2752	19 32 14.8	+27 58 35	−0.7 ± 10.1,15.1 ± 10.7	13.82	0.095 0933 ± 0.000 0015	5 ± 1	341 ± 1		WD	ell,puls	8,9,10
HS0705+6700	07 10 42.1	+66 55 44	−3.2 ± 1.6,−3.5 ± 1.8	14.92	0.095 646 65 ± 0.000 000 39	−36.4 ± 2.9	85.8 ± 3.7		dM	refl,ecl	11
SDSSJ08205+0008	08 20 53.5	+00 08 43	2.5 ± 4.6, −7.1 ± 4.6	15.17	0.096 ± 0.001	9.5 ± 1.3	47.4 ± 1.9		bd	refl,ecl	12
PG1336−018	13 38 48.1	−02 01 49	−6.5 ± 2.0, −12.5 ± 2.1	13.75	0.101 015 999 ± 0.000 000 002	–	78.6 ± 0.6		dM	refl,ecl,puls	13,14
NSVS14256825	20 20 00.5	+04 37 56	5.1 ± 2.7, −2.0 ± 3.0	13.23	0.110 374 230 ± 0.000 000 002	−12.1 ± 1.5	73.4 ± 2.0		dM	refl,ecl	15
HS2231+2441	22 34 21.5	+24 56 57	13.9 ± 1.4,−20.7 ± 1.7	14.15	0.110 5880 ± 0.000 0005	–	49.1 ± 3.2		dM	refl,ecl	16
UVEXJ0328+5035	03 28 55.2	+50 35 30	−4.7 ± 4.6, −1.2 ± 2.2	14.26	0.110 17 ± 0.000 11	44.9 ± 0.7	64.0 ± 1.5		dM	refl	17
HW Vir	12 44 20.2	−08 40 17	9.5 ± 1.5, −16.0 ± 1.6	10.69	0.115 ± 0.008	−13.0 ± 0.8	84.6 ± 1.1		dM	refl,ecl	18
EC10246−2707	10 26 56.6	−27 22 59	−4.4 ± 2.9, −7.2 ± 2.1	14.38	0.118 507 9936 ± 0.000 000 0009	–	71.6 ± 1.7		dM	refl,ecl	19
PG1043+760	10 47 05.0	+75 44 23	5.1 ± 1.5, 8.9 ± 1.9	13.53	0.120 1506 ± 0.000 0003	24.8 ± 1.4	63.6 ± 1.4		dM		20
OGLE BUL-SC16335	18 09 48.2	−26 41 49	60.0 ± 5.3, 9.0 ± 6.6	16.5	0.122	36.4 ± 19.6	92.5 ± 26.2		dM	refl,ecl	21,22
2M1938+4603	19 38 32.6	+46 03 59	2.8 ± 0.6, −2.7 ± 0.7	12.06	0.125 765 300 ± 0.000 000 021	20.1 ± 0.3	65.7 ± 0.6		dM	refl,ecl,puls	23
EC00404−4429	00 42 48.4	−44 13 25	21.6 ± 1.3, 9.8 ± 1.4	13.67	0.128 34 ± 0.000 04	33.0 ± 2.9	152.8 ± 3.4				24
KIC7335517	18 43 06.8	+42 59 18	−2.8 ± 4.9, −8.7 ± 4.4	15.60	0.137 29 ± 0.000 02	–	–		dM	refl	25,26
SDSSJ0830+4751	08 30 06.2	+47 51 50	1.1 ± 3.8, −10.0 ± 4.2	16.04	0.147 80 ± 0.000 07	49.9 ± 0.9	77.0 ± 1.7		WD		27
ASAS102322−3737	10 23 21.9	−37 37 00	−27.4 ± 1.3,−20.9 ± 0.9	11.58	0.139 269 40 ± 0.000 000 04	–	81 ± 3		dM	ecl,refl	28
KIC6614501	19 36 50.0	+42 01 44	42.8 ± 8.6, 12.8 ± 9.1	16.09	0.157 497 47 ± 0.000 000 25	−6.5 ± 1.5	97.2 ± 2.0		WD	ell,dop	29
2M1533+3759	15 33 49.4	+37 59 28	−0.6 ± 1.3, −19.9 ± 3.1	13.61	0.161 770 42 ± 0.000 000 01	−3.4 ± 5.2	71.1 ± 1.0		dM	refl,ecl	30
SDSSJ1920+3722	19 20 59.8	+37 22 20	1.7 ± 5.6, 4.5 ± 6.5	15.74	0.168 876 ± 0.000 35	16.8 ± 2.0	59.8 ± 2.5		dM	refl,ecl	31
HS2333+3927	23 35 42.5	+39 44 27	0.6 ± 4.7, 3.9 ± 4.8	14.79	0.171 8023 ± 0.000 0009	−31.4 ± 2.1	89.6 ± 3.2		dM	refl	32
GALEX J0805−1058	08 05 10.9	−10 58 34	−23.2 ± 1.8, −27.3 ± 1.5	12.25	0.173 703 ± 0.000 002	58.2 ± 0.9	29.2 ± 1.3		dM, bd?	33	
BPS CS 22169−0001	03 56 23.3	−15 09 19	−3.3 ± 1.7, 2.2 ± 1.6	12.85	0.1780 ± 0.0003	2.8 ± 0.3	14.9 ± 0.4			refl?	34
GALEX J0751+0925	07 51 47.1	+09 25 26	−9.6 ± 1.6, −9.9 ± 2.0	14.09	0.178 319 ± 0.000 005	15.5 ± 1.6	147.7 ± 2.2		WD		33
HE1415−0309	14 18 20.9	−03 22 54	–	15.14	0.192 ± 0.004	104.7 ± 9.5	152.4 ± 11.2		WD		22
HS1741+2133	17 43 19.0	+21 32 38	−12.1 ± 2.3, 4.2 ± 2.5	13.99	0.20 ± 0.01	−112.8 ± 2.7	157.0 ± 3.4		WD		17
SDSSJ0823+1136	08 23 32.1	+11 36 41	–	16.65	0.207 07 ± 0.000 02	135.1 ± 2.0	169.4 ± 2.5				27
SDSSJ1138−0035	11 38 40.7	−00 35 32	−10.2 ± 2.7, −27.2 ± 3.3	14.47	0.207 536 ± 0.000 002	23.3 ± 3.7	162.0 ± 3.8		WD		35
PG1432+159	14 35 18.9	+15 40 14	2.9 ± 1.4, −25.7 ± 1.9	13.90	0.224 89 ± 0.000 32	−16.0 ± 1.1	120.0 ± 1.4		WD		4,36
SDSSJ1625+3632	16 25 42.1	+36 32 19	–	19.36	0.2324 ± 0.0396	−95.0 ± 2.1	58.4 ± 2.7				37
PG2345+318	23 48 07.5	+32 04 48	5.4 ± 1.8, −3.1 ± 2.1	14.16	0.240 9458 ± 0.000 0083	−10.6 ± 1.4	141.2 ± 1.1				36
SDSSJ2046−0454	20 46 13.4	−04 54 19	10.9 ± 13.4, −11.4 ± 10.9	16.32	0.243 11 ± 0.000 01	87.6 ± 5.7	134.3 ± 7.8				35
PG1329+159	13 31 53.6	+15 41 18	−18.1 ± 1.2, −8.6 ± 1.7	13.51	0.249 699 ± 0.000 002	−22.0 ± 1.2	40.2 ± 1.1		dM	refl	20
FBS0117+396	01 20 22.9	+39 50 59	−4.5 ± 5.1, −1.7 ± 5.7	15.34	0.252013 ± 0.000013	−47.3 ± 1.3	37.3 ± 2.8		dM	puls,refl	38
SDSSJ1654+3037	16 54 04.2	+30 37 02	7.4 ± 5.3, −8.4 ± 3.3	15.41	0.253 57 ± 0.000 01	40.5 ± 2.2	126.1 ± 2.6				35
AA Dor	05 31 40.4	−69 53 02	−13.6 ± 1.2, 52.2 ± 1.3	11.14	0.2614 ± 0.0002	1.6 ± 0.1	40.2 ± 0.1		dM/bd	refl,ecl	39
HE0532−4503	05 33 40.5	−45 01 35	6.7 ± 4.8, −14.7 ± 4.8	16.08	0.2656 ± 0.0001	8.5 ± 0.1	101.5 ± 0.2				40
GALEXJ0321+4727	03 21 39.6	+47 27 19	60.1 ± 1.6, −8.5 ± 0.9	11.72	0.265 856 ± 0.000 003	69.6 ± 2.2	60.8 ± 4.5		dM	refl,puls	41,42
CPD-64°481	05 47 59.3	−64 23 03	−1.9 ± 1.0, −30.1 ± 0.9	11.29	0.277 263 15 ± 0.000 000 08	93.5 ± 0.1	23.8 ± 0.1		bd	refl	43
KBS13	19 26 09.4	+37 20 08	4.0 ± 1.7, −9.9 ± 2.1	13.63	0.2923 ± 0.0004	7.5 ± 0.1	22.8 ± 0.2		dM	refl	44
SDSSJ1021+3010	10 21 51.6	+30 10 11	–	18.22	0.2966 ± 0.0001	−28.4 ± 4.8	114.5 ± 5.2				27
HS2043+0615	20 46 20.8	+06 26 25	2.5 ± 5.9, −9.4 ± 6.3	15.42	0.3015 ± 0.0003	−43.5 ± 3.4	73.7 ± 4.3		dM	refl	22
PG0941+280	09 43 54.6	+27 46 59	−14.7 ± 1.1, −40.1 ± 2.8	13.26	0.311	73.0 ± 4.9	141.7 ± 19.4		WD	ecl	22
PHL457	23 19 24.5	−08 52 37	−11.2 ± 2.3, −10.9 ± 2.4	12.95	0.3131 ± 0.0002	20.7 ± 0.2	13.0 ± 0.2		bd	refl,puls	43
PG1528+104	15 31 10.4	+10 15 01	−18.9 ± 1.4, −7.2 ± 1.7	13.38	0.331 ± 0.001	−49.3 ± 1.0	53.3 ± 1.6		WD		23
PG1438−029	14 40 52.8	−03 08 53	7.8 ± 1.5, −42.9 ± 1.8	13.79	0.336	–	32.1			refl	45
GALEX J2205−3141	22 05 51.8	−31 41 05	22.3 ± 0.9, −2.1 ± 1.6	12.30	0.341 543 ± 0.000 008	−19.4 ± 1.7	47.8 ± 2.2		dM	refl	33

Table C1 – *continued*

Object	RA (J2000)	Dec. (J2000)	$\mu_\alpha \cos\delta$, μ_δ (mas yr^{-1})	V (mag)	Period (d)	γ (km s^{-1})	K (km s^{-1})	e	Sec. type	Variable	Ref.
PG1101+249	11 04 31.7	+24 39 43	−29.9 ± 1.9, 19.2 ± 2.3	12.78	0.353 86 ± 0.000 14	−0.8 ± 0.9	134.6 ± 1.3		WD		36
PG1232−136	12 35 18.7	−13 55 09	−44.0 ± 1.7, 5.4 ± 1.7	13.27	0.3630 ± 0.0003	4.1 ± 0.3	129.6 ± 0.4	0.060 ± 0.005			34
Feige 48	11 47 14.5	+61 15 32	−28.1 ± 3.2, −6.3 ± 2.7	13.42	0.376 ± 0.003	−47.9 ± 0.1	28.0 ± 0.2		WD	puls	46
GD 687	01 10 18.5	−34 00 26	−1.3 ± 1.6, −16.1 ± 1.6	14.08	0.377 65 ± 0.000 02	32.3 ± 3.0	118.3 ± 3.4		WD		47
KIC11179657	19 02 22.0	+48 50 53	–	–	0.3945 ± 0.0002	–	–		dM	refl,puls	26,48
V 1405 Ori	04 44 56.9	+14 21 50	3.6 ± 4.3, −10.9 ± 4.7	15.14	0.398	−33.6 ± 5.5	85.1 ± 8.6		dM	refl,puls	22,49
KIC2438324	19 21 12.9	+37 45 51	–	–	0.398 4944 ± 0.000 0035	–	–		dM	ref,puls	50
KPD1946+4340	19 47 42.9	+43 47 31	−9.2 ± 2.7, −1.4 ± 3.1	14.28	0.403 7503 ± 0.000 0002	−5.5 ± 1.0	164.0 ± 1.9		WD	ell,ecl,dop	20,51
SDSSJ0951+0347	09 51 01.3	+03 47 57	−4.8 ± 4.0, −9.5 ± 3.6	15.90	0.4159 ± 0.0007	111.1 ± 2.5	84.4 ± 4.2				27
[CW83] 1419−09	14 22 40.3	−09 17 22	−6.0 ± 0.9, −36.9 ± 1.0	12.12	0.4178 ± 0.0002	42.3 ± 0.3	109.6 ± 0.4	0.039 ± 0.005			34
HE0929−0424	09 32 02.1	−04 37 37	−3.1 ± 4.6, −6.4 ± 4.4	16.16	0.4400 ± 0.0002	41.4 ± 1.0	114.3 ± 1.4				40
KIC2991403	19 27 15.9	+38 08 08	–	–	0.443 12 ± 0.000 08	–	–		dM	refl,puls	52,53
HE0230−4323	02 32 54.7	−43 10 28	−8.5 ± 1.5, −0.9 ± 1.5	13.77	0.4515 ± 0.0002	16.6 ± 1.0	62.4 ± 1.6		dM	refl,puls	34,54
GALEXJ2349+3844	23 49 47.6	+38 44 42	−4.3 ± 1.6, −2.5 ± 1.1	11.72	0.462 516 ± 0.000 005	2.0 ± 1.0	87.9 ± 2.2	0.06±0.02	WD	puls	41,42
KUV16256+4034	16 27 16.5	+40 27 29	−19.7 ± 0.9, −13.6 ± 0.6	12.49	0.4776 ± 0.0008	−90.9 ± 0.9	38.7 ± 1.2		WD		24
BPS CS 22879−149	20 57 15.3	−38 11 51	11.9 ± 2.4, −10.8 ± 2.4	14.24	0.478[a]	21.9 ± 2.5	63.5 ± 2.8				22
HE1318−2111	13 21 15.6	−21 27 18	4.5 ± 1.7, −0.7 ± 2.0	14.77	0.487 502	48.9 ± 0.7	48.5 ± 1.2				55,56
PG1544+488	15 46 11.7	+48 38 37	−47.5 ± 1.4, 32.7 ± 1.1	12.79	0.496 ± 0.002	86.6 ± 0.5/95.0 ± 0.4	−25.5 ± 0.4		He-sdB		57
SDSSJ1726+2744	17 26 24.1	+27 44 19	8.0 ± 3.7, −9.1 ± 3.8	15.99	0.501 98 ± 0.000 05	−36.7 ± 4.8	118.9 ± 3.7				35
PG1743+477	17 44 26.4	+47 41 47	0.7 ± 1.2, 12.4 ± 1.3	13.79	0.515 561 ± 0.000 002	−65.8 ± 0.8	121.4 ± 1.0				20
GALEX J0507+0348	05 07 35.7	+03 48 14	11.7 ± 3.0, −4.0 ± 3.3	14.24	0.528 127 ± 0.000 013	96.2 ± 1.8	68.2 ± 2.5		WD		33
PG0001+275	00 03 55.6	+27 48 37	3.3 ± 1.9, −20.4 ± 1.2	13.32	0.529 842 ± 0.000 005	−44.7 ± 0.5	92.8 ± 0.7				34
PG1519+640	15 20 31.4	+63 52 08	24.5 ± 1.0, 33.8 ± 1.3	12.39	0.539 ± 0.003	0.9 ± 0.8	36.7 ± 1.2		WD		24
HE1059−2735	11 01 24.8	−27 51 42	−11.4 ± 2.4, 2.0 ± 2.4	15.56	0.555 624	−44.7 ± 0.6	87.7 ± 0.8				55,56
PG0101+039	01 04 21.7	+04 13 37	11.7 ± 0.7, −29.3 ± 1.0	12.06	0.569 899 ± 0.000 001	7.3 ± 0.2	104.5 ± 0.3		WD	ell,puls	58
EC20182−6534	20 22 51.3	−65 25 20	−12.6 ± 1.3, −9.2 ± 2.3	13.29	0.598 819 ± 0.000 006	13.5 ± 1.9	59.7 ± 3.2				24
PG1725+252	17 27 57.4	+25 08 36	−20.1 ± 1.4, 7.4 ± 1.2	13.06	0.601 507 ± 0.000 003	−60.0 ± 0.6	104.5 ± 0.7				20
PG1247+554	12 50 04.3	+55 06 03	−76.5 ± 3.6, −7.3 ± 2.0	12.26	0.602 740 ± 0.000 006	13.8 ± 0.6	32.2 ± 1.0				59
HD188112	19 54 31.4	−28 20 21	33.7 ± 0.7, 22.5 ± 1.2	10.18	0.606 5812 ± 0.000 0005	26.7 ± 0.2	188.4 ± 0.2		WD		34
PG1648+536	16 49 59.9	+53 31 32	0.9 ± 1.3, −15.4 ± 2.1	14.09	0.610 9107 ± 0.000 0004	−69.9 ± 0.9	109.0 ± 1.3		WD		24
SDSSJ1522−0130	15 22 22.1	−01 30 18	–	17.81	0.671 62 ± 0.000 03	−79.5 ± 2.7	80.1 ± 3.5				27
SDSSJ2256+0656	22 56 38.3	+06 56 51	−2.0 ± 3.7, −1.1 ± 4.3	15.31	0.7004 ± 0.0001	−7.3 ± 2.1	105.3 ± 3.4				35
EC22202−1834	22 22 58.1	−18 19 10	10.3 ± 1.8, −15.7 ± 1.7	13.80	0.704 71 ± 0.000 05	−5.5 ± 3.9	118.6 ± 5.8				24
PG1248+164	12 50 50.3	+16 10 03	11.6 ± 2.0, −8.8 ± 2.2	14.46	0.732 32 ± 0.000 02	−16.2 ± 1.3	61.8 ± 1.1				20
JL82	21 36 01.3	−72 48 27	15.0 ± 1.2, −17.6 ± 0.9	12.37	0.7371 ± 0.0005	−1.6 ± 0.8	34.6 ± 1.0		dM	refl,puls	34,60
PG0849+319	08 52 54.6	+31 43 37	−10.8 ± 1.6, −9.6 ± 1.8	14.58	0.745 07 ± 0.000 01	64.0 ± 1.5	66.3 ± 2.1				20
SDSSJ1505+1108	15 05 13.5	+11 08 37	−17.7 ± 8.3, −29.4 ± 8.0	15.38	0.747 73 ± 0.000 05	−77.1 ± 1.2	97.2 ± 1.8				35
EQ Psc	23 34 34.6	−01 19 37	−8.7 ± 1.8, −40.4 ± 1.3	12.78	0.801[b]	–	–		dM	refl,puls	61
EC02200−2338	02 22 19.8	−23 24 56	34.2 ± 1.6, −12.3 ± 1.0	12.01	0.8022 ± 0.0007	20.7 ± 2.3	96.4 ± 1.4				24
KPD2215+5037	22 17 29.7	+50 52 59	9.7 ± 4.4, 14.4 ± 2.8	13.64	0.809 146 ± 0.000 002	−7.2 ± 1.0	86.0 ± 1.5				24
Ton S 183	01 01 17.6	−33 42 45	−7.1 ± 1.2, −15.2 ± 1.0	12.60	0.8277 ± 0.0002	50.5 ± 0.8	84.8 ± 1.0				34
EC13332−1424	13 35 53.5	−14 40 13	−12.6 ± 1.8, 16.6 ± 2.0	13.40	0.827 94 ± 0.000 01	−53.2 ± 1.8	104.1 ± 3.0				24
PG1627+017	16 29 35.3	+01 38 19	−2.0 ± 2.1, −9.7 ± 4.4	12.94	0.829 2056 ± 0.000 0014	−54.2 ± 0.3	70.1 ± 0.1		WD	puls	62
EC21556−5552	21 59 00.7	−55 38 04	3.4 ± 1.3, 6.4 ± 1.3	13.09	0.8340 ± 0.0007	31.4 ± 2.0	65.0 ± 3.4				24
PG1230+052	12 33 12.6	+04 57 38	−10.6 ± 2.4, −17.6 ± 2.3	13.24	0.837 177 ± 0.000 003	−43.1 ± 0.7	40.4 ± 1.2		WD		24
PG1116+301	11 19 04.8	+29 51 53	−13.0 ± 3.3, −7.7 ± 4.1	14.37	0.856 21 ± 0.000 03	−0.2 ± 1.1	88.5 ± 2.1				20
PG0918+029	09 21 28.2	+02 46 02	−23.9 ± 2.4, −22.0 ± 1.4	13.30	0.876 79 ± 0.000 02	104.4 ± 1.7	80.0 ± 2.6				20
EC12408−1427	12 43 30.0	−14 43 49	−24.1 ± 1.6, 6.2 ± 1.9	12.83	0.902 43 ± 0.000 01	−52.2 ± 1.2	58.6 ± 1.5				24
HE2135−3749	21 38 44.2	−37 36 15	26.5 ± 1.4, −0.8 ± 1.2	13.90	0.9240 ± 0.0003	45.0 ± 0.5	90.5 ± 0.6				40
PB5333	23 19 55.3	+04 52 35	28.7 ± 3.3, −26.6 ± 2.2	12.81	0.925 60 ± 0.000 12	−95.3 ± 1.3	22.4 ± 0.8				63
HS2359+1942	00 02 08.5	+19 59 13	−12.1 ± 2.8, −1.7 ± 3.9	15.64	0.932 61 ± 0.000 05	−96.1 ± 6.0	107.4 ± 8.3		WD		22

Table C1 – *continued*

Object	RA (J2000)	Dec. (J2000)	$\mu_\alpha \cos\delta$, μ_δ (mas yr^{-1})	V (mag)	Period (d)	γ (km s^{-1})	K (km s^{-1})	e	Sec. type	Variable	Ref.
PG1452+198	14 54 39.8	+19 37 01	0.8 ± 1.8, −17.9 ± 1.3	12.48	0.964 98 ± 0.000 04	−9.1 ± 2.1	86.8 ± 1.9				24
SDSSJ1508+4940	15 08 29.0	+49 40 50	–	17.52	0.967 164 ± 0.000 009	−60.0 ± 10.7	93.6 ± 5.8				27
PG1000+408	10 03 54.3	+40 34 18	−1.7 ± 1.9, −15.9 ± 1.6	13.29	1.049 343 ± 0.000 005	56.6 ± 3.4	63.5 ± 3.0		WD		24
SDSSJ1132−0636	11 32 41.6	−06 36 52	–	16.27	1.06 ± 0.02	8.3 ± 2.2	41.1 ± 4.0				27
GALEX J1731+0647	17 31 53.7	+06 47 06	−18.9 ± 2.0, −1.3 ± 2.1	14.09	1.173 34 ± 0.000 04	−39.1 ± 3.0	87.7 ± 3.0		WD		33
HE1421−1206	14 24 08.8	−12 20 20	−7.8 ± 2.8, −6.8 ± 2.2	15.51	1.188	−86.2 ± 1.1	55.5 ± 2.0				55
PG2331+038	23 33 58.2	+04 03 56	−10.2 ± 2.8, −16.7 ± 3.3	14.63	1.204 964 ± 0.000 003	−9.5 ± 1.1	93.5 ± 1.9				24
HE1047−0436	10 50 26.9	−04 52 36	−6.4 ± 2.5, 0.1 ± 2.7	14.95	1.213 253	25	94		WD		64
GALEX J2254−5515	22 54 44.1	−55 15 05	29.7 ± 1.3, 6.2 ± 1.5	12.12	1.227 02 ± 0.000 05	4.2 ± 2.0	79.7 ± 2.6		WD		33
PG0133+114	01 36 26.2	+11 39 32	22.0 ± 1.7, −20.3 ± 1.7	12.30	1.237 87 ± 0.000 03	−0.3 ± 0.2	82.0 ± 0.3	0.025 ± 0.005			34
PG1512+244	15 14 32.5	+24 10 41	−41.9 ± 1.1, 3.0 ± 0.9	13.18	1.269 78 ± 0.000 02	−2.9 ± 1.0	92.7 ± 1.5				20
[CW83] 1735+22	17 37 26.4	+22 08 58	−24.2 ± 0.8, 0.1 ± 1.6	11.86	1.280 ± 0.006	20.6 ± 0.4	104.6 ± 0.5		WD		34
SDSSJ0118−0025	01 18 57.2	−00 25 46	5.3 ± 3.8, −9.6 ± 4.2	14.80	1.30 ± 0.02	37.7 ± 1.8	54.8 ± 2.9				27
HE2150−0238	21 52 35.8	−02 24 32	–	16.08	1.3209 ± 0.0050	−32.5 ± 0.9	96.3 ± 1.4				40
KPD2040+3955	20 42 33.9	+40 05 42	−12.9 ± 2.6, −14.1 ± 3.1	14.48	1.482 860 ± 0.000 004	−16.4 ± 1.0	94.0 ± 1.5		WD		24
SDSSJ0023−0029	00 23 24.0	−00 29 53	24.1 ± 2.8, 8.5 ± 7.1	15.58	1.4876 ± 0.0001	16.4 ± 2.1	81.8 ± 2.9				35
HD49798	06 48 04.7	−44 18 58	−5.1 ± 1.0, 6.0 ± 1.0	8.29	1.547 671 ± 0.000 011	13.5 ± 2.2	119.2 ± 3.2		WD/N	ecl,X-ray	65,66
KIC7664467	18 56 07.1	+43 19 19	–	–	1.559110	–	–			puls	48,53
HD171858	18 37 56.7	−23 11 35	−16.8 ± 1.4, −21.2 ± 1.4	9.86	1.632 80 ± 0.000 05	62.5 ± 0.1	87.8 ± 0.2		WD		34
PG1403+316	14 05 59.8	+31 24 37	−25.2 ± 2.0, 2.7 ± 1.8	13.50	1.738 46 ± 0.000 01	−2.1 ± 0.9	58.5 ± 1.8				24
PG1716+426	17 18 03.9	+42 34 13	8.2 ± 1.3, −19.4 ± 1.6	13.93	1.777 32 ± 0.000 05	−3.9 ± 0.8	70.8 ± 1.0			puls	20,67
SDSSJ1346+2817	13 46 32.6	+28 17 22	−14.0 ± 3.9, −7.4 ± 4.2	14.91	1.96 ± 0.03	1.2 ± 1.2	85.6 ± 3.4				27
NGC 188/II-91	00 47 52.3	+85 19 08	−5.7 ± 6.7, −1.2 ± 6.4	16.07	2.15	–	22.0:				68
PG1300+279	13 02 41.8	+27 40 42	−7.8 ± 1.5, −7.8 ± 1.9	14.26	2.2593 ± 0.0001	−3.1 ± 0.9	62.8 ± 1.6				20
CPD-20° 1123	06 06 13.4	−20 21 07	9.3 ± 1.4, −15.4 ± 1.3	12.17	2.3098 ± 0.0003	−6.3 ± 1.2	43.5 ± 0.9				69
HD149382	16 34 23.3	−04 00 52	−8.7 ± 0.8, −1.9 ± 0.5	8.94	2.391 ± 0.002	25.3 ± 0.1	2.3 ± 0.1		bd		70
PG1538+269	15 40 23.4	+26 48 30	7.8 ± 1.4, −5.1 ± 1.7	13.86	2.500	–	75		WD		71,72
GALEX J1632+0759	16 32 01.4	+07 59 40	7.0 ± 1.1, −2.7 ± 1.3	12.76	2.9516 ± 0.0006	−31.6 ± 2.7	54.9 ± 4.6		WD		33,73
PG1253+284	12 56 04.9	+28 07 19	−11.8 ± 1.2, 0.5 ± 1.5	12.76	3.016 34 ± 0.000 05	17.8 ± 0.6	24.8 ± 0.9				24
PG0958−073	10 00 47.3	−07 33 31	−43.1 ± 1.8, −2.2 ± 3.2	13.56	3.180 95 ± 0.000 07	90.5 ± 0.8	27.6 ± 1.4				24
KIC10553698A	19 53 08.4	+47 43 00	36.1 ± 4.5, 11.5 ± 4.3	14.90	3.387 ± 0.014	52.1 ± 1.5	64.8 ± 2.2		WD	puls,dop	74
KPD0025+5402	00 28 29.0	+54 19 15	−8.9 ± 7.6, −8.3 ± 3.8	13.91	3.571 ± 0.001	−7.8 ± 0.7	40.2 ± 1.1				20
PB7352	22 55 43.2	−06 59 40	−2.0 ± 1.0, 2.1 ± 1.1	12.26	3.621 66 ± 0.000 05	−2.1 ± 0.3	60.8 ± 0.3				34
PG0934+186	09 37 16.3	+18 25 11	−14.8 ± 1.3, −9.5 ± 0.8	13.13	4.050 ± 0.01	7.7 ± 3.2	60.3 ± 2.4				24
Ton S 135	00 03 22.1	−23 38 58	4.2 ± 2.5, −17.6 ± 1.7	13.28	4.122 ± 0.008	−3.7 ± 1.1	41.4 ± 1.5				34
EC20369−1804	20 39 46.5	−17 54 04	9.2 ± 1.3, −8.3 ± 1.6	13.35	4.5095 ± 0.0004	7.2 ± 1.6	51.5 ± 2.3				24
SDSSJ1832+6309	18 32 49.0	+63 09 10	2.1 ± 4.6, 6.1 ± 4.5	15.70	5.4 ± 0.2	−32.5 ± 2.1	62.1 ± 3.3				27
PG0839+399	08 43 12.7	+39 44 50	−3.5 ± 1.9, −10.7 ± 2.2	14.34	5.622 ± 0.002	23.2 ± 1.1	33.6 ± 1.5				20
PG1244+113	12 47 06.6	+11 03 14	6.6 ± 1.7, −0.7 ± 3.2	14.14	5.752 11 ± 0.000 09	7.4 ± 0.8	54.4 ± 1.4				24
CD-24° 731	01 43 48.5	−24 05 10	84.3 ± 2.0, −48.6 ± 1.2	11.72	5.85 ± 0.30	20 ± 5	63 ± 3		WD		34
HE1115−0631	11 18 11.6	−06 47 32	−13.8 ± 2.7, −10.3 ± 3.2	15.08	5.870	87.1 ± 1.3	61.9 ± 1.1				55,56
PG0907+123	09 10 25.4	+12 08 27	−9.1 ± 1.4, −3.6 ± 1.7	13.92	6.1163 ± 0.0006	56.3 ± 1.1	59.8 ± 0.9			puls	20,75
PG1032+406	10 35 16.6	+40 21 14	−84.1 ± 3.4, −38.1 ± 3.9	11.47	6.779 ± 0.001	24.5 ± 0.5	33.7 ± 0.5				20
SDSSJ0952+6258	09 52 38.9	+62 58 18	1.9 ± 2.7, −13.8 ± 3.3	14.69	6.98 ± 0.04	−35.4 ± 3.6	62.5 ± 3.4		WD		27
HE1448−0510	14 51 13.1	−05 23 17	1.1 ± 2.4, −6.1 ± 2.7	14.61	7.1588 ± 0.0130	−45.5 ± 0.8	53.7 ± 1.1				40
PG1439−013	14 42 27.5	−01 32 46	−9.3 ± 1.8, −1.4 ± 2.2	13.87	7.2914 ± 0.0005	−53.7 ± 1.6	50.7 ± 1.5				24
SDSSJ0321+0538	03 21 38.8	+05 38 40	0.5 ± 3.7, −5.8 ± 4.4	15.05	7.4327 ± 0.0004	−16.7 ± 2.1	39.7 ± 2.8				27
PHL861	00 51 03.9	−19 59 59	1.5 ± 2.6, −28.8 ± 1.7	14.83	7.4436 ± 0.0150	−26.5 ± 0.4	47.9 ± 0.4				40
PG0940+068	09 42 55.0	+06 35 37	11.3 ± 2.4, −4.0 ± 2.7	13.69	8.330 ± 0.003	−16.7 ± 1.4	61.2 ± 1.4				59
Feige108	23 16 12.4	−01 50 35	−0.4 ± 1.0, −14.1 ± 1.0	13.00	8.7465 ± 0.0010	45.8 ± 0.6	50.2 ± 1.0				63
EC20260−4757	20 29 34.1	−47 47 26	−3.6 ± 1.3, 0.0 ± 1.3	13.80	8.952 ± 0.002	56.5 ± 1.6	57.1 ± 1.9				24

Table C1 – *continued*

Object	RA (J2000)	Dec. (J2000)	$\mu_\alpha \cos\delta$, μ_δ (mas yr^{-1})	V (mag)	Period (d)	γ (km s^{-1})	K (km s^{-1})	e	Sec. type	Variable	Ref.
FF Aqr	22 00 36.4	−02 44 27	36.0 ± 0.6, −10.7 ± 0.8	9.57	9.208 03 ± 0.000 04	24.5 ± 1.7	116.5 ± 2.1		K0III	ecl,refl	76,77
PG1110+294	11 13 04.5	+29 07 46	−7.3 ± 1.3, −8.5 ± 1.9	14.11	9.415 ± 0.002	−15.2 ± 0.9	58.7 ± 1.2				20
KIC11558725	19 26 34.2	+49 30 30	−28.6 ± 5.5, −5.7 ± 5.3	14.86	10.0545 ± 0.0048	−66.1 ± 1.4	58.1 ± 1.7			puls,dop	78
PG1558−007	16 01 14.0	−00 51 42	−8.7 ± 3.1, −15.8 ± 4.5	13.54	10.3495 ± 0.0006	−71.9 ± 0.7	42.8 ± 0.8				24
LB1516	23 01 56.1	−48 03 48	9.1 ± 1.7, 1.2 ± 1.4	12.86	10.3598 ± 0.0005	14.3 ± 1.1	48.6 ± 4.4		WD	puls	22,79
CS1246	12 49 37.6	−63 32 10	−11.2 ± 3.7, −1.2 ± 3.7	14.37	14.104 ± 0.011	67.3 ± 1.7	16.6 ± 0.6			puls	80
KIC7668647	19 05 06.4	+43 18 31	−11.2 ± 5.6, −36.2 ± 5.7	15.22	14.1742 ± 0.0042	−27.4 ± 1.3	38.9 ± 1.9		WD	puls,dop	81
PG1619+522	16 20 38.8	+52 06 09	−4.3 ± 0.9, 10.4 ± 0.7	13.24	15.357 ± 0.008	−52.5 ± 1.1	35.2 ± 1.1				20
PG0919+273	09 22 39.8	+27 02 25	23.3 ± 0.8, −27.1 ± 1.1	12.66	15.5830 ± 0.0005	−68.6 ± 0.6	41.5 ± 0.8				24
EGB 5	08 11 12.8	+10 57 17	−17.9 ± 1.5, 9.7 ± 1.9	13.81	16.537 ± 0.003	68.5 ± 0.7	16.1 ± 0.8	0.098 ± 0.048			82
HD 185510	19 39 38.8	−06 03 49	22.8 ± 1.1, −27.4 ± 1.1	8.47	20.661 87 ± 0.000 58	−21.9 ± 0.1	93.7 ± 2.5		K0III/IV	ecl,refl?	83,84
PG0850+170	08 53 23.7	+16 49 35	0.8 ± 1.4, −6.8 ± 1.6	14.00	27.81 ± 0.05	32.2 ± 2.8	33.5 ± 3.1			puls	20,85
59 Cyg	20 59 49.6	+47 31 15	7.3 ± 1.0, 2.5 ± 1.0	4.75	28.1871 ± 0.0011	−10.4 ± 0.8	121.3 ± 1.1	0.141 ± 0.008	Be		86
FY CMa	07 26 59.5	−23 05 10	−7.8 ± 1.0, 4.8 ± 1.0	5.56	37.257 ± 0.003	31.2 ± 1.7	128.2 ± 2.2		Be		87
ϕ Per	01 43 39.6	+50 41 19	24.6 ± 1.0, −14.0 ± 1.0	4.06	126.6731 ± 0.0071	−6.1 ± 0.5	81.3 ± 0.6		Be		88,89
BD-11° 162	00 52 15.1	−10 39 46	−29.6 ± 1.0, −30.1 ± 1.7	11.17	421 ± 3	2.3 ± 0.2	7.9 ± 0.3		G		90
PG1701+359	17 03 21.5	+35 48 49	−57.9 ± 4.0, 20.4 ± 0.9	13.20	738 ± 4	−120.1 ± 0.2	–	0.07 ± 0.04	G/K		91
PG1104+243	11 07 26.2	+24 03 11	−65.9 ± 1.2, −25.1 ± 1.2	11.32	753.2 ± 0.8	−15.7 ± 0.1	6.5 ± 0.8		F/K		92
PG1018−047	10 21 10.6	−04 56 20	−15.1 ± 2.1, −11.9 ± 2.6	13.32	755.9 ± 5.1	38.0 ± 0.9	12.6 ± 0.8	0.246 ± 0.052	K4-K6		93
PG1449+653	14 50 36.1	+65 05 52	−21.7 ± 2.1, 13.6 ± 1.0	13.62	909 ± 2	−135.5 ± 0.2	12.8 ± 1.1	0.11 ± 0.02	G/K		91
PG1338+611	13 40 14.7	+60 52 48	14.5 ± 0.9, −61.4 ± 0.8	11.62	937.5 ± 1.1	32.6 ± 0.1	15.2 ± 1.8	0.15 ± 0.02	G2-G7		92,94
BD+34° 1543	07 10 07.7	+34 24 54	35.2 ± 1.0, −61.8 ± 0.8	10.16	972 ± 2	33.1 ± 0.2	19.3 ± 0.2	0.16 ± 0.01	MS		94
PG1317+123	13 19 53.6	+12 03 58	−6.9 ± 1.1, −1.6 ± 1.1	11.41	1179 ± 12	40.3 ± 0.2	15.5 ± 1.7		G8V		92
BD-7° 5977	23 17 46.8	−06 28 31	7.3 ± 1.7, 1.1 ± 1.3	10.45	1195 ± 30	−8.73 ± 0.02	6.1 ± 0.8		K2III		95
BD+29° 3070	17 38 21.2	+29 08 47	−6.4 ± 0.5, 22.1 ± 0.9	10.34	1283 ± 63	−57.6 ± 0.9	16.6 ± 0.6	0.15 ± 0.01	MS		94
TYC3871-835-1	15 15 38.2	+56 53 45	−33.7 ± 0.6, 3.2 ± 0.5	11.41	1363 ± 25	−15.03 ± 0.03	4.8 ± 0.3		G0		95

Variable: puls – sdB pulsator, refl – reflection effect, ecl – eclipsing binary, ell – ellipsoidal variations, dop – Doppler beaming.

References: (1) Vennes et al. (2012); (2) Geier et al. (2013a); (3) Schaffenroth et al. (2014b); (4) Maxted et al. (2002); (5) O'Toole et al. (2006); (6) Koen, Orosz & Wade (1998); (7) Orosz & Wade (1999); (8) Maxted et al. (2000b); (9) Billeres et al. (2000); (10) Geier et al. (2007); (11) Drechsel et al. (2001); (12) Geier et al. (2011d); (13) Kilkenny et al. (2000); (14) Vučković et al. (2007); (15) Almeida et al. (2012); (16) Østensen et al. (2007); (17) Kupfer et al. (2014); (18) Edelmann (2008); (19) Barlow et al. (2013a); (20) Morales-Rueda et al. (2003); (21) Polubek et al. (2007); (21) Geier et al. (2014); (23) Østensen et al. (2010a); (24) Copperwheat et al. (2011); (25) Østensen et al. (2011); (26) Telting et al. (2012a); (27) Kupfer et al. (2015); (28) Schaffenroth et al. (2013); (29) Silvotti et al. (2012); (30) For et al. (2010); (31) Schaffenroth et al. (2014a); (32) Heber et al. (2004); (33) This work; (34) Edelmann et al. (2005); (35) Geier et al. (2011a); (36) Moran et al. (1999); (37) Kilic et al. (2011); (38) Østensen et al. (2013); (39) Müller, Geier & Heber (2010); (40) Karl et al. (2006); (41) Kawka et al. (2010); (42) Kawka et al. (2012); (43) Schaffenroth et al. (2014c); (44) For et al. (2008); (45) Green, For & Hyde (2005); (46) O'Toole, Heber & Benjamin (2004); (47) Geier et al. (2010a); (48) Østensen et al. (2010b); (49) Reed et al. (2010); (50) Pablo, Kawaler & Green (2011); (51) Bloemen et al. (2011); (52) Kawaler et al. (2010); (53) Telting et al. (2014a); (54) Kilkenny, Koen & Worters (2010); (55) Geier et al. (2011c); (56) Napiwotzki et al. (2004); (57) Şener & Jeffery (2014); (58) Geier et al. (2008); (59) Maxted et al. (2000a); (60) Koen (2009); (61) Jeffery & Ramsay (2014); (62) For et al. (2006); (63) Edelmann et al. (2004); (64) Napiwotzki et al. (2001); (65) Thackeray (1970); (66) Mereghetti et al. (2013); (67) Reed et al. (2004); (68) Green et al. (2004); (69) Naslim et al. (2012); (70) Geier et al. (2009); (71) Foss, Wade & Green (1991); (72) Saffer, Livio & Yungelson (1998); (73) Barlow et al. (2014); (74) Østensen et al. (2014); (75) Koen & Green (2010); (76) Vaccaro & Wilson (2003); (77) Vaccaro et al. (2007); (78) Telting et al. (2012b); (79) Koen et al. (2010); (80) Barlow, Dunlap & Clemens (2011); (81) Telting et al. (2014b); (82) Geier et al. (2011b); (83) Jeffery et al. (1992); (84) Fekel et al. (1993); (85) Green et al. (2003); (86) Peters et al. (2013); (87) Peters et al. (2008); (88) Božić et al. (1995); (89) Gies et al. (1998); (90) Østensen & Van Winckel (2012); (91) Barlow et al. (2013b); (92) Barlow et al. (2012); (93) Deca et al. (2012); (94) Vos et al. (2013); (95) Vos, Østensen & Van Winckel (2014).

[a]Alternate P = 0.964 d.

[b]Based on Kepler light curves.

Table C2. Kinematics (U, V, W), stellar parameters and absolute V magnitude (M_V) of known binaries.

Name	U (km s^{-1})	V (km s^{-1})	W (km s^{-1})	$T_{\rm eff}$ (K)	log g (c.g.s.)	M_V (mag)	Ref.	Name	U (km s^{-1})	V (km s^{-1})	W (km s^{-1})	$T_{\rm eff}$ (K)	log g (c.g.s.)	M_V (mag)	Ref.
CD−30 11223	41	−8	9	30150	5.72	4.62	1	HS2043+0615	21	−89	−42	26157	5.28	3.81	26
SDSSJ1622+4730	248	−209	69	29000	5.65	4.53	2	PG0941+280	−41	−151	11	29400	5.43	3.94	16
PG1017−086	−38	45	20	30300	5.61	4.32	3	PHL457	56	−1	−9	26500	5.38	4.04	35
NGC6121−V46	38	1	15	16197	5.75	6.58	4	PG1528+104	−38	−63	−3	27200	5.46	4.18	36
KPD0422+5421	44	−54	−3	25000	5.40	4.22	5	PG1438−029	101	−96	−90	27700	5.50	4.25	29
KPD1930+2752	−39	31	42	35200	5.61	4.02	6	GALEX J2205−3141	−30	−7	3	28650	5.68	4.63	24
HS0705+6700	17	−26	−34	28800	5.40	3.91	7	PG1101+249	−43	19	−12	29700	5.90	5.09	37
SDSSJ08205+0008	39	−40	1	26700	5.48	4.27	8	PG1232−136	−90	−46	12	29600	5.71	4.63	25
PG1336−018	13	−45	−13	31327	5.59	4.20	9	Feige 48	−45	−71	−44	29500	5.54	4.21	38
NSVS14256825	−6	−7	−10	40000	5.50	3.55	10	GD 687	60	−58	−15	24350	5.32	4.05	26
HS2231+2441	8	−59	−107	28370	5.39	3.92	11	KIC11179657	10	3	7	26000	5.14	3.47	39
UVEXJ0328+5035	−16	41	−14	28500	5.50	4.19	12	V 1405 Ori	59	−73	−6	35100	5.66	4.14	16
HW Vir	18	8	−12	28488	5.63	4.51	13	KIC2438324	9	3	7	27098	5.69	4.77	40
EC10246−2707	12	−9	−28	28900	5.64	4.51	14	KPD1946+4340	43	−17	53	34200	5.43	3.61	25
PG1043+760	18	50	9	27600	5.39	3.98	15	SDSSJ0951+0347	−38	−61	79	29800	5.48	4.04	19
OGLE BUL−SC16335	−36:	448:	−579:	31500	5.70	4.46	16	[CW83] 1419−09	53	−58	3	–	–	(4.3)	
2M1938+4603	16	24	3	29564	5.43	3.93	17	HE0929−0424	3	−68	−24	29602	5.69	4.58	26
EC00404−4429	−67	−15	−34	–	–	(4.3)		KIC2991403	9	3	7	27300	5.43	4.10	39
KIC7335517	85	−20	4	–	–	(4.3)		HE0230−4323	32	19	−18	31552	5.60	4.20	26
ASAS102322−3737	−6	−7	−39	25300	5.38	4.13	18	GALEX J2349+3844	17	7	5	23770	5.38	4.24	24
SDSSJ0830+4751	−37	−88	42	28400	5.60	4.45	19	KUV16256+4034	−5	−93	−28	23100	5.38	4.30	36
KIC6614501	−150	68	−163	23700	5.70	5.80	20	BPS CS 22879−149	−10	−41	−51	–	–	(4.3)	
2M1533+3759	64	−36	7	29230	5.58	4.33	21	HE1318−2111	67	−1	28	36254	5.42	3.48	41
SDSSJ1920+3722	−33	35	15	27500	5.40	4.01	22	PG1544+488	−136	2	148	32800	5.33	3.65	42
HS2333+3927	7	−20	40	36500	5.70	4.18	23	SDSSJ1726+2744	57	−21	−88	32600	5.84	4.74	28
GALEX J0805−1058	−20	−49	−12	22320	5.68	5.86	24	PG1743+477	−48	−41	−24	27600	5.57	4.43	43
BPS CS 22169−0001	9	16	2	39300	5.60	3.82	25	GALEX J0507+0348	−74	−66	8	23990	5.42	4.33	24
GALEX J0751+0925	−5	−24	−34	30620	5.74	4.63	24	PG0001+275	42	−68	−29	25400	5.30	3.92	25
HE1415−0309	69	−15	89	29520	5.56	4.26	26	PG1519+640	−18	50	−42	30600	5.72	4.58	36
HS1741+2133	−85	−98	40	35600	5.30	3.21	27	HE1059−2735	−143	8	−57	40966	5.38	3.24	41
SDSSJ0823+1136	−90	−60	66	31200	5.79	4.71	19	PG0101+039	15	−39	−22	27500	5.53	4.34	44
SDSSJ1138−0035	34	−144	−63	31200	5.54	4.08	28	EC20182−6534	28	−29	35	–	–	(4.3)	
PG1432+159	55	−47	−30	26900	5.75	4.93	29	PG1725+252	−58	−69	63	26560	5.03	3.15	45
SDSSJ1625+3632	−27	−55	−60	23570	6.12	6.86	30	PG1247+554	−60	−42	22	32366	6.11	5.42	46
PG2345+318	1	−17	−1	27500	5.70	4.76	29	HD188112	25	20	−11	21500	5.66	5.88	47
SDSSJ2046−0454	39	−56	−212	31600	5.54	4.05	28	PG1648+536	68	−62	−36	31400	5.62	4.27	36
PG1329+159	−24	−48	−12	29100	5.62	4.44	15	SDSSJ1522−0130	−49	4	−49	25200	5.47	4.36	19
FBS0117+396	72	−13	8	29370	5.48	4.07	31	SDSSJ2256+0656	24	−2	15	28500	5.64	4.54	28
SDSSJ1654+3037	100	32	−30	24900	5.39	4.18	28	EC22202−1834	−4	−59	−20	–	–	(4.3)	
AA Dor	−66	8	−19	37800	5.51	3.65	32	PG1248+164	67	5	−18	26600	5.68	4.78	15
HE0532−4503	182	−91	52	25710	5.33	3.97	26	JL82	−35	−36	3	26500	5.22	3.64	25
GALEX J0321+4727	−104	−39	45	27990	5.34	3.83	24	PG0849+319	−77	−65	−18	28900	5.37	3.83	15
CPD−64°481	48	−70	−41	27500	5.60	4.51	33	SDSSJ1505+1108	19	−232	−59	33200	5.80	4.60	28
KBS13	32	7	−15	33970	5.87	4.73	34	EQ Psc	74	−60	−27	–	–	(4.3)	
SDSSJ1021+3010	25	11	−19	30400	5.67	4.47	19	EC02200−2338	−20	−50	8	–	–	(4.3)	

Table C2 – *continued*

Name	U (km s^{-1})	V (km s^{-1})	W (km s^{-1})	$T_{\rm eff}$ (K)	log g (c.g.s.)	M_V (mag)	Ref.	Name	U (km s^{-1})	V (km s^{-1})	W (km s^{-1})	$T_{\rm eff}$ (K)	log g (c.g.s.)	M_V (mag)	Ref.
KPD2215+5037	−40	−11	30	29600	5.64	4.45	36	PG1253+284	−13	−9	24	–	–	(4.3)	
Ton S 183	46	−21	−38	27600	5.43	4.08	25	PG0958−073	−116	−84	−20	26100	5.58	4.57	35
EC13332−1424	−68	40	9	–	–	(4.3)		KIC10553698A	−167	111	−155	27423	5.44	4.12	51
PG1627+017	−25	−30	−29	23500	5.40	4.32	25	KPD0025+5402	57	15	−27	28200	5.37	3.88	43
EC21556−5552	22	13	−25	–	–	(4.3)		PB7352	11	8	14	25000	5.35	4.07	25
PG1230+052	2	−37	−57	27100	5.47	4.22	36	PG0934+186	−18	−27	−26	35800	5.65	4.08	36
PG1116+301	−23	−41	−12	32500	5.85	4.77	15	Ton S 135	21	−38	8	25000	5.60	4.70	52
PG0918+029	−57	−93	15	31700	6.03	5.27	29	EC20369−1804	3	−13	−26	–	–	(4.3)	
EC12408−1427	−64	15	−24	–	–	(4.3)		SDSSJ1832+6309	−61	−24	−19	26800	5.29	3.79	19
HE2135−3749	−21	−1	−77	30000	5.84	4.92	48	PG0839+399	−22	−62	−3	37800	5.53	3.70	43
PB5333	−22	−121	29	37900	5.81	4.40	29	PG1244+113	44	21	12	36300	5.54	3.78	36
HS2359+1942	141	−21	81	31434	5.56	4.11	26	CD−24°731	−33	−103	7	35400	5.90	4.73	53
PG1452+198	26	−18	−8	29400	5.75	4.74	36	HE1115−0631	−40	−130	1	40443	5.80	4.30	41
SDSSJ1508+4940	5	−30	−44	29600	5.73	4.68	19	PG0907+123	−43	−34	10	27280	5.54	4.38	45
PG1000+408	−20	−56	52	36400	5.54	3.78	45	PG1032+406	−69	−57	−13	31290	5.78	4.68	45
SDSSJ1132−0636	10	1	12	46400	5.89	4.53	19	SDSSJ0952+6258	31	−74	13	27700	5.59	4.47	19
GALEX J1731+0647	−23	−73	73	27780	5.35	3.87	24	HE1448−0510	−1	−14	−52	34760	5.53	3.84	26
HE1421−1206	−72	−54	−67	29600	5.55	4.23	25	PG1439−013	−45	−17	−23	–	–	(4.3)	
PG2331+038	96	−41	−13	27200	5.58	4.48	36	SDSSJ0321+0538	37	−22	3	30700	5.74	4.62	19
HE1047−0436	−26	−20	8	30200	5.66	4.46	49	PHL861	108	−162	11	29668	5.50	4.10	26
GALEX J2254−5515	−26	0	−16	31070	5.80	4.74	24	PG0940+068	56	8	15	–	–	(4.3)	
PG0133+114	−4	−42	−6	29600	5.66	4.50	43	Feige108	25	14	−38	35880	6.26	5.61	45
PG1512+244	−50	−58	56	29900	5.74	4.68	15	EC20260−4757	61	−2	−14	–	–	(4.3)	
[CW83] 1735+22	21	−9	56	38000	5.54	3.71	25	FF Aqr	0	8	−29	32000	6.00	3.47[a]	54
SDSSJ0118−0025	0	−44	−46	27900	5.55	4.36	19	PG1110+294	4	−31	−19	30100	5.72	4.62	15
HE2150−0238	−5	−16	30	30200	5.83	4.88	25	KIC11558725	114	−120	149	27910	5.41	4.01	55
KPD2040+3955	103	−28	14	27900	5.54	4.33	36	PG1558−007	−29	−86	−44	20300	5.00	3.58	56
SDSSJ0023−0029	−177	−30	5	29200	5.69	4.61	28	LB1516	−5	−1	−14	25200	5.41	4.21	35
HD49798	5	−4	3	–	–	(4.3)		CS1246	−5	−82	0	28500	5.46	4.09	57
KIC7664467	9	3	7	26800	5.17	3.49	39	KIC7668647	273	−91	−29	27700	5.50	4.25	58
HD171858	73	−3	3	27200	5.30	3.78	25	PG1619+522	−19	−33	−27	32300	5.98	5.11	39
PG1403+316	−47	−36	24	31200	5.75	4.61	36	PG0919+273	95	−20	−22	32900	5.90	4.87	36
PG1716+426	88	−5	−33	27400	5.47	4.19	15	EGB 5	−83	9	−2	34500	5.85	4.65	59
SDSSJ1346+2817	−31	−96	28	28800	5.46	4.06	19	HD185510	−8	−30	−32	31000	6.50	1.10[a]	60
NGC188/II−91	10	5	6	–	–	(4.3)		PG0850+170	1	−37	17	27100	5.37	3.97	15
PG1300+279	1	−41	4	29600	5.65	4.48	15	59 Cyg	−4	−7	−1	52100	5.00	−3.45[a]	61
CPD−20°1123	54	−28	17	23500	4.90	3.09	50	FY CMa	−18	−11	−3	45000	4.30	−2.51[a]	62
HD149382	30	7	20	34200	5.89	4.77	29	Φ Per	−6	−22	0	53000	4.20	−2.80[a]	63
PG1538+269	43	13	−19	25200	5.30	3.94	29	BD−11°162	58	−4	−4	35000	5.90	4.16[a]	64

Table C2 – *continued*

Name	U (km s^{-1})	V (km s^{-1})	W (km s^{-1})	$T_{\rm eff}$ (K)	log g (c.g.s.)	M_V (mag)	Ref.	Name	U (km s^{-1})	V (km s^{-1})	W (km s^{-1})	$T_{\rm eff}$ (K)	log g (c.g.s.)	M_V (mag)	Ref.
GALEX J1632+0759	−3	3	−34	38110	5.38	3.31	24	PG1701+359	−110	−145	61	33010	5.91	4.53[a]	45
PG1104+243	−51	−54	−48	33500	5.85	3.95[a]	65	PG1317+123	12	−9	44	37000	5.80	3.75[a]	69
PG1018−047	−22	−59	−19	30500	5.50	3.97[a]	66	BD−7°5977	−28	−9	5	29000	5.02	0.21[a]	65
PG1449+653	−68	−125	−82	28150	5.50	3.85[a]	67	BD+29°3070	−42	−30	−8	28500	5.76	3.59[a]	68
PG1338+611	85	−24	82	27400	5.54	3.89[a]	68	TYC3871−835−1	−31	−49	28	22500	5.12	3.24[a]	65
BD+34°1543	−12	−66	28	36700	5.92	3.55[a]	68								

[a] M_V estimated for the spectral composite.

References: (1) Vennes et al. (2012); (2) Schaffenroth et al. (2014a); (3) Maxted et al. (2002); (4) O'Toole et al. (2006); (5) Koen et al. (1998); (6) Geier et al. (2007); (7) Drechsel et al. (2001); (8) Geier et al. (2011b); (9) Vučković et al. (2007); (10) Almeida et al. (2012); (11) Østensen et al. (2007); (12) Verbeek et al. (2012); (13) Edelmann (2008); (14) Barlow et al. (2013b); (15) Maxted et al. (2001); (16) Geier et al. (2014); (17) Østensen et al. (2010c); (18) Schaffenroth et al. (2013); (19) Kupfer et al. (2015); (20) Silvotti et al. (2012); (21) For et al. (2010); (22) Schaffenroth et al. (2014b); (23) Heber et al. (2004); (24) Németh et al. (2012); (25) Geier et al. (2010b); (26) Lisker et al. (2005); (27) Edelmann et al. (2003); (28) Geier et al. (2011c); (29) Saffer et al. (1994); (30) Kilic et al. (2011); (31) Østensen et al. (2013); (32) Müller et al. (2010); (33) O'Toole et al. (2005); (34) For et al. (2008); (35) Geier et al. (2013b); (36) Copperwheat et al. (2011); (37) Edelmann et al. (1999); (38) Heber et al. (2000); (39) Østensen et al. (2010a); (40) Liebert et al. (1994); (41) Stroeer et al. (2007); (42) Şener & Jeffery (2014); (43) Morales-Rueda et al. (2003); (44) Geier et al. (2008); (45) Billéres et al. (2002); (46) Kepler et al. (1995); (47) Heber et al. (2003); (48) Karl et al. (2006); (49) Napiwotzki et al. (2001); (50) Naslim et al. (2012); (51) Østensen et al. (2014); (52) Heber (1986); (53) O'Toole & Heber (2006); (54) Vaccaro et al. (2007); (55) Telting et al. (2012a); (56) Heber et al. (2002); (57) Barlow et al. (2010); (58) Telting et al. (2014b); (59) Geier et al. (2011d); (60) Jeffery & Simon (1997); (61) Peters et al. (2013); (62) Peters et al. (2008); (63) Gies et al. (1998); (64) Ulla & Thejll (1998); (65) Vos et al. (2014); (66) Deca et al. (2012); (67) Aznar Cuadrado & Jeffery (2001); (68) Vos et al. (2013); (69) Thejll et al. (1995).

MNRAS **450,** 3514–3548 (2015)